

Utah State University

DigitalCommons@USU

All Graduate Theses and Dissertations

Graduate Studies

5-1998

Predicting Transpiration rates of Hydroponically-Grown Plant Communities in Controlled Environments

Oscar Monje
Utah State University

Follow this and additional works at: <https://digitalcommons.usu.edu/etd>



Part of the [Plant Sciences Commons](#)

Recommended Citation

Monje, Oscar, "Predicting Transpiration rates of Hydroponically-Grown Plant Communities in Controlled Environments" (1998). *All Graduate Theses and Dissertations*. 6754.
<https://digitalcommons.usu.edu/etd/6754>

This Dissertation is brought to you for free and open access by the Graduate Studies at DigitalCommons@USU. It has been accepted for inclusion in All Graduate Theses and Dissertations by an authorized administrator of DigitalCommons@USU. For more information, please contact digitalcommons@usu.edu.



PREDICTING TRANSPIRATION RATES OF
HYDROPONICALLY-GROWN PLANT COMMUNITIES
IN CONTROLLED ENVIRONMENTS

by

Oscar Monje

A dissertation submitted in partial fulfillment
of the requirements for the degree

of

DOCTOR OF PHILOSOPHY

in

Plant Science

Approved:

UTAH STATE UNIVERSITY
Logan, Utah

1998

Copyright © Oscar Monje 1998
All Rights Reserved

ABSTRACT

Predicting Canopy Transpiration of Plant Communities
in Controlled Environments

by

Oscar Monje, Doctor of Philosophy

Utah State University, 1998

Major Processor: Dr. Bruce Bugbee
Department: Plants, Soils, and Biometeorology

Canopy transpiration is a major factor determining crop evapotranspiration and energy budgets. Unfortunately the development of robust models of canopy transpiration is hindered by a lack of reliable data due to the difficulties of making canopy-scale measurements. However, measurements of canopy water vapor and carbon fluxes via gas exchange techniques are possible in controlled environments. Simultaneous measurements of transpiration, photosynthesis, and canopy temperature were made in wheat and soybean communities. These data were used to calculate chamber aerodynamic and canopy stomatal conductances, and to model the response of canopy transpiration to CO₂ concentration and vapor pressure deficit. Canopy stomatal conductance was found to decrease diurnally by 20-30% in well-watered crops grown under constant environmental conditions. The magnitude of this diurnal decrease in the canopy stomatal conductance of wheat and soybean decreased

with increasing ambient CO₂ concentrations. Eight models describing how canopy stomatal conductance responds to environmental changes were incorporated into a canopy transpiration model. The results and methods developed in this study will allow future physiologically-based canopy transpiration models to incorporate these models for predicting the response of transpiration rates in controlled environments.

(127 Pages)

ACKNOWLEDGMENTS

I would like to thank my mentor, Dr. Bruce Bubgee, for teaching me to adhere to what theory predicts when the measurement instrumentation used in these studies may have suggested otherwise. I would also like to thank him for trusting in me to explain these observations in my own terms and for his guidance in career matters.

I would also like to thank the members of my committee for their insightful comments and for challenging me to excel in the completion of this dissertation. I would also like to thank all the faculty and staff of the Plants, Soils, and Biometeorology Department at Utah State University for providing an excellent environment for learning and for providing much insight of how things are done in the academic world.

Finally, I would like to thank my wife, Maki, my son, Daniel, my father, Alberto, and Sichirou Fujiwara because this work would not have been possible without their love, patience, and continued support.

Oscar Monje

CONTENTS

	Page
ABSTRACT	iii
ACKNOWLEDGMENTS	v
LIST OF TABLES	viii
LIST OF FIGURES	ix
CHAPTER	
1. PREDICTING TRANSPIRATION RATES OF PLANT COMMUNITIES	1
Introduction	1
Literature review	2
Objectives	8
References	10
2. DETERMINING CANOPY STOMATAL CONDUCTANCE FROM RADIATIVE AND AERODYNAMIC CANOPY TEMPERATURE MEASUREMENTS	13
Abstract	13
Introduction	14
Materials and methods	16
Results	26
Discussion	40
References	43
3. FACTORS CONTROLLING DIURNAL CHANGES IN CANOPY STOMATAL CONDUCTANCE	45
Abstract	45
Introduction	45
Materials and methods	48
Results and discussion	51
References	57

4.	MODELING CANOPY TRANSPIRATION IN CONTROLLED ENVIRONMENTS	59
	Abstract	59
	Introduction	59
	Materials and methods	61
	Results and discussion	77
	Conclusions	88
	References	89
5.	SUMMARY AND CONCLUSIONS	92
	Abstract	92
	Conclusions	109
	References	111
	CURRICULUM VITAE	113

LIST OF TABLES

Table	Page
4.1	Definitions of the eight stomatal conductance models 69
4.2	Parameterization coefficients for stomatal conductance models 70
4.3	Parameterization coefficients for fGs functions. 73
4.4	Comparison of wheat canopy stomatal conductance models in predicting canopy transpiration using the Penman-Monteith equation. 82
4.5	Comparison of soybean canopy stomatal conductance models in predicting canopy transpiration using the Penman-Monteith equation. 83

LIST OF FIGURES

Figure	Page
2.1 Wind speed profiles of (A) wheat and (B) soybean canopies measured at several stages of the life cycle.	27
2.2 The effect of incident PPF on the air temperature profiles above and within a wheat canopy.	28
2.3 Air temperature profiles above and within a wheat canopy.	30
2.4 Diurnal course of canopy energy balance components: net radiation, latent heat flux, sensible heat flux, and photosynthesis in (A) wheat and (B) soybean.	30
2.5 The energy balance fluxes of soybean canopies, of the same age, affected by the (A) absence and (B) presence of a water filter under the HPS lamps.	32
2.6 The regression of sensible heat flux versus the radiative canopy-to-air temperature (solid line).	32
2.7 The radiative ΔT_{IR} (Method 1) and the aerodynamic ΔT_A (Method 2) influenced by PPF_o and by wind speed.	34
2.8 The radiative ΔT_{IR} , measured as a function of the height at which the infrared transducers were positioned above or within the canopy.	34
2.9 The ΔT_{Height} determined by Method 3 as a function of PPF_o	35
2.10 Sensible heat flux and the canopy-to-air temperature differences as a function of time of day, corresponding to the energy fluxes in Figure 2.5.	35
2.11 Daily courses of (A) canopy surface stomatal conductance (G_C) and (B) canopy stomatal conductance (G_S) for a mature wheat canopy grown at a PPF of $1600 \mu\text{mol m}^{-2} \text{s}^{-1}$	38
2.12 Diurnal course of the decoupling coefficient in (A) wheat and (B) soybean.	38
2.13 The coupling coefficient, $(1-\Omega)$, as a function of canopy G_S in wheat and soybean canopies measured at $400 \mu\text{mol mol}^{-1} \text{CO}_2$	39

Figure	Page
3.1 A sequence of 6 days where CO ₂ enrichment was decreased every two days. The corresponding changes in canopy Tr (A), canopy-air temperature difference (B), and canopy G _s (C) were continuously recorded as CO ₂ concentration was changed.	52
3.2 The data in Fig. 3.1 were expressed as a function of the photoperiod to illustrate the effects of CO ₂ concentration on the diurnal patterns in canopy G _s	52
3.3 Wheat canopy stomatal conductance (A) expressed as a fraction of the conductance measured at 380 μmol mol ⁻¹ and (B) expressed as a fraction of the maximum conductance observed during the day	56
3.4 Water use efficiency improved as the CO ₂ concentration increased	56
4.1 A flow diagram of the transpiration model. The chart illustrates the main subroutines and the iterative loop used to calculate canopy temperature.	65
4.2 The fGS functions for (A) wheat and (B) soybean. These functions describe the response of canopy stomatal conductance to CO ₂ enrichment as a function of the photoperiod.	80
4.3 A comparison between predicted vs. observed transpiration. This figure compares the accuracy of the eight canopy G _s models and the two transpiration models.	80
4.4 The Akaike information criterion (AIC) as a function of model complexity. The greater the number of parameters then the likelihood that a given model gave the best fit was reduced.	84
4.5 A comparison between predicted vs. observed wheat (A) and soybean (B) canopy GS for the eight stomatal conductance algorithms.	84
4.6 Single parameter sensitivity plots for the wheat BW2 model (A) and the soybean AJ2 model (B).	86
4.7 A comparison between predicted vs. observed wheat canopy stomatal conductance (A) and transpiration rate (B) as a function of vapor pressure deficit.	86

Figure	Page
4.8 Soybean canopy photosynthesis and dark respiration (A) measured in the 20 m ² Biomass Production Chamber (BPC) at the Kennedy Space Center.	88
5.1 (A) Average daytime and nighttime canopy transpiration rates measured for the life cycle of a wheat (cv. Apogee) crop. (B) The ratio of nighttime to daytime transpiration rate increases as the life cycle progresses.	96
5.2 Canopy G _s (A), Tr (B), and G _s vs.Tr (C) as a function of vapor pressure deficit (VPD) measured at 700 (red), 1000 (green), and 1200 (blue) μmol mol ⁻¹ CO ₂	96
5.3 Simulated canopy G _s (A), Tr (B), and G _s vs.Tr (C) as a function of VPD at two PPF levels (600 and 1400 μmol ⁻² s ⁻¹).	104
5.4 Observed (A) and simulated (B) canopy G _s in soybean at four CO ₂ concentrations (400, 600, 800, and 1200 μmol mol ⁻¹).	104
5.5 The observed diurnal courses in canopy G _s (A), Pnet (B), Tr (C), T _{canopy} (D), and chamber VPD (E) as a function of the photoperiod (fPD) for the soybean experiment described in Fig. 5.4.	106
5.6 The simulated diurnal courses in canopy G _s (A), Pnet (B), Tr (C), T _{canopy} (D), and chamber VPD (E) as a function of the photoperiod (fPD) for the soybean experiment described in Fig. 5.4.	107
5.7 The responses of daytime wheat and soybean G _s (A) and Tr (B) to CO ₂ concentration at a PPF of 1400 μmol m ⁻² s ⁻¹ were simulated with the same inputs as in the wheat experiment (Fig. 5.3).	108

CHAPTER 1
PREDICTING TRANSPIRATION RATES
OF PLANT COMMUNITIES

Introduction

The ability to predict canopy transpiration (T_r) rates in controlled environments (CEs) has many applications: the design of automated environmental control systems, reducing costs in commercial production systems, improved growth chamber design, and generating performance envelopes for plant-based bioregenerative systems (Sirko *et al.*, 1992). Although many models predict how transpiration will respond to environmental parameters (i.e., radiation, temperature, vapor pressure deficit, and CO_2 concentration), the majority of these models have been developed for field conditions. There are several inherent differences between field and chamber environments, and many empirical assumptions are made in the derivation of field models. These differences were not large enough to warrant the development of an entirely new model, but they caused us to modify existing models of stomatal conductance for modeling canopy T_r in CEs. Simulation experiments with a validated T_r model will help identify the combinations of environmental parameters having the greatest impact on transpiration and can, therefore, reduce the number of experiments required to select between competing chamber designs.

CEs are unique compared to the field: electric lighting and CO_2 -enrichment are frequently used; the spectral quality of incident radiation can be controlled by choosing the lighting system; the ratio of photosynthetic to total shortwave radiation is 42-46% in the field and 50-80% in CEs; spatial scales are small ($<5 \text{ m}^2$) with the potential for edge effects to be

important; photosynthetic photon flux (PPF) and temperature vary spatially; wind speed and turbulence vary spatially and temporally; chamber wind direction can be bottom to top, or left to right; and humidities above 75% are common, even at high irradiances. Although environmental parameters can be manipulated with greater ease in CEs than in the field, the lack of data characterizing the behavior of plant communities in CEs hinders efforts to develop predictive models of water fluxes in these systems. In addition, measurements made in any given CE growth chamber may not be transferrable to other chambers because of differences in side-lighting, CO₂-enrichment, chamber wind speed and direction, and in the fraction of longwave radiation reaching the plants (Bubenheim *et al.*, 1988; Sinclair *et al.*, 1992).

Literature review

Stomatal conductance models

Mechanistic transpiration models are typically based on measurements and models of single-leaf conductance (g), which are first used to predict single leaf transpiration and finally to estimate canopy transpiration. This approach assumes that the cumulative behavior of stomata of all the leaves in a canopy can be estimated from the behavior of stomata on a single leaf.

Single leaf stomatal conductance. Several approaches for modeling the response of single-leaf stomatal conductance (g) to the environment have been used. Single leaf stomatal conductance has been: 1) modeled from radiation measurements (Aphalo and Jarvis, 1993; Monteith, 1995); 2) correlated with [CO₂] and net photosynthesis (Farquhar and Wong, 1974;

Farquhar and von Caemmerer, 1982); 3) modeled assuming that environmental factors act independently in determining g (Jarvis, 1976; $g = f(\text{PPFabs}) * f(\text{Tleaf}) * f(\text{Ds}) * f(\text{CO}_2) * f(\psi)$); 4) related empirically to net photosynthesis, ambient CO_2 , and humidity (Ball *et al.*, 1987; Leuning, 1995); 5) linearly related to transpiration rates (Monteith, 1995); and 6) related to the osmotic gradient between guard and epidermal cells (Dewar, 1995).

Recent studies indicate that stomata respond to the rate of transpiration (Tr) rather than to humidity (Dewar, 1995; Monteith, 1995; Mott and Parkhurst, 1991). Typically, stomatal conductance decreases linearly as Tr increases, perhaps due to a negative feedback that optimizes water use efficiency. This linear decrease in g vs. Tr , commonly observed in field plants, can be expressed as Equation 1:

$$g = a - b * \text{Tr} \quad (1)$$

where a and b are empirical constants (Dewar, 1995). There have been reports that average stomatal conductance may also increase with Tr in very dry atmospheres, due to patchy (heterogenous) stomatal closure (Monteith, 1995; Mott and Parkhurst, 1991). However, these reports are speculative and the observed responses were determined in unusual environmental conditions.

Canopy stomatal conductance. Several models have been developed for estimating the surface conductance of vegetation (G_c), which includes the canopy stomatal conductance (G_s). The most widely used model was the big-leaf model developed by Monteith (1963). This model assumes that the canopy exchanges sensible and latent heat with the atmosphere from a theoretical surface that possesses the physiological properties of a leaf. The surface

conductance of vegetation is assumed to depend only on stomatal conductance of the individual leaves and the total leaf area, when soil evaporation is negligible (Lhomme, 1991). The main problem with this single-layer model is that there is no simple way to estimate the mean leaf stomatal conductance for the vegetation from direct measurements of single leaf stomatal conductance.

In contrast, multilayer models treat the canopy as a continuous or discrete set of horizontal planes, each one absorbing net radiation and transferring sensible and latent heat. The mean leaf stomatal conductance in each layer can then be estimated from various scaling-up techniques. Mean canopy stomatal conductance has been: 1) weighted according to leaf position in sun and shade environments (Sinclair *et al.*, 1976); 2) weighted by the leaf area and leaf angle class present in each layer (Sellers *et al.*, 1986); 3) estimated from the bulk average conductance of sunlit and shaded horizontal leaves (Bailey and Davies, 1981); or 4) estimated from the mean stomatal conductance of the sunlit horizontal leaves in the top 25% of the LAI (Whitehead *et al.*, 1981).

Leuning *et al.* (1995) recently used a multilayer model of canopy photosynthesis and transpiration to study the response of canopy nitrogen- and radiation use efficiencies to plant nutritional status and to the diffuse component of incident radiation. They developed Equation 2 to describe the response of leaf stomatal conductance (g) for CO_2 to environmental changes:

$$g = g_0 + a_1 \cdot P_{\text{net}} / [(C_s - \Gamma) \cdot (1 + D_s / D_{s0})] \quad (2)$$

where, g_0 = stomatal conductance at the light compensation point,
 P_{net} = leaf net photosynthesis,
 Γ = the CO_2 compensation point,
 a_1, D_{s0} = empirical coefficients,

C_s = CO₂ concentration at the leaf surface, and
 D_s = vapor pressure deficit at leaf temperature.

In this semi-empirical approach, P_{net} determines the maximal stomatal conductance that can be attained. This model predicts stomatal responses to irradiance, temperature, humidity, and CO₂ since P_{net} , D_s , and C_s depend on these environmental parameters. Their model also scales leaf g to the canopy stomatal conductance (G_s ; Equation 3):

$$G_s = LAI * (F_{sun} * g_{sun} + F_{shade} * g_{shade}) \quad (3)$$

where, LAI = leaf area index,
 F_{sun} , F_{shade} = fractions of sunlit and shaded leaves at each level, and
 g_{sun} , g_{shade} = the corresponding stomatal conductances.

Canopy transpiration models

Most transpiration models have been developed and calibrated for field situations and they are useful starting points for transpiration modeling in CEs. The Penman-Monteith equation is more mechanistic and has been suggested for modeling transpiration in CE chambers (Sirko *et al.*, 1992). Unfortunately, the Penman-Monteith model requires horizontally and temporally homogenous wind and temperature profiles within and above the plant canopies. These profiles occur in large vegetated surfaces with a stable boundary layer above the canopy. A well-defined, equilibrium boundary layer is established from the prolonged interaction between the air flowing above the canopy and the canopy itself (Monteith and Unsworth, 1990). The boundary layer becomes thicker with increasing fetch and its rate of growth is commonly assumed to be on the order of 1 m per 100 m of fetch. Once this equilibrium boundary layer exists, the transport of heat, water vapor, and CO₂ can

be modeled from the wind speed and air temperature at a given reference height, stomatal and leaf boundary layer conductances, canopy temperature, and the aerodynamic resistance (Campbell, 1977; Huband and Monteith, 1986; Thornley and Johnson, 1990). In contrast, the fetch of even the largest, well ventilated, walk-in plant growth chambers is far too small for a distinct boundary layer to be formed above the canopy and applying a field-calibrated Penman-Monteith equation would not be possible unless there was some procedure for determining the aerodynamic resistance in a growth chamber.

Mechanistic models define the canopy in terms of the inclination, orientation, and distribution of individual leaves and estimate canopy transpiration and photosynthesis from canopy radiation interception and energy balance components (Stockle, 1992). In these models, the leaf radiation balance is calculated in layers from estimates of the direct and diffuse shortwave fluxes and longwave radiation fluxes (Norman, 1979). Several factors such as the extinction of radiation with depth, the fractional area of sunlit and shaded leaves, and sunlit leaf orientation affect the leaf radiation balance and must be calculated by the model. The typical modeling approach (De Wit, 1965) divides the canopy into thin layers (0.1-0.5 LAI), and the leaves in each layer are divided into as many as nine leaf inclination and azimuth angle classes. However, simplified models divide the foliage elements into three leaf inclination and azimuth angle classes, resulting in negligible losses of accuracy (Goudriaan, 1988). Further simplifications, which consider only two foliage fractions (sunlit and shaded) and an average irradiance per layer, result in less than 4% errors in photosynthesis and transpiration. In comparison, modeling the canopy as a single layer and with average

irradiance may result in errors ranging up to 9% (Stockle, 1992).

Chamber aerodynamic resistance

A well-defined method for determining the chamber aerodynamic resistance in CEs is required since this term governs the exchange of heat and water vapor between the canopy and the air above it. In fact, canopy transpiration cannot be estimated directly from the canopy stomatal conductance because sensible heat and water vapor fluxes are exchanged with the air above the canopy across the boundary layer surrounding the vegetation (Baldocchi *et al.*, 1983). The overall boundary layer resistance of the canopy is the sum of the canopy resistance to water vapor and the aerodynamic resistance. This 'bulk' surface conductance, the inverse of the surface resistance to water vapor, can be used to determine the canopy stomatal conductance from measurements of T_r , humidity, and air and canopy temperatures when the aerodynamic resistance term is known (Monteith and Unsworth, 1990). The aerodynamic resistance may be estimated from the sensible heat flux and the canopy-to-air temperature difference obtained with infrared thermometers. The radiative canopy-to-air temperature difference can be compared with the temperature difference necessary to solve the energy balance equation for both transpiration and sensible heat, assuming a given aerodynamic resistance, but this method requires a detailed description of the canopy energy balance (Bugbee *et al.*, 1996).

Controlled environments

CEs offer the benefit of constant environmental conditions (PPF, temperature, CO₂,

humidity). Constant PPF levels result in significant reductions in model complexity, as typical diurnal fluctuations of incoming radiation caused by changing cloud cover, solar zenith angle and elevation, and diurnal changes in temperature commonly found in field situations are avoided. In addition, sealed plant chambers facilitate nondestructive measurements of water and CO₂ fluxes (Bugbee, 1992), which can be used for model development. These unique features of plant chambers greatly simplify the acquisition of data for model parameterization and validation. However, each CE chamber has a unique environment because of the many types of artificial lighting and the different combinations of CO₂-enrichment, PPF, temperature, and wind set points that are possible. This variability in conditions means that empirical relationships determined from measurements made in a given chamber may not be valid in other chambers.

Empirical models developed for the field, which only fit observed data or rely on crop coefficients, are of little use in CEs. Mechanistic models should be more portable to CEs, but substantial recalibration may be required. However, this may not be entirely possible since the sensitivity of stomata to environmental factors in hydroponically grown plants may be different from field plants. Such differences could cause relationships between rates of physiological processes and plant parameters determined from field plants to be of limited use for interpreting or predicting the behavior of plants in CEs. These differences can substantially affect the portability of models developed in CEs to the field, and vice versa.

Objectives

The objective of this study is to develop a model for predicting the instantaneous

canopy transpiration rates and energy fluxes of crops grown hydroponically in CEs. A semi-empirical, canopy-level transpiration model that avoids the complexity of scaling from the single leaf to the canopy will be developed from canopy-level measurements. In principle, a canopy-level model should require fewer inputs than current mechanistic models based on single-leaf inputs; however, this approach relies on accurate measurements of canopy Tr and of energy balance components for model calibration and validation. The validation procedure is designed to evaluate how the model will behave in other chamber systems (Power, 1993). The best predictive model will be used to predict Tr using inputs collected in another chamber. This is a critical test since the usefulness of the predictions will depend on their validity in different chamber systems. Sensitivity analyses will be conducted to test the relative importance of both environmental and stomatal factors in determining transpiration rates. This analysis will be used to rank the model inputs with respect to their effect on transpiration, and for determining the precision required in specifying model inputs.

Models describing the responses of both erectophile (wheat) and planophile (soybean) canopy architectures to environmental changes will be calibrated using data collected during short-term exposures (hours to one day). The models will predict canopy stomatal conductance, and predict canopy transpiration using the Penman-Monteith equation together with measurements of chamber aerodynamic conductance. These models will be validated against independent data sets obtained in the same chamber used to collect the calibration data sets, and then ranked according to their accuracy and simplicity. The algorithms for predicting canopy transpiration in this study have been developed for use in future

physiologically-based, controlled environment, canopy transpiration models.

References

- Aphalo PJ, Jarvis PG.** 1993. An analysis of Ball's empirical model of stomatal conductance. *Annals of Botany* **72**, 321-327.
- Bailey WG, Davies JA.** 1981. Bulk stomatal control on evaporation. *Boundary-Layer Meteorology* **20**, 401-415.
- Baldocchi DD, Verma SB, Rosenberg NJ.** 1983. Characteristics of air flow above and within soybean canopies. *Boundary-Layer Meteorology* **25**, 43-54.
- Ball JT, Woodrow IE, Berry JA.** 1987. A model predicting stomatal conductance and its contribution to the control of photosynthesis under different environmental conditions. In: Biggens J, ed. *Progress in photosynthesis research*. The Hague: Martinus Nijhoff Publishers, 221-224.
- Bubenheim DL, Bugbee B, Salisbury FB.** 1988. Radiation in controlled environments: Influence of lamp type and filter material. *J. Amer. Soc. Hort. Sci.* **113**, 468-474.
- Bugbee B.** 1992. Steady state gas exchange in growth chambers: system design and operation. *HortScience* **27**, 770-776.
- Bugbee B, Monje O, Tanner B.** 1996. Quantifying energy and mass transfer in crop canopies. *Advances in Space Research* **18**, 149-156.
- Campbell GS.** 1977. *An introduction to environmental biophysics*. New York: Springer-Verlag.
- Dewar RC.** 1995. Interpretation of an empirical model for stomatal conductance in terms of guard cell function. *Plant, Cell and Environment* **18**, 365-372.
- De Wit CT.** 1965. Photosynthesis of leaf canopies. *Agricultural Research Report. Wageningen.* **663**.
- Farquhar GD, von Caemmerer S.** 1982. Modelling of photosynthetic response to environmental conditions. In: Lange OL, Nobel PS, Osmond CB, Ziegler H, eds. *Physiological plant ecology II: water relations and carbon assimilation*, Vol.12 B. Berlin: Springer-Verlag, 549-587.

- Farquhar GD, Wong SC.** 1974. An empirical model of stomatal conductance. *Aust. J. of Plant Physiology* **20**, 69-82.
- Goudriaan J.** 1988. The bare bones of leaf angle distribution in radiation models for canopy photosynthesis and energy exchange. *Agric. Forest Meteorology* **43**, 155-159.
- Huband NDS, Monteith JL.** 1986. Radiative surface temperature and energy balance of a wheat canopy. I. Comparison of radiative and aerodynamic temperature. *Boundary-Layer Meteorology* **36**, 1-17.
- Jarvis PG.** 1976. The interpretation of the variations in leaf water potential and stomatal conductance found in canopies in the field. *Philosophical Trans. Of the Royal Soc. London.* **273B**, 593-610.
- Leuning R.** 1995. A critical appraisal of a combined stomatal-photosynthesis model for C₃ plants. *Plant, Cell and Environment* **18**, 339-357.
- Lhomme JP.** 1991. The concept of canopy resistance: historical survey and comparison of different approaches. *Agric. Forest Meteorol.* **54**, 227-240.
- Monteith JL.** 1963. Gas exchange in plant communities. In: Evans LT, ed. *Environmental control of plant growth*. New York: Academic Press, 95-102.
- Monteith JL.** 1995. A reinterpretation of stomatal responses to humidity. *Plant, Cell and Environment.* **18**, 357-364.
- Monteith JL, Unsworth MH.** 1990. *Principles of environmental physics*. New York: Chapman and Hall, Inc.
- Mott KA, Parkhurst DF.** 1991. Stomatal response to humidity in air and in helox. *Plant, Cell and Environment* **14**, 509-515.
- Norman JM.** 1979. Modeling the complete canopy. In: Barfield BJ, Jones JW, eds. *Predicting photosynthesis for ecosystem models II*. Boca Raton: CRC Press.
- Power M.** 1993. The predictive validation of ecological and environmental models. *Ecological Modelling* **68**, 33-50.
- Sellers PJ, Mintz Y, Sud YC, Dalcher A.** 1986. A simple biosphere model (SiB) for use within general circulation models. *J. Atmospheric Science.* **43**, 305-331.

Sinclair TR, Murphey CE, Knoerr KR. 1976. Development and evaluation of simplified models simulating canopy photosynthesis and transpiration. *J. Appl. Ecology* **13**, 813-829.

Sinclair TR, Shiraiwa T, Hammer GL. 1992. Variation in crop radiation-use efficiency with increased diffuse radiation. *Crop Science* **32**, 1281-1284.

Sirko RJ, McCormack AC, Edeen MA. 1992. Plant canopy transpiration in bioregenerative life support systems: The link between mechanistic and empirical models. *22nd International Conference of Environmental Design*. Seattle: American Institute of Aeronautics and Astronautics, SAE No. 921356, 1-5.

Stockle CO. 1992. Canopy photosynthesis and transpiration estimates using radiation interception models with different levels of detail. *Ecological Modelling* **60**, 31-44.

Thornley JHM, Johnson IR. 1990. *Plant and crop modeling: a mathematical approach to plant and crop physiology*. New York: Oxford University Press.

Whitehead D, Okali DUU, Fasehun FE. 1981. Stomatal response to environmental variables in two tropical forest species during the dry season in Nigeria. *J. Appl. Ecology* **18**, 571-587.

CHAPTER 2
DETERMINING CANOPY STOMATAL CONDUCTANCE
FROM RADIATIVE AND AERODYNAMIC CANOPY
TEMPERATURE MEASUREMENTS

Abstract

Radiative canopy temperature of hydroponically grown wheat and soybean crops was measured with infrared thermometers. Sensible heat flux was calculated by subtraction from measurements of net radiation, latent heat flux, and canopy photosynthesis. Canopy surface conductance, which includes the chamber aerodynamic conductance, was obtained from the ratio of canopy transpiration to the canopy-to-air vapor pressure gradient. The chamber aerodynamic conductance was determined from sensible heat flux and the radiative canopy-to-air temperature difference and used to compute canopy stomatal conductance from canopy surface conductance. The average chamber aerodynamic conductance was $5.5 \text{ mol m}^{-2} \text{ s}^{-1}$ (0.14 m s^{-1}) in wheat, and $2.5 \text{ mol m}^{-2} \text{ s}^{-1}$ (0.06 m s^{-1}) in soybean canopies. Canopy stomatal conductance was computed from canopy surface conductance and the chamber aerodynamic conductance. The radiative canopy temperature was related to the aerodynamic canopy temperature by an offset, which varied as a function of photosynthetic photon flux. The chamber coupling coefficient, which quantifies the amount of transpiration controlled by stomatal movements, was 0.7 in both soybean and wheat. This degree of coupling is comparable to coupling found in field situations, which suggests that canopy stomatal conductances in well-ventilated controlled environments are comparable to conductances in

the field.

Introduction

Canopy stomatal conductance (G_s) is perhaps the most important property of a vegetated surface, because it regulates the rate of water loss in response to energy demands imposed by the environment surrounding it. This regulatory function is reflected in canopy temperature, which in turn, determines the direction of energy fluxes between the vegetation and its environment. Canopy stomatal conductance has traditionally been estimated using complex averaging algorithms based on single leaf stomatal conductance (Jones, 1992). Measurements of stomatal conductance are relatively easier to make in single leaves compared to canopies. However, scaling stomatal conductance from the single leaf to the canopy is complicated by the spatial variability of temperature, light, vapor pressure, and wind within a plant community, resulting from the interaction between the environment and canopy architecture (Jarvis, 1976; Monteith and Unsworth, 1990).

In field situations, Baldocchi *et al.* (1991) caution against equating the 'bulk' or canopy surface conductance (G_c) to estimates of canopy G_s derived from single leaf measurements. Canopy G_c , calculated from the stand-level latent heat exchange, may include contributions from soil evaporation because the aerodynamic surface temperature in the field represents sensible heat exchange from both foliage and soil. Canopy G_s may be computed from canopy G_c , obtained from transpiration measurements using the Penman-Monteith equation, if the aerodynamic conductance (g_A) is known. However, the determination of g_A in controlled environments is not as straightforward as in the field, where it can be obtained

using the log-wind profile approximation (Monteith and Unsworth, 1990).

The radiative canopy temperature has been used for determining g_A from simultaneous measurements of radiative canopy-air temperature difference and sensible heat flux (Smith *et al.*, 1989), or from a linear relation between canopy-air temperature difference and the vapor pressure difference (O'Toole and Real, 1986). However, these approaches are strongly dependent on the relation between the radiative and aerodynamic canopy temperatures. Considerable errors may be incurred from the use of the radiative canopy temperature as an estimate of the aerodynamic canopy temperature, since only the latter solves the energy balance equation that governs the magnitude and direction of evaporative and sensible heat fluxes (Smith *et al.*, 1989; Baldocchi *et al.*, 1991). A systematic difference of -1°C between radiative and aerodynamic temperatures was found by Huband and Monteith (1986), although differences ranging from 2 - 6°C have been observed (Baldocchi *et al.*, 1991). In the field, radiative temperature measurements depend on view and sun angles, degree of crop cover, soil-canopy temperatures, the spatial variability in canopy emissivity, and atmospheric attenuation (Kimes *et al.*, 1983). Additional errors due to sensor field of view and due to fluctuations in sensor body temperature can also introduce variability in radiative measurements of canopy temperature (Bugbee *et al.*, 1997). Errors of 1°C in the surface-to-air temperature can cause errors of approximately 40 W m^{-2} in estimates of latent heat flux.

The g_A represents the mechanism of turbulent transfer of heat, mass, and momentum between a canopy and its environment, and also influences the degree of stomatal control of transpiration. The degree of stomatal control, typically described by a dimensionless coupling

coefficient ($1 - \Omega$), quantifies how much must canopy conductance change to restrict transpiration by a given amount. The coupling coefficient depends on factors such as ventilation rate, or size of the crop, that alter the ratio between g_A and G_S (Jones, 1992). Jarvis and McNaughton (1986) note that stomatal conductances determined in controlled environment chambers often do not apply to field situations, as poor coupling in CEs results in minimal feedback between stomatal conductances and the saturation deficit within the canopy, and the impact of stomata on the transpiration rate is large.

In this study, the radiative canopy temperature, together with energy balance measurements, were used to determine the chamber g_A of fully-covered wheat and soybean canopies grown hydroponically in controlled environments. The chamber g_A was then used to compute canopy G_S from measurements of canopy transpiration. Furthermore, the chamber coupling coefficient was computed from the ratio between G_S and g_A to compare canopy conductances measured in this system with conductances in the field, or in other chamber systems.

Materials and methods

Cultural and environmental conditions

Wheat (*Triticum aestivum* L. cv. Veery-10) and soybean (*Glycine max* L. cv. Hoyt) canopies were grown in sealed, water-cooled, controlled-environment chambers (Model EGC-13, Environmental Growth Chambers, Chagrin Falls, OH). Two plant canopies of the same species were grown simultaneously in two chambers, each fitted with two 21 cm deep, 30 L hydroponic tubs. Wheat was planted in a 10 mm layer of inert media (Isolite, size CG-2,

Sumitomo Corp., Denver, CO) at a density of 1100 plants m^{-2} . Soybean seeds were germinated in moist Isolute and transplanted when the hypocotyls had elongated to at least 4 cm (about 6 days). The soybean plants were supported by closed cell foam plugs in a blue Styrofoam lid, and were evenly spaced at a planting density of 60 plants m^{-2} .

A fixed area, reflective enclosure was built around the hydroponic tubs within each chamber to reduce edge effects and side lighting. Lighting was provided by four 1000-W high pressure sodium lamps, which were adjusted to achieve $\pm 5\%$ PPF uniformity over the crop surface. The incident PPF (PPF_0) was 1400 $\mu\text{mol m}^{-2} \text{s}^{-1}$ and 900 $\mu\text{mol m}^{-2} \text{s}^{-1}$ during the growth of wheat and soybean, respectively. Longwave radiation from the lamps was removed by a 10 cm deep, recirculating, chilled water filter. The PPF_0 was measured at the top of the canopy with a quantum sensor (Model LI-190SB, LI-COR, Lincoln, NE), and was maintained constant throughout the life cycle by lowering the canopy platform as the plants grew taller.

Average air temperature was $23.0 \pm 0.3^\circ\text{C}$, the barometric pressure was 86 kPa, and the chamber CO_2 setpoint was varied between 400-1400 $\mu\text{mol mol}^{-1}$. The root zone was a recirculating hydroponic system controlled at $23 \pm 0.2^\circ\text{C}$ and pH 5.7 for the duration of the experiments. The solution was replenished daily with refill solution to provide ample nutrients over the life cycle.

Gas exchange system

The gas exchange system used was previously described in Bugbee (1992), except for the following modifications: 1) a dew point hygrometer was added to measure transpiration rates continuously, 2) two solid-state multiplexers (Model AM-25T, Campbell Scientific,

Logan, UT) with PRT temperature references were used for precision thermocouple measurements, and 3) two infrared transducers were used to measure radiative canopy temperature in each chamber. Data acquisition and control was performed with a dedicated datalogger (Model CR-10T, Campbell Scientific, Logan, UT).

Gas exchange in each chamber was measured every 8 minutes. Shoot net photosynthesis, P_{net} , and dark respiration rates were calculated from the difference between pre- and post-chamber CO_2 concentrations (ΔCO_2), multiplied by the mass flow rate of air (MF; $mol\ s^{-1}$) through the chambers. CO_2 concentration in pre- and post-chamber air was measured using two infrared gas analyzers (IRGA; Model LI-6251, LI-COR, Lincoln, NE). ΔCO_2 was measured by a differential IRGA, and pre-chamber air was controlled within $\pm 2\ \mu mol\ mol^{-1}$ from the setpoint by an absolute IRGA and a mass flow controller (Model 820, Sierra Instruments, Monterey, CA). Air flow into the chambers was measured with mass flow meters (Model 730, Sierra Instruments, Monterey, CA). Chamber evapotranspiration (ET) was determined from the difference in mole fraction of water vapor between pre- and post-chamber air (ΔX_{H_2O}), multiplied by MF into the chamber ($ET = \Delta X_{H_2O} \cdot MF$). ΔX_{H_2O} was determined from sequential measurements of pre- and post-chamber air dewpoint made with a dewpoint hygrometer (Model Dew-10, General Eastern, Watertown, MA).

Wind speed

Wind speed was measured with calibrated, heat transfer needle anemometers (Campbell Scientific, Logan, UT). These anemometers were well-suited for working in controlled environments because they are small, have fast responses, and are omnidirectional.

These needle anemometers were calibrated in a wind tunnel for windspeeds between 0.05 to 5 m s⁻¹ (Bugbee *et al.*, 1996), which makes them very useful for making wind measurements within the canopy foliage. The effect of wind speed on the canopy-air temperature difference was studied by changing the chamber fan speed settings from low to either medium or high settings.

Temperature measurements

Mean air temperature was measured with a manifold of aspirated thermocouples placed at a reference location above the canopy. The reference air temperature was measured at 20 cm above the canopy because the air at higher locations was warmed by the lamps at the top of the chamber. Ten Type-E thermocouples were placed within the manifold, through which air was aspirated at about 1-2 m s⁻¹. The thermocouples were shielded from incident radiation by plastic tubing wrapped in aluminum foil, and aspiration was provided by a household vacuum cleaner (2 hp motor).

Canopy temperature in each chamber was measured by two nadir-viewing, wide field of view, infrared transducers (Exergen ir/tc 37) positioned 10 cm above the canopy. Infrared transducer output was affected by sensor body temperature, and position above the top of the canopy. The effect of sensor body temperature was minimized by adding aluminum jackets to each infrared transducer to increase their thermal mass, and by using measurements of sensor body temperature to correct their output. The calibration procedures, field of view considerations, and the functions used to correct for sensor body temperature are described in Bugbee *et al.* (1997).

Canopy sensible heat flux

Sensible heat flux (H) quantifies energy exchange, due to conduction and convection between the canopy and the chamber air. Sensible heat flux was calculated from Equation 1:

$$H = R_{\text{net}} - LE - P \quad (1)$$

where, R_{net} = net radiation,
 LE = latent heat flux, and
 P = energy storage in photosynthesis.

The LE included water vapor fluxes due to canopy ET, and P was determined from canopy photosynthesis. This simple model allows comparison of energy fluxes in a common energy currency (W m^{-2}), and allows H to be determined by residual. However, it ignores thermal storage within the canopy.

Net radiation, evapotranspiration, and photosynthesis

Net radiation (R_{net}) was estimated from Equation 2. The fraction of incident PPF absorbed by the canopy (PPF_{abs}) was calculated from the product of radiation capture and PPF_0 (Gallo and Daughtry, 1986). PPF_{abs} measured with a quantum sensor and the fraction of absorbed, non-photosynthetic, shortwave radiation (NPSW_{abs}) was measured with a pyranometer. This approach for determining R_{net} was preferable to direct measurements with a net radiometer because there are two problems with net radiometers in controlled environments. First, most net radiometers are calibrated for field operation, where the fraction of longwave radiation is much smaller than in controlled environments. Second, the dimensions of the chambers placed the net radiometer close to the top of the foliage, where self-shading led to significant overestimates of the net radiation flux. These problems

indicated that a more accurate estimate of net radiation could be made from its components (Equation 2) than could be measured directly.

$$R_{\text{net}} = \text{PAR}_{\text{abs}} + \text{NPSW}_{\text{abs}} - \uparrow\text{Lc} + \downarrow\text{Lg} \quad (2)$$

where, PAR_{abs} = absorbed photosynthetic radiation,
 NPSW_{abs} = absorbed non-photosynthetic shortwave radiation,
 $\uparrow\text{Lc}$ = longwave radiation emitted by the canopy, and
 $\downarrow\text{Lg}$ = longwave radiation emitted by the glass filter.

The longwave radiation components ($\uparrow\text{Lc}$ and $\downarrow\text{Lg}$) were obtained from their surface temperatures and emissivities. The contributions from $\uparrow\text{Lc}$ and $\downarrow\text{Lg}$ were small, and nearly canceled each other as the surface temperatures of the glass, the canopy, and the reflective chamber walls were similar. This situation is not commonly encountered in field environments.

NPSW_{abs} depended on the spectral properties of the incident radiation, and on the canopy reflection coefficient, ρ_c . Since canopy reflection does not equal leaf reflection due to internal shading within the canopy, it was derived from a scattering coefficient (σ) using equations given by Equation 3 (Goudriaan and van Laar, 1994):

$$\rho_c = [1 - (1 - \sigma)^2] / [1 + (1 - \sigma)^2] \quad (3)$$

The scattering coefficient varied with the wavelength of the radiation, and equaled the sum of the fractions of reflected and transmitted light by a single leaf. The values of σ used were 0.2 in the visible, and 0.8 in the near-infrared. NPSW_{abs} was calculated from $(1 - \rho_c)$, thus it equaled $0.62 \cdot \text{PPF}_0$ for $\rho_c = 0.38$ and $\sigma = 0.8$ in the near-infrared.

Net radiation was varied by either changing PPF_0 with neutral density filters (window screen filters), or by removing the water filter under the lamps. The water filter under the lamps reduced the amount of longwave radiation impinging on the canopy, thereby increasing

the ratio of PAR_{abs} to R_{net} (Bubenheim *et al.*, 1988). This ratio was 83 % of R_{net} in a chamber with a water filter below the lamps, but was only 64 % of R_{net} when the water filter was removed.

Chamber ET consisted of canopy transpiration (Tr) and evaporation (E) from the hydroponic solution through the porous media (Equation 4).

$$ET = Tr + E \quad (4)$$

Initially, evaporation through the porous media separating the shoot environment from the root hydroponic environment was 10% of R_{net} in an empty chamber without plants. The planting media holder was modified by doubling the thickness of porous media through which the plants grew, and by sealing the edges of the tubs in which the media rested. These modifications reduced E to about 2% of R_{net} , which made the ET essentially equal to Tr . This ensured that the aerodynamic canopy temperature calculated from energy balance measurements was entirely due to the flux of sensible heat from the foliage to the air at the reference height above the canopy.

P represented the conversion of energy in radiation into stored chemical energy via canopy photosynthesis. P was computed from P_{net} measured using gas exchange techniques (Bugbee, 1992). Although this term is typically neglected in energy balance measurements in the field, P was included in the energy balance equation because it may represent up to 10% of R_{net} in CEs. This is because most of the longwave radiation was removed by the water filter under the lamps and PAR represents a much higher fraction of the total radiation.

Chamber aerodynamic conductance

The highly turbulent conditions within the growth chambers, due to forced convection by the fans of the heat exchanger, preclude the use of wind profile equations for the calculation of aerodynamic conductance. Instead, energy transfer in the air within the canopy was described by an analog of Ohm's Law, which relates the surface-to-air temperature difference to sensible heat loss from the surface (Equation 5; Monteith and Unsworth, 1990).

$$H = \rho C_p * g_A * (T_{\text{canopy,IR}} - T_{\text{air}}) \quad (5)$$

where, ρ = the density of air,
 C_p = the heat capacity of air,
 g_A = the chamber aerodynamic conductance, and
 $T_{\text{canopy,IR}} - T_{\text{air}}$ = the radiative canopy-air temperature difference.

The canopy surface was measured radiatively by the infrared transducers. This radiative canopy temperature ($T_{\text{canopy,IR}}$) was used to calculate the radiative canopy-air temperature difference ($\Delta T_{\text{IR}} = T_{\text{canopy,IR}} - T_{\text{air}}$). Radiative ΔT_{IR} and H were varied by changing ambient CO_2 level and PPF_0 , which should maintain the chamber g_A constant as it does not respond to changes in these factors. In this approach, the slope of a linear regression of H versus ΔT_{IR} was used to determine the chamber g_A (Smith *et al.*, 1989). This procedure assumes that the slope between H and ΔT_{IR} equals the aerodynamic canopy-to-air temperature difference ($\Delta T_A = T_{\text{canopy, H}} - T_{\text{air}}$). In this context, the chamber g_A represented the conductance of heat transfer between the leaves at the canopy temperature and the air temperature at the reference height above the canopy.

Canopy-to-air temperature difference

Normally, g_A is determined from H and ΔT_A , or from the log-wind relationship as is done in the field, but Equation 5 employs ΔT_{IR} instead, therefore, the relation between the radiative ΔT_{IR} and the aerodynamic ΔT_A was investigated. The canopy-to-air temperature difference, with respect to the air temperature at the reference height above the canopy, was measured using three separate methods.

Method 1. The radiative canopy temperature measured by the infrared transducers was used to calculate ΔT_{IR} (as previously described). The radiative ΔT_{IR} was also measured by placing the infrared transducers at several heights from the top of the canopy to characterize its response to sensor placement.

Method 2. The aerodynamic canopy-air temperature difference, ΔT_A , was computed from H and chamber g_A by rearranging Equation 5 to solve for the temperature difference. This aerodynamic ΔT_A is the canopy-air temperature difference that explains the observed sensible heat flux, and that solves the energy balance exactly.

A comparison between the canopy-air temperature differences obtained using Methods 1 and 2 was made to evaluate the effect of using the radiative versus the aerodynamic canopy temperature in the calculation of H . The Offset observed between the observed ΔT_{IR} and the calculated ΔT_A is essentially the value of ΔT_{IR} when H is zero (Equation 6). The behavior of the Offset between the radiative and aerodynamic canopy-air ΔT s was studied by varying the radiation incident on the canopy.

$$\text{Offset} = \Delta T_A + \Delta T_{IR} \quad (6)$$

Method 3. The canopy-air temperature difference was also estimated from air temperature profiles, assuming that the temperature of the air within the canopy equilibrated with the foliage temperature. This third method provided estimates of the canopy-air temperature difference at different depths within the canopy (ΔT_{Depth}). Comparisons between Method 3 versus Methods 1 and 2 were made to examine how much 'depth' of the canopy was responsible for the observed ΔT_A , and for evaluating if the radiative ΔT_{IR} integrated the temperature profile appropriately.

Canopy conductance

Surface G_C was calculated from the ratio of canopy transpiration to the canopy-air vapor pressure gradient (expressed as a mole fraction; Equation 7). The canopy-air vapor

$$G_C = \text{Tr} * 1 / [X_{\text{h20}}(T_{\text{canopy,H}}) - X_{\text{h20}}(T_{\text{air}})] \quad (7)$$

pressure gradient was determined at the aerodynamic canopy temperature ($T_{\text{canopy,H}}$) and used to compute canopy G_S from Equation 8. Surface G_C and canopy G_S were also calculated using

$$G_S = G_C * g_A / (g_A - G_C) = ((1/G_C) - (1/g_A))^{-1} \quad (8)$$

the radiative canopy temperature to evaluate the error incurred in substituting radiative with aerodynamic canopy temperature.

Chamber coupling coefficient

Canopy transpiration depends on the magnitude of the boundary layer surrounding the canopy. At low boundary layer conductances, the canopy transpiration rate operates at the equilibrium transpiration rate ($T_{\text{eq}} = s/(s+\gamma)*(R_n - G)$), where G is the soil heat flux

(assumed negligible in our chamber), s is the ratio of the slope of the relation between saturation vapor pressure and temperature, and γ is the psychrometric constant. Conversely, the transpiration rate in large boundary layers is proportional to the product of stomatal conductance and the vapor pressure deficit, D_s , imposed at the leaf surface ($T_{imp} = \rho C_p / \gamma * G_c * D_s$). This relation, which depends on the degree of coupling between the environmental conditions at the surface and the airstream above the canopy, was described in terms of a decoupling coefficient, Ω (Equation 9; Jarvis and McNaughton, 1986).

$$T_r = \Omega * T_{eq} + (1 - \Omega) * T_{imp} \quad (9)$$

Ω is a dimensionless factor that assumes values between 0 and 1, depending on the magnitudes of the chamber g_A and canopy G_s (Equation 10).

$$\Omega = (\epsilon + 1) / [\epsilon + (g_A / G_s)] \quad (10)$$

Ω was computed from chamber g_A , canopy G_s , and the ratio of the increase of latent heat content to the increase of sensible heat content of saturated air, $\epsilon (= s/\gamma)$ (Jones, 1992).

Results

Wind speed

The average wind speed profiles above and within wheat and soybean canopies were measured at various stages of the life cycle (Fig. 2.1). Chamber air was recirculated by forced convection resulting in considerable spatial variability in the wind speed profile. The wind speed at any given plane above the canopy was highly variable in time, typically ranging from 0.5 to 2.4 m s⁻¹ in wheat (Fig. 2.1A), and from 0.4 to 1.4 m s⁻¹ in soybean (Fig. 2.1B). Wind speed within the canopies was more uniform and lower in the uppermost layers of foliage.

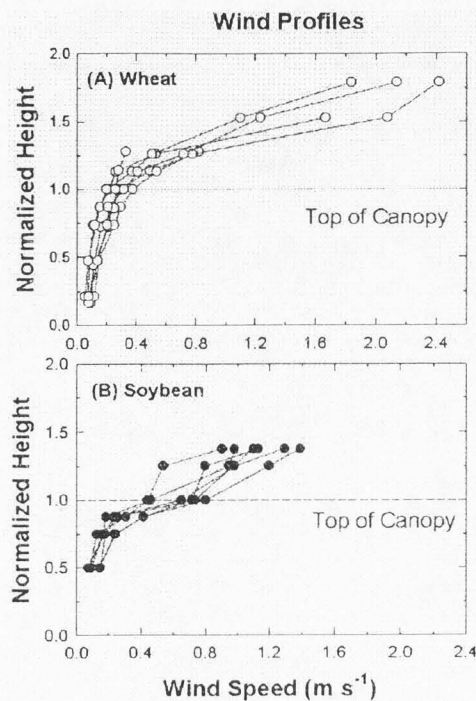


Figure 2.1 Wind speed profiles of (A) wheat and (B) soybean canopies measured at several stages of the life cycle. The canopy heights are normalized to the canopy height, which changed during the course of the life cycles.

Chamber temperature profiles

The vertical air temperature profile within the growth chamber, measured with the manifold of aspirated thermocouples, was also spatially variable. These large air temperature gradients within the canopies in the chamber were probably due to vertical differences in transpiration rates, and due to turbulent mixing above the canopy surface (Fig. 2.2). The vertical air temperature profiles were homogenous in an empty, dark chamber (data not shown) since there was no foliage to trap pockets of air, and because the surfaces within the chamber (glass and chamber walls, and the surface of the growth media) equilibrated at nearly the same temperature. The vertical temperature profiles above and within a 20-day-old wheat canopy varied the most during the photoperiod (Fig. 2.2), as heat from the lamps warmed the

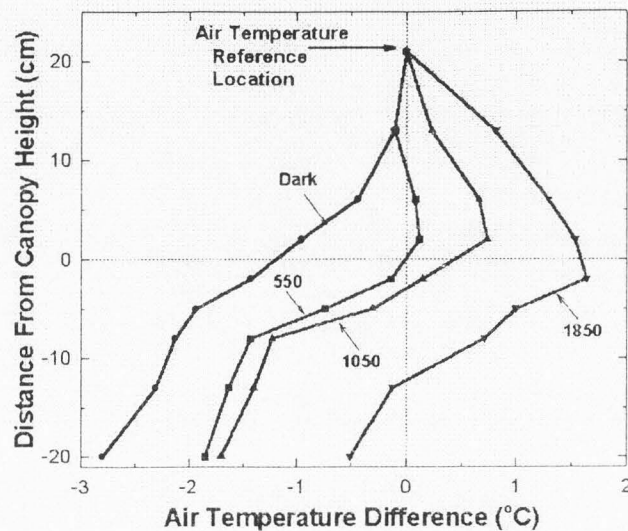


Figure 2.2 The effect of incident PPFD on the air temperature profiles above and within a wheat canopy. The top of the canopy was warmer as most of the incident radiation was absorbed by the top layers of foliage during the photoperiod, and cooler in the dark. The canopy was warmer than the reference air temperature only at incident light levels greater than $600 \mu\text{mol m}^{-2} \text{s}^{-1}$.

foliage within the chamber. In the light, the uppermost leaves of the canopy absorbed most of the incoming radiation and became warmer than the lower leaves. At night, the entire canopy was cooler than air temperature due to evaporative cooling and the uppermost leaves were warmer than the lower leaves because they received sensible heat from the air above the canopy. Air temperature within the canopy could differ by $1\text{--}5^\circ\text{C}$ from the reference air temperature above the canopy depending on the magnitude of the latent heat flux. These temperature differences increased as the net radiation incident on the canopy increased, but were positive only when PPFD was greater than $550 \mu\text{mol m}^{-2} \text{s}^{-1}$ (Fig. 2.2).

The manual wind speed setting in the chamber also affected the temperature profiles within the canopy because this regulated fan speed and, therefore, the amount of forced

convection in the chamber. However, the largest temperature difference with respect to the reference air temperature above the canopy, was observed at the low wind setting compared to either the medium or high settings (Fig. 2.3). This suggests that there is a threshold in turbulence above which an increase in wind speed does not continue to affect canopy-air heat exchange.

Energy balance components

Canopy energy balance was predominantly influenced by R_{net} , LE, and H in both wheat (Fig. 2.4A) and soybean (Fig. 2.4B) canopies. The effect of P on the energy balance was small, but reached 7-10% at high PPF. In wheat, H was more negative (the vegetation became cooler) whenever LE exceeded net radiation. The soybean canopy remained cooler than the air temperature because LE was always greater than the net radiation. Canopy temperature increased during the photoperiod and H increased correspondingly as the canopy warmed. The increase in canopy temperature was brought about by a diurnal decrease in stomatal conductance. In the dark, the canopy was always cooler than air temperature because R_{net} was negligible and 'dark' transpiration rate remained high.

The energy balance components of two soybean canopies of the same age varied when the water filter under the HPS lamps was removed (Fig. 2.5). When the water filter was removed (Fig. 2.5A), R_{net} increased but PPF_0 remained the same, as this reduced the ratio of photosynthetic to non-photosynthetic shortwave radiation from 83:17 to 66:34. The increased net radiation only affected H. The higher longwave radiation resulted in warmer leaves during the photoperiod, which is reflected in the higher H. In the canopy with the water filter,

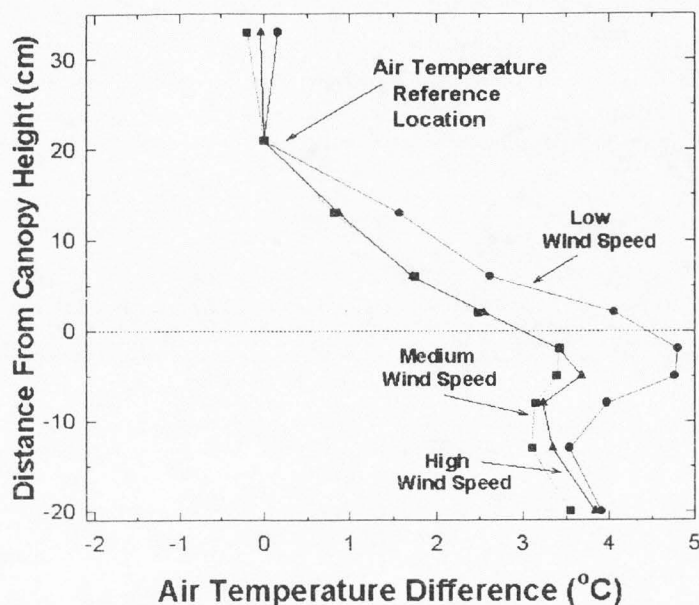


Figure 2.3 Air temperature profiles above and within a wheat canopy. The air temperature profile was measured with a manifold of shielded, aspirated thermocouples at different wind speed settings. The profile is expressed as the difference between air temperature within the canopy and air temperature measured at the reference height located 20 cm above the canopy.

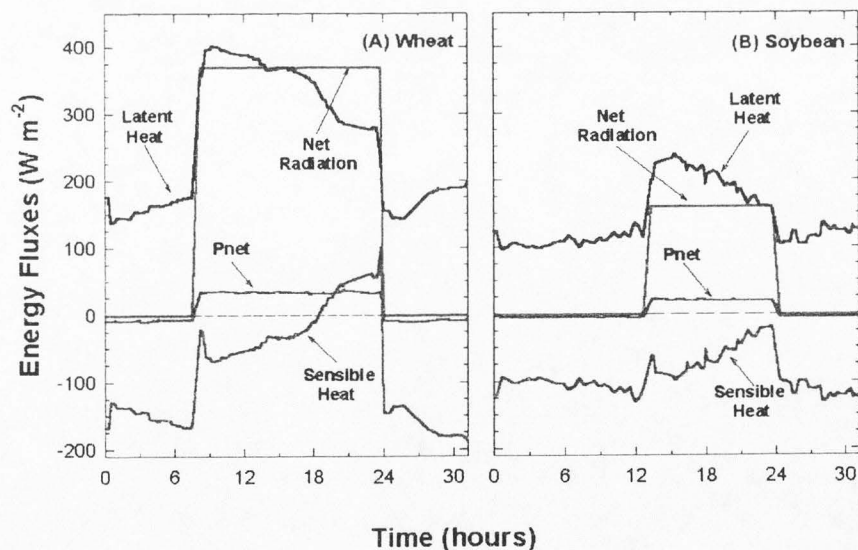


Figure 2.4 Diurnal course of canopy energy balance components: net radiation, latent heat flux, sensible heat flux, and photosynthesis in (A) wheat and (B) soybean. Sensible heat flux was calculated from direct measurements of the other three components.

photosynthesis and LE were unchanged since PPF_o remained constant, but the reduced longwave radiation resulted in cooler leaves and caused a small decrease in H during the photoperiod (Fig. 2.5B). In the dark, the energy balance components were similar in both canopies.

Chamber aerodynamic conductance

The chamber g_A , calculated from the slope of H versus radiative ΔT_{IR} , was $5.5 \text{ mol m}^{-2} \text{ s}^{-1}$ in wheat and $2.5 \text{ mol m}^{-2} \text{ s}^{-1}$ in soybean, which correspond to aerodynamic resistances of 7.5 s m^{-1} and 16.5 s m^{-1} , respectively. As expected, the chamber g_A did not respond to changes in ambient CO_2 (wheat, Fig 2.6) since the slopes of H versus ΔT_{IR} at each CO_2 concentration were the same (separate regressions not shown). The dashed line represents the plot of H versus ΔT_A , which was determined by adding a constant Offset to ΔT_{IR} (Equation 6). This Offset was about 0.7°C and equals the value of ΔT_{IR} when H is zero. The chamber g_A was subsequently used for calculating ΔT_A from H, and for computing canopy G_s from the surface G_c .

Canopy-to-air temperature difference

The radiative ΔT_{IR} (Method 1) was influenced by PPF_o and by wind speed (Fig. 2.7). As PPF increased from dark to $1500 \mu\text{mol m}^{-2} \text{ s}^{-1}$, ΔT_{IR} increased linearly from 0°C to $+4^\circ\text{C}$ at low wind speed (Fig. 2.7A, top), and increased from -1°C to $+2^\circ\text{C}$ at the high wind speed setting (Fig. 2.7B, top). The Offset correction required to make the radiative ΔT_{IR} equal the aerodynamic ΔT_A did not vary with wind speed (Fig. 2.7, bottom graphs). At constant PPF,

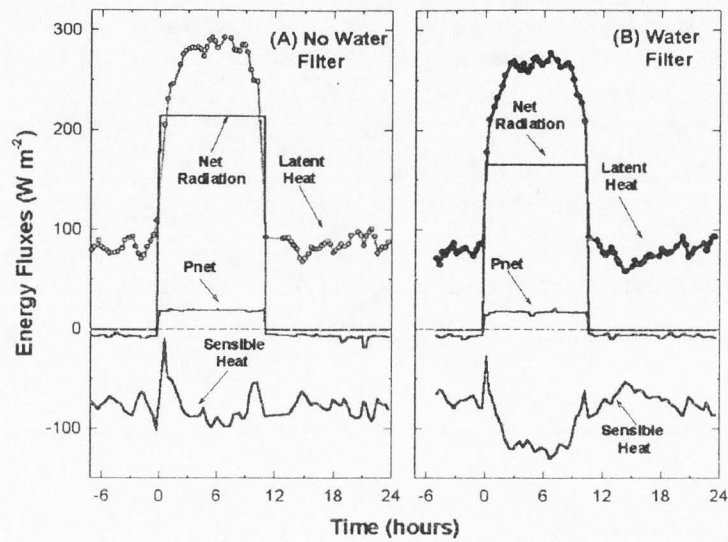


Figure 2.5 The energy balance fluxes of soybean canopies of the same age, affected by the (A) absence and (B) presence of a water filter under the HPS lamps.

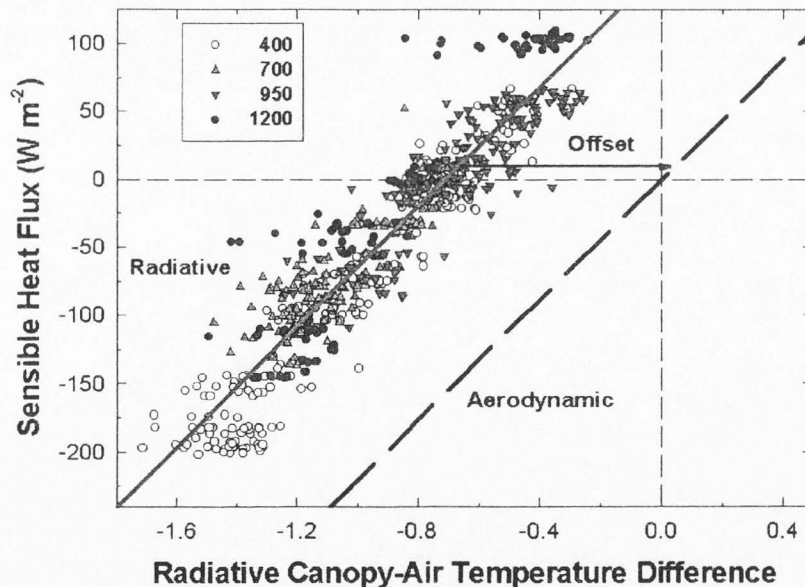


Figure 2.6 The regression of sensible heat flux versus the radiative canopy-to-air temperature (solid line). The slope of the line is proportional to the aerodynamic conductance for heat transfer between the foliage and the air at the reference height above the canopy. The dashed line denotes the corresponding relation between sensible heat flux and the aerodynamic canopy-air temperature difference. A constant Offset (Eqn. 5) was needed to make the radiative canopy-to-air temperature difference equal the aerodynamic temperature difference. The offset equals 0.75°C for this wheat canopy. The CO_2 concentrations used were 400, 700, 950, and $1200 \mu\text{mol mol}^{-1}$.

the radiative ΔT_{IR} decreased as ambient CO_2 increased from 400 to 1200 $\mu\text{mol mol}^{-1}$ (Fig. 2.6) because stomatal conductance declined, which resulted in less evaporative cooling, and the canopy became warmer. Although the aerodynamic ΔT_{A} (Method 2) also increased linearly with increasing PPF_0 (Figs. 2.7A, B), it had a steeper slope than the ΔT_{IR} increase (e.g. from -3°C to $+4^\circ\text{C}$ at the low wind setting; Fig. 2.7A). The radiative ΔT_{IR} , measured as a function of the height at which the infrared transducers were positioned above or within the canopy, also increased in a linear fashion with increasing PPF_0 (Fig. 2.8), but with a smaller slope.

There was also a linear relation between ΔT_{Depth} (Method 3) and PPF_0 (Fig. 2.9). The contributions from each layer of foliage (thin solid lines) to the average ΔT_{Depth} were simulated by successively including deeper layers in the average (dashed lines; Fig. 2.9).

Method 1 versus method 2. The radiative ΔT_{IR} did not equal zero when H was zero (Fig. 2.6), and was often opposite in sign to the aerodynamic ΔT_{A} (Figs. 2.10A, B, bottom). This means that ΔT_{IR} cannot be used to determine H. In fact, H predicted from ΔT_{IR} often has an opposite sign to H (Fig. 2.10, top) determined from the energy balance equation (Equation 1). However, relative changes in the magnitude of ΔT_{IR} as a function of time paralleled the relative changes in H during the day, suggesting that there was a consistent difference between ΔT_{IR} and ΔT_{A} (Fig. 2.10). This constant difference, or Offset, supports the validity of Equation 5. Although the Offset remained constant at all CO_2 concentrations, it was linearly dependent on PPF_0 (Fig. 2.7, bottom graphs). In wheat grown at a light level of 1600 $\mu\text{mol m}^{-2} \text{s}^{-1}$, an Offset equal to $+0.7^\circ\text{C}$ was required to make ΔT_{IR} equal ΔT_{A} when

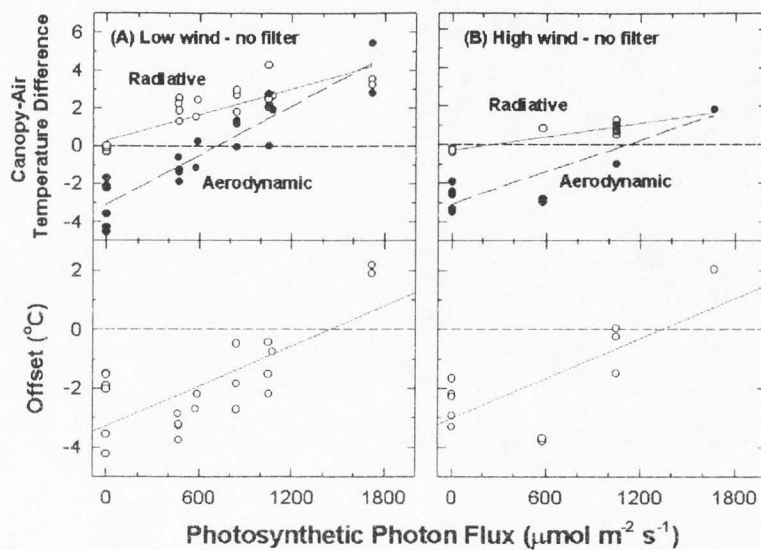


Figure 2.7 The radiative ΔT_{IR} (Method 1) and the aerodynamic ΔT_{A} (Method 2) were influenced by PPF_0 and by wind speed. As PPF_0 increased from dark to $1500 \text{ mol m}^{-2} \text{ s}^{-1}$, ΔT_{IR} increased linearly from 0°C to $+4^\circ\text{C}$ at low wind speed (A, top), and increased from -1°C to $+2^\circ\text{C}$ at the high wind speed setting (B, top). The Offset correction required to make the radiative ΔT_{IR} equal the aerodynamic ΔT_{A} did not vary with wind speed (A and B, bottom graphs).

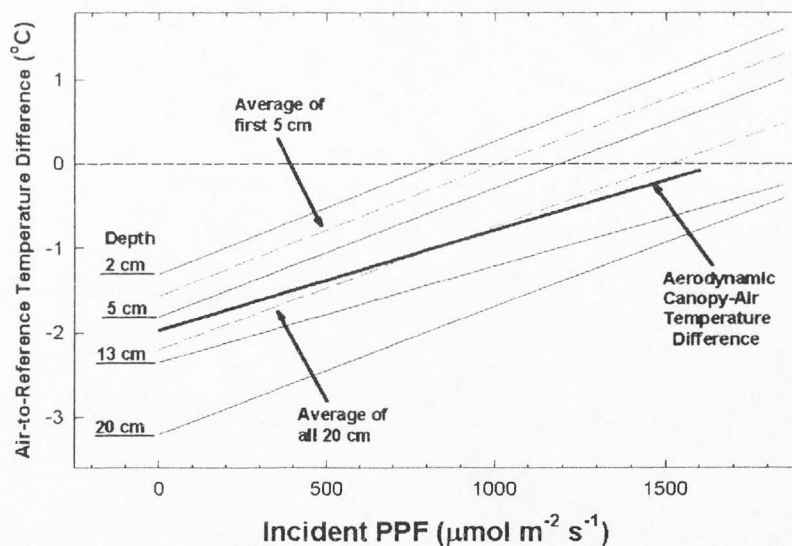


Figure 2.8 The radiative ΔT_{IR} , measured as a function of the height at which the infrared transducers were positioned above or within the canopy, also increased in a linear fashion with increasing PPF_0 , but with a smaller slope than the corresponding aerodynamic ΔT_{A} .

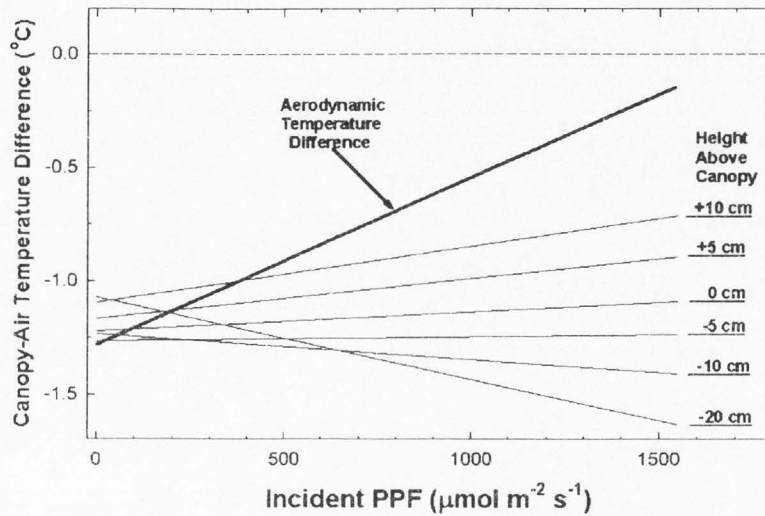


Figure 2.9 The ΔT_{Height} determined by Method 3 as a function of PPF_0 . The average ΔT_{Height} (dashed lines) mimicked the behavior of the aerodynamic ΔT_A (dark solid line) (both relations had nearly equal slopes). However, this comparison suggests that the entire canopy height contributed to the observed aerodynamic ΔT_A . The entire profile (down to 20 cm below the top of the canopy) had to be averaged in order to match the measured dependence of ΔT_A on PPF_0 .

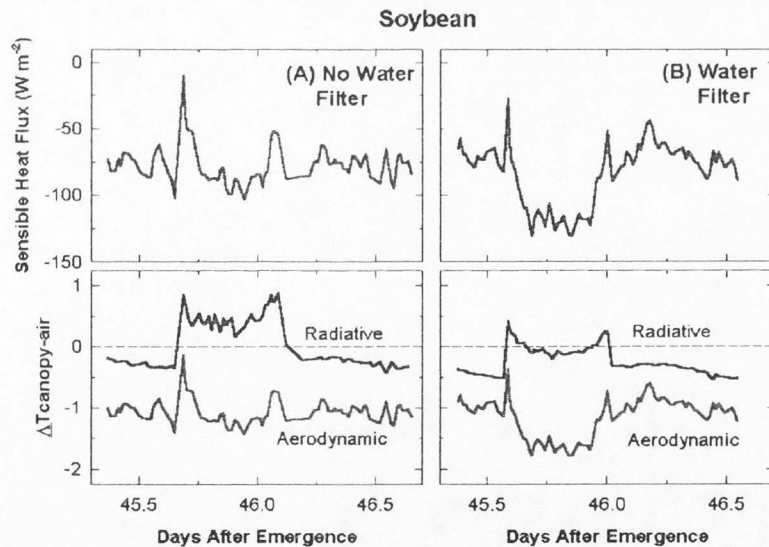


Figure 2.10 Sensible heat flux and the canopy-to-air temperature differences as a function of time of day, corresponding to the energy fluxes in Figure 2.5. Radiative canopy-air temperature difference (ΔT_{IR}) was always greater than the aerodynamic canopy-air temperature difference (ΔT_A), but the difference was a constant offset. Canopy-air temperature difference increased during the photoperiod, as it began to warm up and sensible heat increased correspondingly. The radiative ΔT_{IR} was positive during the photoperiod, when sensible heat flux determined from energy balance measurements was negative.

H was zero (Fig. 2.6).

Method 3 versus methods 1 and 2. Generally, the average ΔT_{Height} (dashed lines; Fig. 2.9) mimicked the behavior of the aerodynamic ΔT_A (dark solid line; Fig. 2.9) as a function of PPF_o (both relations had nearly equal slopes). However, this comparison suggests that the entire canopy height contributed to the observed aerodynamic ΔT_A . The entire profile (down to 20 cm below the top of the canopy) had to be averaged in order to match the measured dependence of ΔT_A on PPF_o . On the other hand, the dependence of the radiative ΔT_{IR} on PPF_o had a much smaller slope than either ΔT_A (thin lines versus solid line; Fig. 2.8) or ΔT_{Height} (dashed lines; Fig. 2.9). The observed ΔT_{IR} was consistently smaller than the values of ΔT_A and ΔT_{Height} in the dark, but it was closer to them at mid-values of PPF, and approached them only at the higher PPFs (Fig. 2.7, top graphs).

Canopy conductance

In wheat in a chamber with $g_A = 5.5 \text{ mol m}^{-2} \text{ s}^{-1}$, the average surface G_C calculated from transpiration measurements (Equation 6) using the radiative ΔT_{IR} , was $1.58 \text{ mol m}^{-2} \text{ s}^{-1}$ (solid line), while the surface G_C determined from the aerodynamic ΔT_A was $1.49 \text{ mol m}^{-2} \text{ s}^{-1}$ (dashed line; Fig. 2.11A). Thus, neglecting to correct for the Offset between ΔT_{IR} and ΔT_A resulted in only a 6.1% underestimation in the surface G_C . The average radiative and aerodynamic values of canopy G_S , calculated using a g_A of $5.5 \text{ mol m}^{-2} \text{ s}^{-1}$ and the corresponding surface G_C , were $2.27 \text{ mol m}^{-2} \text{ s}^{-1}$ (0.057 m s^{-1}) and $2.08 \text{ mol m}^{-2} \text{ s}^{-1}$ (0.053 m s^{-1}) (Equation 8; Fig. 2.11B), respectively. Computing the canopy G_S radiatively (ie. using the observed ΔT_{IR}) differs from G_S determined aerodynamically by only 8.4%. The error incurred

if the surface G_C was assumed to equal the canopy G_S , that is, without taking the chamber g_A into account was large (-40%) (Fig. 2.11A versus 2.11B). Furthermore, assuming literature values of g_A corresponding to less turbulent field conditions (e.g., Luchiarri and Riha, 1991; $g_A = 2 \text{ mol m}^{-2} \text{ s}^{-1}$) resulted in a 32.5% underestimation of the canopy G_C (Fig. 2.11A).

In soybean (data from Fig. 2.5), the radiative G_C was $0.56 \text{ mol m}^{-2} \text{ s}^{-1}$ and the aerodynamic surface G_C was $0.75 \text{ mol m}^{-2} \text{ s}^{-1}$ (data not shown). In contrast to wheat, neglecting to correct for the Offset between the radiative ΔT_{IR} and the aerodynamic ΔT_A caused a larger (33.7%) underestimation of the surface G_C . The average radiative and aerodynamic values of canopy G_S (using a chamber g_A of $2.5 \text{ mol m}^{-2} \text{ s}^{-1}$) were $0.73 \text{ mol m}^{-2} \text{ s}^{-1}$ and $1.08 \text{ mol m}^{-2} \text{ s}^{-1}$, respectively. This represents a difference of 49.2%. The error in canopy G_S , computed assuming that the surface G_C equaled the canopy G_S , was of similar magnitude to that found wheat (-45.2%), but the error in canopy G_S calculated with literature values of g_A was only 6.9%.

Chamber coupling coefficient

The canopy decoupling coefficient (Ω , Equation 10; Figs. 2.12A, B) was 0.2 in the dark in both wheat and soybean (Figs. 2.12A, B). During the photoperiod, Ω increased to near 0.7 at $400 \mu\text{mol mol}^{-1} \text{ CO}_2$ in both wheat and soybean canopies, but Ω was only 0.3-0.4 at $1200 \mu\text{mol mol}^{-1} \text{ CO}_2$. There was a diurnal fluctuation in Ω caused by a corresponding fluctuation in canopy G_S , assuming g_A remained constant throughout the course of the photoperiod. The chamber coupling coefficient, $(1-\Omega)$, at $400 \mu\text{mol mol}^{-1} \text{ CO}_2$ for wheat and soybean is plotted as a function of canopy G_S (using the data in Fig. 2.12). The coupling

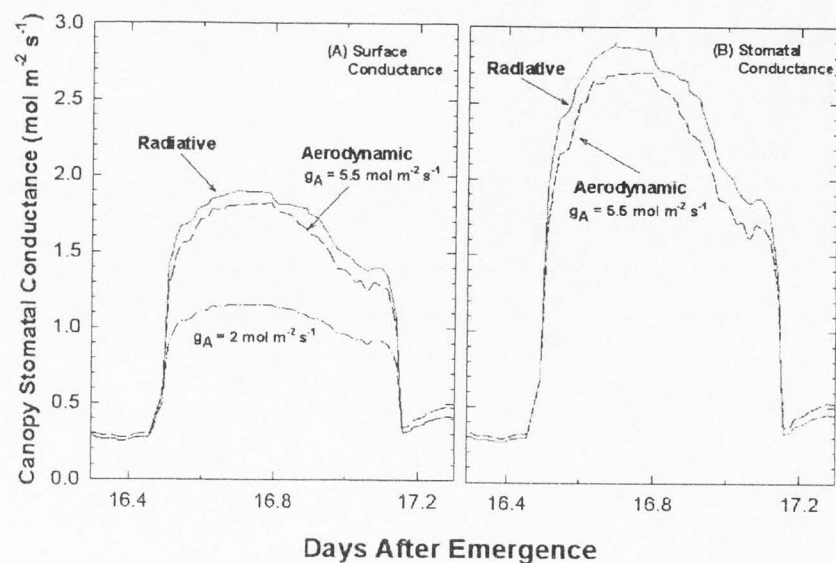


Figure 2.11 Daily courses of (A) canopy surface stomatal conductance (G_c) and (B) canopy stomatal conductance (G_s) for a mature wheat canopy grown at a PPF of $1600 \mu\text{mol m}^{-2} \text{s}^{-1}$. The conductances were calculated using radiative (solid lines) and aerodynamic (dashed lines) canopy-air temperature differences.

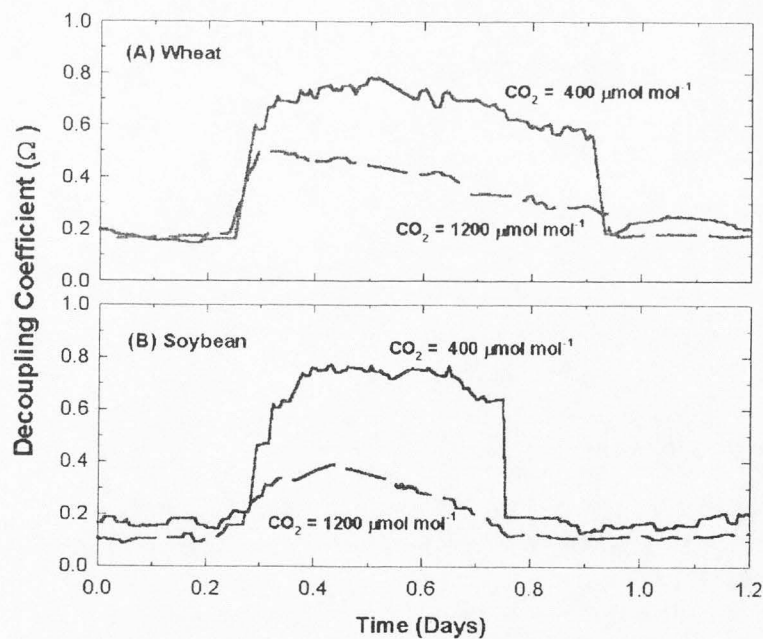


Figure 2.12 Diurnal course of the decoupling coefficient in (A) wheat and (B) soybean. The decoupling coefficient, Ω , was 0.2 in the dark, and increased to near 0.8 at $400 \mu\text{mol mol}^{-1}$ CO_2 during the photoperiod, but Ω was only 0.3-0.4 at $1200 \mu\text{mol mol}^{-1}$ CO_2 .

coefficient decreased nonlinearly as canopy G_s increased during the course of the photoperiod (symbols), and decreased as the chamber g_A became smaller (solid lines; Fig. 2.13). There was less coupling in the soybean canopies because they had a smaller g_A than the wheat canopies.

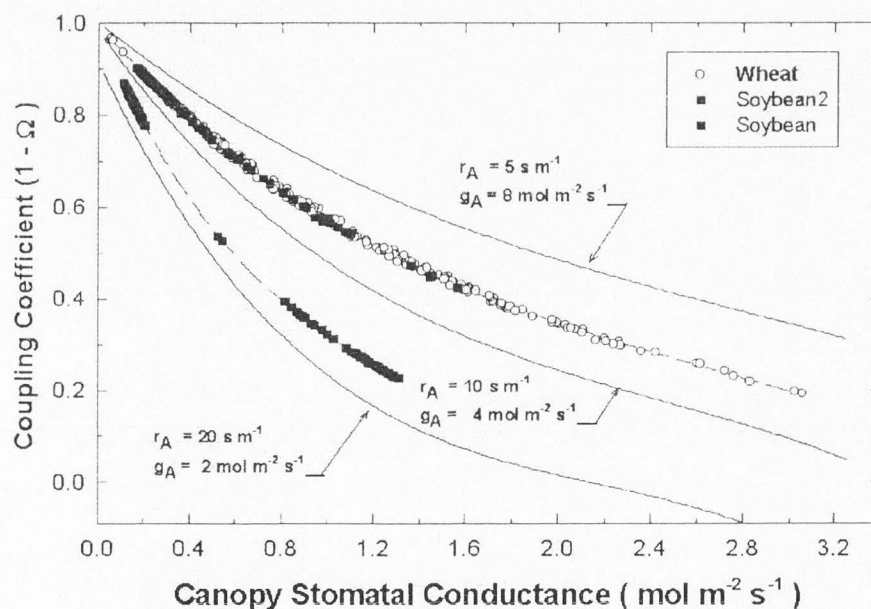


Figure 2.13 The coupling coefficient, $(1-\Omega)$, as a function of canopy G_s in wheat (open symbol) and soybean (closed symbol) canopies measured at $400 \mu\text{mol mol}^{-1} \text{CO}_2$. The coupling coefficient decreased as canopy G_s increased during the photoperiod. The solid lines represent simulated coupling coefficients for increasing chamber aerodynamic conductance (g_A). These were calculated for g_A of 2, 4, and $8 \text{ mol m}^{-2} \text{ s}^{-1}$.

Discussion

The goals of the current research were to compute canopy G_s from direct measurements of 'bulk' or surface G_c , to explore the relation between the radiative ΔT_{IR} and the aerodynamic ΔT_A in controlled environments, and to quantify the degree of coupling between transpiration and canopy G_s in controlled environments.

The difficulty in accomplishing the first of these goals lies in determining the chamber g_A , which cannot be obtained aerodynamically from wind profile measurements, as is typically done in the field. Instead, we used an empirical approach to determine chamber g_A from the relationship between sensible heat fluxes and the associated canopy-air temperatures. The canopy G_s for wheat at $400 \mu\text{mol mol}^{-1} \text{CO}_2$ ($2.08 \text{ mol m}^{-2} \text{s}^{-1}$) in this study is similar to field canopy G_s values ($1.82 \text{ mol m}^{-2} \text{s}^{-1}$ or 22 s m^{-1}) reported by Hatfield (1985) at sea level, under optimal available soil water. Our canopy G_s values are expected to be higher because they were measured at an elevation of 4800 ft and a lower barometric pressure (86 kPa; Daunicht and Brinkhans, 1992). Soybean canopy G_s was $1.08 \text{ mol m}^{-2} \text{s}^{-1}$, nearly one-half the values found in wheat probably due to less leaf area and because they were measured at a lower PPF. Soybean canopy G_s was also slightly higher than typical conductances measured in field crops (O'Toole and Real, 1986). These results suggest that the approach developed in this study, for estimating canopy G_s from surface G_c measurements in controlled environments, yields values of similar magnitude to conductances reported in field studies.

The need for accurate estimates of g_A is apparent from an examination of the large (>40%) errors in canopy G_s incurred when surface G_c was assumed to equal canopy G_s . The

magnitude of these errors is important because this causes corresponding errors in transpiration rates calculated from these conductances. Thus, neglecting g_A results in greater errors in transpiration than the errors in g_A caused by the difference between the radiative and aerodynamic canopy-air temperature differences. The chamber g_A for wheat ($5.5 \text{ mol m}^{-2} \text{ s}^{-1}$ or 0.14 m s^{-1}) and for soybean ($2.5 \text{ mol m}^{-2} \text{ s}^{-1}$ or 0.06 m s^{-1}) canopies fall near the range of typical values of aerodynamic conductances of field crops (ranging from $3.2\text{-}10 \text{ mol m}^{-2} \text{ s}^{-1}$ or $0.08\text{-}0.25 \text{ m s}^{-1}$; O'Toole and Real, 1986).

The second goal of this study was accomplished by measuring the canopy-air temperature difference using 3 separate methods. The radiative ΔT_{IR} was found to differ from the aerodynamic ΔT_A by a constant Offset. These findings are similar to previous studies conducted in the field (Huband and Monteith, 1986; Smith *et al.*, 1989; Baldocchi *et al.*, 1991). However, the Offset was typically less than 1°C , it was affected by PPF_o , and was not dependent on the amount of forced convection in the chamber. The effect of PPF_o on canopy-air temperature calculated from radiative and aerodynamic canopy temperature measurements, was also compared against direct measurements of air temperature profiles within the canopy (Figs. 2.2 and 2.9). Although this comparison rests on the assumption that the foliage temperature is in equilibrium with the air temperature within the canopy, it allowed us to diagnose what factors may be contributing to the disparity between radiative and aerodynamic canopy temperatures. The slope of aerodynamic ΔT_A versus incident PPF matched the relation obtained with the aspirated thermocouple manifold (ΔT_{Height}); however, the aerodynamic ΔT_A could be predicted only when all the leaf layers were averaged down to a

depth of 20 cm.

These comparisons suggest that the aerodynamic ΔT_A is controlled by the energy balance of all the leaf layers of the wheat canopy, and that the main difference between the radiative and the aerodynamic canopy temperatures exists because the radiative temperature measures temperature mostly from the uppermost leaf layers. This finding is corroborated by measurements of radiative canopy temperatures in the dark, suggesting that the infrared transducers are seeing mostly the upper, warmer leaf layers. Thus, although infrared transducer output is weighted towards the center of their field of view where they would 'see' deeper into the canopy, they are probably not seeing enough depth to accurately represent the true canopy temperature profile. Furthermore, the canopy temperature profile viewed by the transducers also varies with the incident PPF, which would explain why the offset correction also depends on incident PPF.

The third goal of this study was to determine the chamber coupling coefficient because it indicates how applicable measurements of canopy G_s obtained in our system may be in other systems, such as field conditions or other chambers. The results obtained in our chambers are deemed valid in field situations because the coupling coefficients are similar to those measured in the field (Jarvis and McNaughton, 1986). Having similar coupling coefficients between chamber and field implies that feedback between transpiration and the environment around the leaves operates at the same degree in both environments. Our observations are in sharp contrast to studies in glasshouses where poor ventilation results in much smaller aerodynamic conductances than would typically be found in field conditions.

The decoupling coefficients, Ω , of wheat and soybean observed in this study suggest that feedback between stomatal conductances and the saturation deficit within the canopy is taking place in our chambers, and that the amount of feedback is reduced in elevated CO_2 (Fig. 2.12). We found that the coupling coefficient was larger as g_A increased (Fig. 2.13). The coupling coefficient in soybean was lower than in wheat, probably because the lower wind speeds above the canopy (Fig. 2.1) resulted in a smaller chamber g_A for soybean. The coupling for the soybean canopy approaches coupling values typically observed in field studies, where small changes in G_S have little effect on canopy transpiration, and transpiration is dominated by net radiation (Meinzer and Grant, 1989).

References

- Baldocchi DD, Luxmoore RJ, Hatfield JL.** 1991. Discerning the forest from the trees: an essay on scaling canopy stomatal conductance. *Agricultural and Forest Meteorol.* **54**:197-226.
- Bubenheim DL, Bugbee B, Salisbury FB.** 1988. Radiation in controlled environments: Influence of lamp type and filter material. *J. Amer. Soc. Hort. Sci.* **113**, 468-474.
- Bugbee B.** 1992. Steady state gas exchange in growth chambers: system design and operation. *HortScience* **27**, 770-776.
- Bugbee B, Droter M, Monje O, Tanner B.** 1997. Evaluation and modification of commercial infrared transducers for leaf temperature measurement. *Adv. In Space Res.* (In press).
- Bugbee B, Monje O., Tanner B.** 1996. Quantifying energy and mass transfer in crop canopies. *Advances in Space Research* **18**, 149-156.
- Daunicht HJ, Brinkhans HJ.** 1992. Gas exchange and growth of plants under reduced air pressure. *Adv. Space Res.* **12**, 107-114.

Gallo KP, Daughtry CS. 1986. Techniques for measuring intercepted and absorbed photosynthetically active radiation in corn canopies. *Agronomy Journal* **78**, 752-756.

Goudriaan J, van Laar HH. 1994. *Modeling potential crop growth processes: textbook with exercises* Boston: Kluwer Academic Publishers.

Hatfield JL. 1985. Wheat canopy resistance determined by energy balance techniques. *Agronomy Journal* **77**, 279-283.

Huband NDS, Monteith JL. 1986. Radiative surface temperature and energy balance of a wheat canopy. I. Comparison of radiative and aerodynamic temperature. *Boundary-Layer Meteorology* **36**, 1-17.

Jarvis PG. 1976. The interpretation of the variations in leaf water potential and stomatal conductance found in canopies in the field. *Phil. Trans. R. Soc. Lond. B.* **273**, 593-610.

Jarvis PG, McNaughton KG. 1986. Stomatal control of transpiration: Scaling up from leaf to region. *Advances in Ecological Research* **15**, 1-49.

Jones HG. 1992. *Plants and microclimate: a quantitative approach to environmental plant physiology*. New York: Cambridge University Press.

Kimes DS. 1983. Remote sensing of row crop structure and component temperatures using directional radiometric temperatures and inversion techniques. *Remote Sensing Environ.* **13**, 33-55.

Luchiari A, Riha SJ. 1991. Bulk surface conductance and its effect on evapotranspiration rates in irrigated wheat. *Agronomy Journal* **83**, 888-895.

Meinzer FC, Grant DA. 1989. Stomatal control of transpiration from a developing sugarcane canopy. *Plant, Cell, and Environment* **12**, 635-642.

Monteith JL, Unsworth MH. 1990. *Principles of environmental physics* New York: Chapman and Hall, Inc.

O'Toole JC, Real JG. 1986. Estimation of aerodynamic and crop resistances from canopy temperature. *Agronomy J.* **78**, 305-310.

Smith RCG, Barrs HD, Meyer WS. 1989. Evaporation from irrigated wheat estimated using radiative surface temperature: an operational approach. *Agricultural and Forest Meteorology* **48**, 331-344.

CHAPTER 3
FACTORS CONTROLLING DIURNAL CHANGES IN
CANOPY STOMATAL CONDUCTANCE

Abstract

The diurnal course of canopy stomatal conductance often decreases towards the end of the photoperiod, even under constant environmental conditions. This reduction in stomatal conductance has been observed at both the leaf and canopy scales, and in both natural and controlled environments, but its causes remained unexplained. In canopies, the shape and magnitude of these diurnal reductions are strongly influenced by elevated CO₂ concentration. As expected, increasing ambient CO₂ concentration at constant photosynthetic photon flux decreased the maximum stomatal conductance, but it also increased the magnitude of the diurnal reductions. These results could not be explained by diurnal fluctuations in leaf water potentials because CO₂ enrichment results in diminished transpiration rates. The results of this study present indirect evidence that supports the hypothesis that sugar accumulation in guard cell walls is major a controlling mechanism of stomatal aperture at the canopy level.

Introduction

In natural ecosystems, the diurnal course of leaf stomatal conductance (g) has been described by three phases during the photoperiod, where g is controlled by a different predominant factor in each phase (Körner, 1995). In the early morning, g responds to increasing PPF until the potential stomatal conductance is reached. The response to vapor

pressure difference (VPD) then takes over and limits further increases in transpiration until the late afternoon. Körner refers to the last phase, which begins prior to the onset of decreased PPF, as being caused by 'unexplained time-dependent reductions in stomatal conductance relative to morning values'. This effect often results large reductions (~20%) in afternoon g compared to morning values under equal climatic conditions. Similar time-dependent reductions in canopy stomatal conductance (G_s) have also been observed in canopies grown hydroponically under constant environmental conditions (Monje and Bugbee, 1996). Diurnal reductions in G_s lead to declining transpiration rates, which affect crop energy balance and result in increased canopy temperatures. The causes for these diurnal fluctuations in stomatal conductance are undoubtedly related to factors controlling stomatal aperture, however, the exact mechanisms by which this control is exerted have remained elusive (Monteith, 1995; Dewar, 1995).

Previous studies of the mechanisms controlling stomatal aperture at the leaf level have centered mostly on the carbon metabolism associated with K^+ fluxes, since increased guard-cell K^+ has been observed during stomatal opening (Outlaw, 1983). However, recent studies have found that stomata respond to the rate of transpiration rather than to humidity (Mott and Parkhurst, 1991; Dewar, 1995; Monteith, 1995).

The control of stomatal opening has been attributed to moisture availability at higher scales of organization. At regional and ecosystem scales, direct responses of stomata to VPD, as well as responses to rhizosphere moisture depletion via root signaling, have been studied extensively because of their impact on community water relations (Grantz and Meinzer, 1990;

Jones, 1992). The concept of a critical water potential has been used to study the diurnal courses of transpiration of plant canopies growing in field situations under water stress (Olioso *et al.*, 1996), as well as in models of stomatal conductance that account for responses to leaf water potential (Ψ_{leaf}) (Nikolov *et al.*, 1995). When the leaf water status reaches a threshold or 'critical' value of leaf water potential (Ψ_c), the stomatal conductance decreases rapidly in response to drying conditions. Although diurnal changes in Ψ_{leaf} may not be a significant mechanism for controlling stomatal aperture under natural conditions (Tenhunen *et al.*, 1987; Körner, 1995), they may play a major role in controlling stomatal conductance in agricultural situations. Lynn and Carlson (1990) explained control of stomatal conductance in corn as being mediated by Ψ_{leaf} , which was itself determined by environmental factors such as solar flux, VPD, soil water potential (Ψ_{soil}), and root-stem resistance.

In contrast, recent histological studies by Lu *et al.* (1997) support the involvement of sucrose accumulation in the apoplast near guard cell walls as the sensing mechanism for regulating stomatal aperture in response to transpiration. When sucrose efflux from mesophyll cells exceeds the translocation rate, it is transported to the guard cells resulting in reduced stomatal apertures and thus lower stomatal conductance. They hypothesized that sucrose accumulation in the guard cell walls may be responsible, in part, for regulating stomatal aperture *in planta*.

In view of the recent literature, it appears that two possible hypotheses may explain the observed diurnal reductions in stomatal conductance: 1) the first hypothesis suggests that canopy stomatal conductance responds to changes in leaf and stem water potential; 2) the

second hypothesis suggests that stomatal aperture is reduced as sugars carried in the transpiration stream accumulate in guard cell walls in sufficient amounts to elicit stomatal closure. This study explored stomatal responses of plant communities to elevated CO₂ to help explain the time-dependent reductions in stomatal conductance. We reasoned that CO₂ enrichment, at otherwise constant conditions, could be used to decide which of these two mechanisms may be controlling canopy stomatal conductance. CO₂ enrichment results in stomatal closure and leads to reduced transpiration rates, which serves to maintain higher leaf and stem water potentials compared to ambient CO₂ concentrations. The higher CO₂ concentrations also result in a simultaneous increase in photosynthetic sugar production in mesophyll cells. We expected to observe smaller diurnal reductions in stomatal conductance in elevated CO₂ if stomatal aperture was determined by leaf and stem water status, and conversely, larger diurnal reductions if stomatal aperture responded to sugar accumulation.

Materials and methods

Cultural and environmental conditions

Wheat (*Triticum aestivum* L. cv. Veery-10) and soybean (*Glycine max* L. cv. Hoyt) canopies were grown in sealed, water-cooled, controlled-environment chambers (Model EGC-13, Environmental Growth Chambers, Chagrin Falls, OH). Two plant canopies of the same species were grown simultaneously in two chambers, each fitted with two 21 cm deep, 30 L hydroponic tubs. Wheat was planted in 10 mm of inert media (Isolite, size CG-2, Sumitomo Corp., Denver, CO) at a density of 1100 plants m⁻². Soybean seeds were germinated in moist Isolite and transplanted when the hypocotyls had elongated to at least 4

cm (about 6 days). The plants were supported by closed cell foam plugs in a blue Styrofoam lid, and were evenly spaced at a planting density of 60 plants m^{-2} .

A fixed area, reflective enclosure was built around the hydroponic tubs within each chamber to reduce edge effects and side lighting. Lighting was provided by four 1000-W high pressure sodium lamps, which were adjusted to achieve $\pm 5\%$ PPF uniformity over the crop surface. The incident PPF (PPF_0) was $1400 \mu\text{mol}^{-2} \text{s}^{-1}$ and $900 \mu\text{mol}^{-2} \text{s}^{-1}$ during the growth of wheat and soybean, respectively. Longwave radiation from the lamps was removed by a 10 cm deep, recirculating, chilled water filter. The PPF_0 was measured at the top of the canopy with a quantum sensor (Model LI-190SB, LI-COR, Lincoln, NE), and was maintained constant throughout the life cycle by lowering the canopy platform as the plants grew taller.

Average air temperature was $23.0 \pm 0.3^\circ\text{C}$, the barometric pressure was 86 kPa, and the chamber CO_2 setpoint was varied between 400-1400 $\mu\text{mol mol}^{-1}$. The root zone was a recirculating hydroponic system controlled at $23 \pm 0.2^\circ\text{C}$ and pH 5.7 for the duration of the experiments. The solution was replenished daily with refill solution to provide ample nutrients over the life cycle.

Gas exchange system

The gas exchange system used was previously described in Bugbee (1992), except for the following modifications: 1) a dew point hygrometer was added to measure transpiration rates continuously, 2) two solid-state multiplexers (Model AM-25T, Campbell Scientific, Logan, UT) with PRT temperature references were used for precision thermocouple measurements, and 3) two infrared transducers were used to measure radiative canopy

temperature in each chamber. Data acquisition and control was performed with a dedicated datalogger (Model CR-10T, Campbell Scientific, Logan, UT).

Gas exchange in each chamber was measured every 8 minutes. Rates of shoot net photosynthesis and dark respiration were calculated from the difference between pre- and post-chamber concentrations (ΔCO_2), multiplied by the mass flow rate of air (MF; mol s^{-1}) through the chambers. CO_2 concentration of pre-chamber air was controlled within $\pm 2 \mu\text{mol mol}^{-1}$ from the setpoint by an absolute IRGA and a mass flow controller (Model 820, Sierra Instruments, Monterey, CA). Air flow into the chambers was measured with mass flow meters (Model 730, Sierra Instruments, Monterey, CA). Chamber evapotranspiration was determined from the difference in mole fraction of water vapor between pre- and post-chamber air ($\Delta\chi_{\text{h}_2\text{o}}$), multiplied by MF into the chamber. $\Delta\chi_{\text{h}_2\text{o}}$ was determined from sequential measurements of pre- and post-chamber air dewpoint made with a dewpoint hygrometer (Model Dew-10, General Eastern, Watertown, MA).

Canopy stomatal conductance

Canopy stomatal conductance was determined from measurements of surface conductance (G_C) and the chamber aerodynamic conductance (g_A) as described in Chapter 2. Briefly, G_C was calculated from the ratio of canopy transpiration (Tr) to the canopy-air vapor pressure gradient, expressed as a mole fraction ($\chi_{\text{h}_2\text{o}}(T_{\text{canopy,H}}) - \chi_{\text{h}_2\text{o}}(T_{\text{air}})$; Equation 1).

$$G_C = \text{Tr} / [\chi_{\text{h}_2\text{o}}(T_{\text{canopy,H}}) - \chi_{\text{h}_2\text{o}}(T_{\text{air}})] \quad (1)$$

The canopy-air vapor pressure gradient was determined from measurements of the aerodynamic canopy temperature ($T_{\text{canopy,H}}$) and the air temperature above the canopy. Canopy

G_s was calculated from Equation 2. The g_A was obtained from $g_A = H / \rho C_p * (T_{\text{canopy,IR}} - T_{\text{air}})$, where H is the sensible heat flux, ρ is the density of air, C_p is the heat capacity of air, and $(T_{\text{canopy,IR}} - T_{\text{air}})$ is the radiative canopy-air temperature difference.

$$G_s = G_C * g_A / (g_A - G_C) = ((1/G_C) - (1/g_A))^{-1} \quad (2)$$

The chamber g_A was constant for the duration of the measurements as it was found to be independent of changes in ambient CO_2 concentration (Chapter 2).

A whole day of measurements was required to capture the diurnal reduction during the photoperiod. Responses of canopy G_s to elevated CO_2 were determined by first exposing the canopies to a CO_2 concentration of $400 \mu\text{mol mol}^{-1}$ for two consecutive days, then increasing the CO_2 in steps of $350\text{-}450 \mu\text{mol mol}^{-1}$ during the dark period of the second day, and measuring for another 2 days. This was repeated three times using each species leading to CO_2 treatments of $400, 800, \text{ and } 1200 \mu\text{mol mol}^{-1}$.

Results and discussion

A typical sequence of CO_2 enrichment events during the photoperiod is shown for a wheat canopy (Fig. 3.1). The chamber CO_2 was held at $1200 \mu\text{mol mol}^{-1}$ during the first two days, and it was sequentially decreased by about $400 \mu\text{mol mol}^{-1}$ every 2 days. Canopy transpiration increased from 8 to $12 \text{ mmol m}^{-2} \text{ s}^{-1}$ as the chamber CO_2 decreased (Fig 3.1A), which resulted in about a 1°C decrease in the canopy-air temperature due to the increased evaporative cooling (Fig 3.1B). Canopy G_s , calculated using Equation 2, increased as the chamber CO_2 concentration decreased (Fig 3.1C).

Figure 3.1 illustrates two main features that are consistent throughout all our

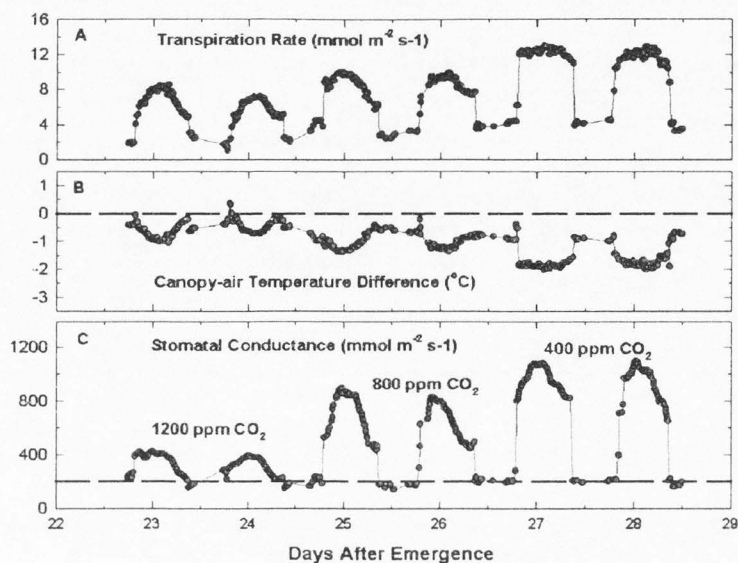


Figure 3.1 A sequence of 6 days where CO₂ enrichment was decreased every two days. The corresponding changes in canopy transpiration rate (A), canopy-air temperature difference (B), and canopy stomatal conductance (C) were continuously recorded as CO₂ concentration was changed. Canopy conductance during the dark period was not close to zero as would be expected in field plants.

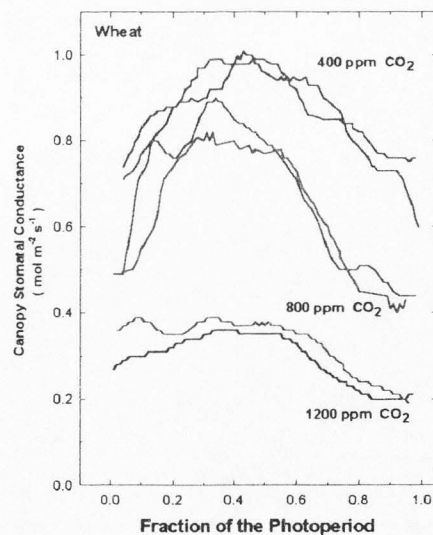


Figure 3.2 The data in Fig. 3.1 were expressed as a function of the photoperiod to illustrate the effects of CO₂ concentration on the diurnal patterns in canopy G_S.

measurements. First, canopy G_s during the dark period (marked by the dashed line in Fig. 3.1C) is not near zero in hydroponic plants. The stomates remain open at night, leading to significant amounts of canopy transpiration, which contrasts results from field studies. The second feature is that canopy G_s typically increased as soon as the lights came on, but it diminished as the photoperiod progresses. This behavior illustrates the diurnal reduction in canopy stomatal conductance. The effect of changes in chamber CO_2 are best seen in Fig. 3.2, which expresses the canopy G_s from Fig. 3.1 as a function of the fraction of the photoperiod.

It appears that the diurnal reduction in stomatal conductance would be mediated by a mechanism that attenuates stomatal aperture at high transpiration rates. We identified two competing hypotheses for explaining the observed diurnal reductions in stomatal conductance: 1) canopy stomatal conductance responds to changes in leaf and stem water potential. In this scheme, stomatal conductance is reduced when leaf water potential falls below a threshold or critical leaf water potential. 2) Sugars produced in mesophyll cells are carried by the transpiration stream, and stomatal aperture is reduced as sugars accumulate in guard cell walls. We used increasing chamber CO_2 concentrations to explore which of these two hypothesis may be controlling G_s in our canopies. Elevated CO_2 results in stomatal closure and leads to reduced transpiration rates, which serves to maintain higher water potentials. The higher CO_2 concentrations also result in a simultaneous increase in sugar production in mesophyll cells.

We expected to observe smaller diurnal reductions in stomatal conductance in

elevated CO_2 if stomatal aperture was being determined by leaf and stem water status. The leaf water potential reflects the diurnal status of water reserves within the plant responsible for supplying the transpiration stream. In field conditions, plant water reserves are replenished from soil water during the night. In the day, the transpiration stream depletes these reserves and the stomata are not affected until a critical leaf water potential is reached. The primary function of a mechanism whereby leaf water potential controls stomatal conductance may serve to maintain favorable leaf temperatures conducive to optimal growth, or to improve canopy water use efficiency (Jones, 1992). The plant water reserves would be depleted over the course of several days as the soil water reserves are depleted in the absence of precipitation or irrigation events. This hypothesis argues that in elevated CO_2 the reduced stomatal conductance would cause a slower depletion of the water reserves within the leaves and stems of the canopy (Lynn and Carlson, 1990). Therefore, the critical water potential at which stomatal closure was triggered would be attained after increasingly longer times into the photoperiod as the chamber CO_2 was increased. Conversely, we would expect no attenuation in conductance at low chamber CO_2 concentrations if the diurnal reductions in stomatal aperture responded to sugar accumulation. There would be no attenuation (i.e., maximum stomatal conductance at $400 \mu\text{mol mol}^{-1}$) until sufficient sucrose accumulated on guard-cell walls to elicit stomatal closure. As CO_2 concentration is increased, net photosynthesis increases resulting in greater export of sucrose from mesophyll cells. Thus we expect that at moderate CO_2 levels (i.e., $600 \mu\text{mol mol}^{-1}$), stomatal closure would occur at an earlier time during the photoperiod than at $400 \mu\text{mol mol}^{-1}$ since sucrose accumulation in

the guard-cell would occur at a faster rate. Then, at even higher CO₂ concentrations (i.e., >900 μmol mol⁻¹), apoplastic sucrose would always be sufficiently high such that stomatal aperture would be permanently reduced compared to low or even moderate levels of CO₂ enrichment.

We found that canopy G_s in higher ambient CO₂ slightly increased the magnitude of the diurnal reductions (Fig. 3.3A), and that CO₂ enrichment also caused the diurnal reductions in G_s to start earlier in the photoperiod (Fig. 3.3B). However, it appears that the effect of CO₂ becomes saturated after 900 μmol mol⁻¹. Our results are in agreement with the mechanism formulated by Lu *et al.* (1997), which argues that when sucrose secretion into the leaf apoplast exceeds the leaf's capacity for removal, accumulation of sucrose in the guard-cell wall would attenuate pore size, resulting in increased water-use efficiency and only a minor decrease in P_{net}. We calculated water use efficiency from our data and also expressed it as a function of the photoperiod (Fig. 3.4). We found that water use efficiency decreased during the early part of the photoperiod as stomatal aperture became maximal. Then, it increased during the photoperiod due to stomatal closure, causing only a small decrease in canopy photosynthesis, as predicted by Lu *et al.* (1997). The decrease in transpiration was accompanied by a simultaneous increase in canopy temperature (Fig. 3.1B).

These findings suggest that the 'sugar accumulation' hypothesis is probably responsible for the diurnal reduction of stomatal conductance in our canopies. It is unlikely

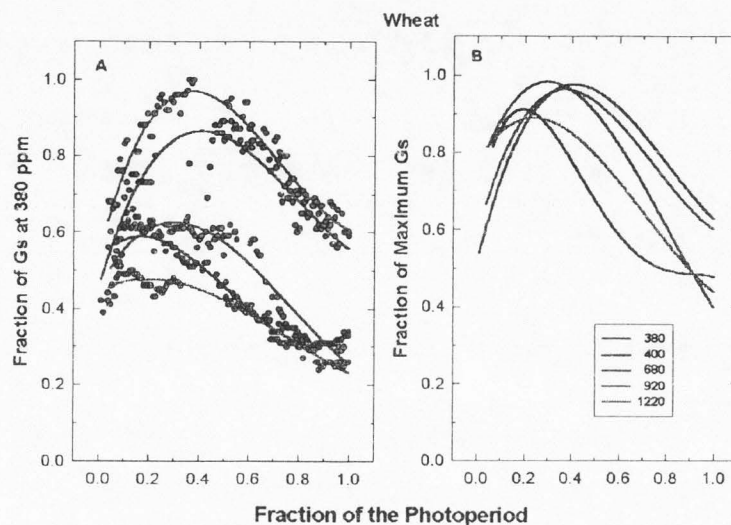


Figure 3.3 Wheat canopy stomatal conductance (A) expressed as a fraction of the conductance measured at 380 $\mu\text{mol mol}^{-1}$ and (B) expressed as a fraction of the maximum conductance observed during the day. Elevated CO₂ altered both the magnitude and caused the diurnal closure of stomata to begin earlier in the photoperiod.

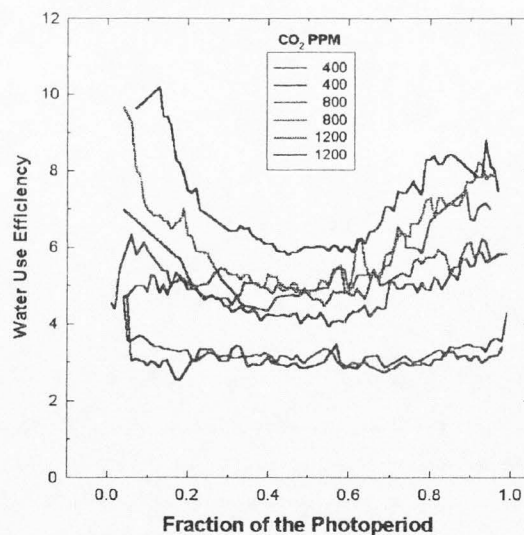


Figure 3.4 Water use efficiency improved as the CO₂ concentration increased. Water use efficiency decreased during the early part of the photoperiod as stomatal aperture became maximal. Then, it increased during the photoperiod due to stomatal closure, causing only a small decrease in canopy photosynthesis.

that the diurnal reductions in stomatal conductance were responding to fluctuating water potentials because the diurnal reductions in canopy Gs became accentuated in spite of conditions leading to higher leaf water potentials.

References

- Bugbee B.** 1992. Steady state gas exchange in growth chambers: system design and operation. *HortScience* **27**, 770-776.
- Dewar RC.** 1995. Interpretation of an empirical model for stomatal conductance in terms of guard cell function. *Plant, Cell and Environment* **18**, 365-372.
- Grantz DA, Meinzer FC.** 1990. Stomatal response to humidity in a sugar cane field: simultaneous porometric and micrometeorological measurements. *Plant, Cell and Environment* **13**, 27-37.
- Jones HG.** 1992. *Plants and microclimate: a quantitative approach to environmental plant physiology*. New York: Cambridge University Press.
- Körner Ch.** 1995. Leaf diffusive conductances in the major vegetation types of the globe. In: Schulze ED, Caldwell M.M., eds. *Ecophysiology of photosynthesis*. The Hague: Springer-Verlag, 463-490.
- Lu P, Outlaw WH Jr, Smith BG, Freed GA.** 1997. A new mechanism for the regulation of stomatal aperture size in intact leaves. *Plant Physiology* **114**, 109-118.
- Lynn BH, Carlson TN.** 1990. A stomatal resistance model illustrating plant vs. external control of transpiration. *Agricultural and Forest Meteorology* **52**, 5-43.
- Monje O, Bugbee B.** 1996. Characterizing photosynthesis and transpiration of plant communities in controlled environments. *Acta Horticulturae. ISHS.* **440**, 123-128.
- Monteith JL.** 1995. A reinterpretation of stomatal responses to humidity. *Plant, Cell and Environment* **18**, 357-364.
- Mott KA, Parkhurst DF.** 1991. Stomatal response to humidity in air and in helox. *Plant, Cell and Environment* **14**, 509-515.

Nikolov NT, Massman WJ, Schoettle AW. 1995. Coupling biochemical and biophysical processes at the leaf level: an equilibrium photosynthesis model for leaves of C₃ plants. *Ecological Modelling* **80**, 205-235.

Olioso A, Carlson TN, Brisson N. 1996. Simulation of diurnal transpiration and photosynthesis of a water stressed soybean crop. *Agricultural and Forest Meteorology* **81**, 41-59.

Outlaw WH Jr. 1983. Current concepts on the role of potassium in stomatal movements. *Physiologia Plantarum* **59**, 302-311.

Tenhunen JD, Pearcy RW, Lange OL. 1987. Diurnal variation in leaf conductance and gas exchange in natural environments. In: Zeiger E, Farquhar GD, Cowan IR, eds. *Stomatal function*. Stanford: Stanford University Press, 321-351.

CHAPTER 4
MODELING CANOPY TRANSPIRATION IN
CONTROLLED ENVIRONMENTS

Abstract

Canopy stomatal conductance and transpiration were measured in controlled environments for calibrating and validating eight canopy stomatal conductance models and two transpiration models. The best predictive combination of these models was selected by using a statistical procedure for evaluating model predictive validity. The Penman-Monteith equation gave slightly better predictions of transpiration than the Ohm's Law analog model in both wheat and soybean canopies. The best single canopy stomatal conductance model was the BWB model, which ranked third in predictive validity for both plant species and required only two parameters. The best predictive canopy stomatal conductance models were the BW2 model for wheat and the AJ2 model for soybean. The main difference between these models was that the wheat BW2 model incorporated a CO₂ concentration dependent function for describing diurnal changes in stomatal conductance, while the soybean AJ2 model did not. This was not expected since soybean stomatal conductance was more sensitive to changes in CO₂ than wheat. Predicted transpiration was very sensitive to small changes in CO₂ concentration, relative humidity, and air temperature.

Introduction

The objective of this study is to develop a model for predicting canopy transpiration

(Tr) in controlled environments (CEs). These estimates of canopy Tr may be used for optimizing designs of future plant-based bioregenerative systems, optimizing resource use in commercial plant production systems, for designing automated environmental control and monitoring systems, and for improving canopy stomatal conductance (G_s) models used in global climate modeling. We found that most canopy transpiration models have been developed for field situations, and that a poor understanding of energy transfer processes in growth chambers hinders efforts to develop reliable models of transpiration in CEs.

Jarvis (1976) analyzed the behavior of stomata and formulated a multiplicative relation to account for stomatal responses to changes in various environmental parameters: PPF, CO₂, temperature, vapor pressure deficit (VPD), and leaf water potential. In such a scheme, each factor independently scales the maximum stomatal conductance to determine the actual g . Several models of stomatal conductance have been formulated since then for predicting transpiration at the leaf, plant, crop, and regional scales (Raupach and Finnigan, 1988; Collatz *et al.*, 1991; Sellers *et al.*, 1992). Transpiration has been modeled using multilayer models where water vapor fluxes leaf layers are integrated to give a total flux, while other models have approximated canopy behavior using a 'big leaf model'. Most transpiration models are based on functions with leaf level parameters, and require additional information concerning the spatial distribution of irradiance, temperature, vapor pressure deficit, CO₂ concentration, and boundary layer conductances within the canopy. Modelers use leaf parameters in their models because canopy transpiration is very difficult to measure in situ.

Problems in adapting field-calibrated models for use in CEs may arise because empirically derived relations describing the energy fluxes of field-grown plants may not be directly applicable to CE-grown plants. This stems from the possibility that the sensitivity of stomata to environmental factors in plants grown in CEs may differ from field plants, or from the occurrence of certain combinations of environmental parameters that would never occur in nature (Jones, 1992). These concerns suggest that transpiration models developed for field plants may not accurately predict transpiration in CEs.

Continuous gas exchange measurements of canopy level CO_2 and water vapor fluxes and simultaneous measurements of canopy temperature allowed us to determine canopy G_s and characterize its response to different environmental regimes. Eight separate canopy stomatal conductance models were developed for predicting transpiration of wheat and soybean canopies. The models were parameterized using canopy G_s measurements collected during short-term exposures (hours to days) of plant canopies to environmental regimes during different stages of their life cycles. The models were compared and ranked by their ability to make accurate predictions of canopy Tr and by their degree of complexity.

Materials and methods

Cultural and environmental conditions

Wheat (*Triticum aestivum* L. cv. Veery-10) and soybean (*Glycine max* L. cv. Hoyt) canopies were grown hydroponically in sealed, water-cooled, controlled-environment chambers (Model EGC-13, Environmental Growth Chambers, Chagrin Falls, OH). Wheat was planted in 10 mm of inert media (Isolite, size CG-2, Sumitomo Corp., Denver, CO) at

a density of 1100 plants m^{-2} . Soybean seeds were germinated in moist Isolite and transplanted when the hypocotyls had elongated to at least 4 cm (about 6 days). The plants were supported by closed cell foam plugs in a blue Styrofoam lid, and were evenly spaced at a planting density of 60 plants m^{-2} . A reflective enclosure was built around the canopies to reduce side lighting. Lighting was provided by four 1000-W high pressure sodium lamps, which were adjusted to achieve $\pm 5\%$ PPF uniformity over the crop surface. The incident PPF (PPF_0) was 400 $\mu mol^{-2} s^{-1}$ and 900 $\mu mol^{-2} s^{-1}$ during the growth of wheat and soybean, respectively. Longwave radiation from the lamps was removed by a 10 cm deep, recirculating, chilled water filter. Average air temperature was $23.0 \pm 0.3^\circ C$, the barometric pressure was 86 kPa, and the chamber CO_2 setpoint was varied between 400-1400 $\mu mol mol^{-1}$. The root zone was a recirculating hydroponic system controlled at $23 \pm 0.2^\circ C$ and pH 5.7 for the duration of the experiments. The solution was replenished daily with refill solution to provide ample nutrients over the life cycle.

Canopy transpiration measurements

The gas exchange system used to measure canopy transpiration (Tr) was previously described in Chapter 3. Canopy evapotranspiration (ET) in the chamber, composed of Tr and evaporation (E) through the porous media (Equation 1), was determined from the difference in mole fraction of water vapor between pre- and post-chamber air (ΔX_{H_2O}), times the mass flow rate of air into the chamber (MF). ΔX_{H_2O} was determined from sequential measurements of pre- and post-chamber air dewpoint made with a dewpoint hygrometer (Model Dew-10, General Eastern, Watertown, MA).

$$ET = Tr + E \cong Tr = \Delta X_{h20} \cdot MF \quad (1)$$

Evaporation (E) through the porous media that separate the shoot environment from the root hydroponic environment was minimized by sealing the edges of the tubs in which the planting media holder rested. E was reduced to about 2% of R_{net} and assumed to be negligible.

Canopy stomatal conductance measurements

Canopy G_s was determined from measurements of surface conductance (G_c) and the chamber aerodynamic conductance (g_A) as described in Chapter 2. Briefly, G_c was calculated from the ratio of Tr to the canopy-air vapor pressure gradient, expressed as a mole fraction ($\chi_{h20}(T_{canopy,H}) - \chi_{h20}(T_{air})$). G_c was obtained by rearranging Equation 2 to solve for G_c .

$$Tr = G_c * [\chi_{h20}(T_{canopy,H}) - \chi_{h20}(T_{air})] \quad (2)$$

The canopy-air vapor pressure gradient was determined from measurements of the aerodynamic canopy temperature ($T_{canopy,H}$) and the air temperature above the canopy. Canopy G_s was calculated from Equation 3.

$$G_s = G_c * g_A / (g_A - G_c) = ((1/G_c) - (1/g_A))^{-1} \quad (3)$$

The g_A was obtained from $g_A = H / \rho C_p * (T_{canopy,IR} - T_{air})$, where H is the sensible heat flux, ρ is the density of air, C_p is the heat capacity of air, and ($T_{canopy,IR} - T_{air}$) is the radiative canopy-air temperature difference. The chamber g_A was constant for the duration of the measurements as it was found to be independent of changes in ambient CO_2 concentration (Chapter 2).

Model structure

The main features of the model are 1) the use of eight different schemes to describe stomatal conductance, 2) the iterative solution of the energy balance equation to obtain T_{canopy} , 3) inclusion of the influence of time of day and CO_2 concentration on G_c , 4) the use of a detailed biochemical model of C3 photosynthesis whenever canopy photosynthesis data was not available, and 5) the use of calibration parameters formulated from direct canopy scale measurements of canopy T_r , net photosynthesis (P_{net}), and G_s . A computer program was developed using the model structure shown in Fig 4.1. The model uses environmental (T_{air} , PPF, CO_2 , and RH) and species dependent parameters to calculate net radiation (R_{net}), canopy P_{net} , G_c , sensible heat flux (H), and T_{canopy} . The canopy temperature is calculated iteratively until the energy balance equation is equal to zero.

Radiation absorption. The canopy leaf area index, LAI, was estimated from the percent of light absorbed by the canopy, Q_{abs} , assuming a light extinction coefficient, K, of 0.3 for wheat (Smart *et al.*, 1994), and a K of 0.71 for soybean (Dougher and Bugbee, unpublished results). The canopy leaf area index was partitioned into sunlit (LAI_{sun}) and into shaded leaf fractions ($\text{LAI}_{\text{shade}}$) using the multilayer model of irradiance penetration described by De Pury and Farquhar (1995). The absorbed irradiance of sunlit and shaded fractions (PPF_{sun} and $\text{PPF}_{\text{shade}}$) were also calculated with the same irradiance model, which uses separate extinction coefficients for diffuse and direct beam radiation. The fraction of diffuse PPF in the chamber was 0.6 (Monje, unpublished results).

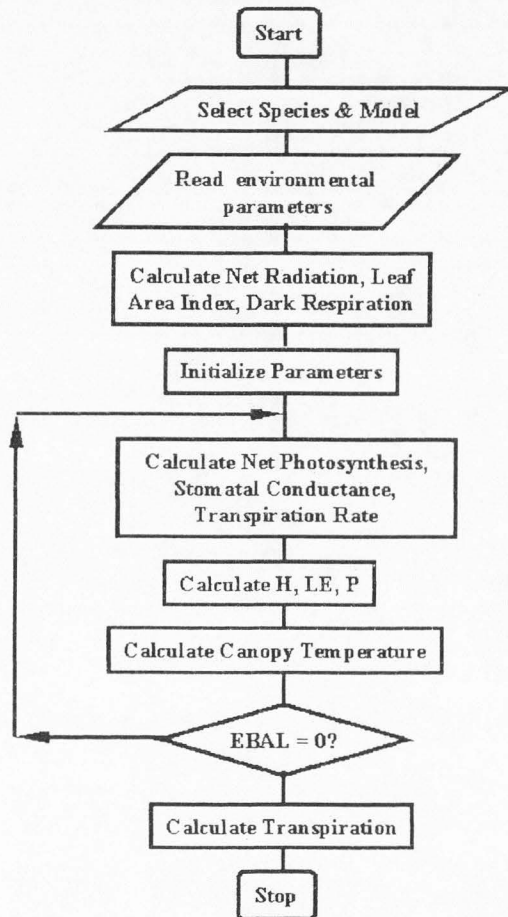


Figure 4.1 A flow diagram of the transpiration model. The chart illustrates the main subroutines and the iterative loop used to calculate canopy temperature.

Canopy photosynthesis. Canopy G_S was calculated from P_{net} measured with the gas exchange system (Chapter 2). However, the model can predict canopy P_{net} whenever measured P_{net} data are not available. The canopy photosynthesis routine calculates canopy gross photosynthetic carbon uptake for each sunlit and shaded leaf fraction according to the procedure described by Evans and Farquhar (1991). In light limited conditions, the photosynthetic rate of carbon uptake is determined by the electron transport rate, J (Sage, 1990). The relationship between J and the absorbed irradiance was described by an asymptotic exponential equation (Equation 6).

$$J = J_{max}' [1 - \exp(-PPF*(1-f)/2*J_{max}')] \quad (6)$$

where, J_{max}' = maximal canopy electron transport rate,
 PPF = incident PPFsun or PPFshade, and
 f = leaf absorption factor.

J_{max}' for each leaf fraction was found by multiplying the maximal electron transport rate per unit leaf area for C_3 plants, J_{max} , by either LAIsun or LAIshade. The dependence of J_{max} on temperature was estimated using Equation 7 (Harley *et al.*, 1992).

$$J_{max} = [\exp(c - \Delta Ha/(R*T_K))/(1+\exp(\Delta S*T_K-\Delta Hd)/(R*T_K))] \quad (7)$$

where, c = a constant (17.8),
 ΔHa = the activation energy,
 R = the gas constant,
 T_K = canopy temperature,
 ΔHd = the energy of deactivation, and
 ΔS = the entropy term.

In light saturated conditions, the maximal gross photosynthetic rate as a function of pCO_2 (the partial pressure of CO_2) was calculated from Equation 8. Γ_* , as a function of temperature, was estimated as described in Long (1991).

$$P_{gmax} = [J*(p_c - \Gamma_*)/(4.5*p_c - 10.5*\Gamma_*)] \quad (8)$$

where, p_c = the pCO_2 at the site of carboxylation, and
 Γ_* = the CO_2 compensation point in the absence of mitochondrial respiration.

Canopy dark respiration (R_t) was calculated from the integrated daily amount of C fixed (DCF, $mol\ m^{-2}\ d^{-1}$) and the carbon use efficiency (CUE; Bugbee and Monje, 1992) (Equations 9-11; Monje and Bugbee, 1998). DCF was obtained from P_{gross} and used to calculate the daily amount of C respired (DCR, $mol\ m^{-2}\ d^{-1}$). These integrated C fluxes are dependent on the length of the photoperiod, PD. Carbon use efficiency, the fraction of daily C fixed that is respired, was 0.65 for wheat and 0.55 for soybean. These values for CUE were assumed constant throughout the life cycle. Canopy photosynthesis was determined from Equation 12.

$$DCF = P_{gross} * (PD/24) * 24 * 3600 * 1e-6 \quad (9)$$

$$DCR = CUE * DCF \quad (10)$$

$$R_t = DCR / (3600 * 1e-6 * 24) \quad (11)$$

$$P_{net} = P_{gross} - R_t \quad (12)$$

Stomatal conductance models

Eight models of daytime canopy G_s were parameterized using separate calibration data sets from wheat and soybean canopies. The calibration data sets included only daytime transpiration, stomatal conductance, and photosynthesis, as well as the necessary environmental variables. The nighttime canopy G_s was not considered in the present formulation of the conductance models. The parameters for each model were obtained using nonlinear regression curve fitting software (SigmaStat 1.0, Jandel Corp.). The equations

describing each model are tabulated in Table 4.1, and the fitting parameters used in each model are shown in Table 4.2. The stomatal conductance models (described below) were adapted from published models or developed using measured data, and represent eight separate hypotheses for describing canopy stomatal conductance. A statistical test of these hypotheses is described in the validation procedure.

Ball Woodrow Berry (BWB). The BWB model is a semi-empirical model developed for calculating leaf stomatal conductance (Ball *et al.*, 1987). Although this model was originally developed for use with single leaves, we applied this model to the canopy scale as was done by Valentini *et al.* (1995). In this model (Equation 13; Table 4.1), daytime canopy G_s responds to relative humidity (h_s) and CO_2 concentration (C_s) at the leaf surface, net photosynthesis (P_{net}) determines maximal G_s , and the constants b_0 and b_1 are obtained by fitting measured data. In its original formulation, this equation described the relation between P_{net} and g_s , which gives realistic predictions of responses to PPF and variables that do not affect the relation between P_{net} and g_s (Aphalo and Jarvis, 1993). However, it is hindered by the need of P_{net} as an input variable, and since it treats changes in temperature and relative humidity via changes in h_s . The BWB is a simple model because it requires few inputs, but may be fundamentally flawed because experiments by Mott and Parkhurst (1991) have shown that stomata respond to the rate of transpiration, and not to h_s .

Aphalo-Jarvis (AJ and AJ2). The AJ model (Equation 14; Table 4.1) is an improved version of the BWB, which replaces h_s by leaf temperature (T_{leaf}) and vapor pressure deficit

Table 4.1. *Definitions of the eight stomatal conductance models*

Model Name and Algorithm	Equation
BWB Model $G_s = b_0 + b_1 * P_{net} * h_s / C_s$	(Equation 13)
AJ Model $G_s = (P_{net} / C_s) * (a_{j1} + a_{j2} * D_s + a_{j3} * T_{canopy})$	(Equation 14)
AJ2 Model $G_s = (P_{net} / C_s) * (a_{j21} + a_{j22} * D_s + a_{j23} * T_{canopy} + a_{j24} * PPF_{abs})$	(Equation 15)
LN Model $G_s = l_1 + l_2 * P_{net} / [(C_s - \Gamma) * (1 + D_s / D_o)]$	(Equation 16)
WF Model $G_s = Q * (w_{f1} + w_{f2} * fPD + w_{f3} * fPD^2)$	(Equation 19)
WF2 Model $G_s = Q * (w_{f21} / C_s) * (w_{f22} + w_{f23} * fPD + w_{f24} * fPD^2)$	(Equation 20)
BW2 Model $G_s = b_{w20} + b_{w21} * (h_s * P_{net} / C_s) * fG_s$	(Equation 21)
BW3 Model $G_s = (b_{w30} + b_{w31} * (h_s * P_{net} / C_s) * fG_s) * PPF_{abs}$	(Equation 22)

Table 4.2. Parameterization coefficients for stomatal conductance models

Parameter	Wheat	r ²	Soybean	r ²
BWB Model (Equation 13)		0.821		0.411
<i>b</i> 0	138.9		117.3	
<i>b</i> 1	153.2		109.5	
AJ Model (Equation 14)		0.857		0.802
<i>a</i> 1	14273.1		-19962.1	
<i>a</i> 2	-7055.5		-10542.9	
<i>a</i> 3	133.7		1716.8	
AJ2 Model (Equation 15)		0.855		0.820
<i>a</i> 21	13408.95		-20244.9	
<i>a</i> 22	-7180.35		-11172.09	
<i>a</i> 23	197.9		1797.54	
<i>a</i> 24	-0.293		-1.226	
LN Model (Equation 16)		0.819		0.414
<i>L</i> 0	183.6		186.0	
<i>L</i> 1	15859.0		10576.0	
Γ	80 μ mol		80 μ mol mol ⁻¹	
<i>D</i> 0	0.8 kPa		0.8 kPa	
WF Model (Equation 19)		0.639		0.310
<i>w</i> 1	0.9006		0.40549	
<i>w</i> 2	0.4655		0.0571	
<i>w</i> 3	-0.8495		-0.1674	
WF2 Model (Equation 20)		0.832		0.504
<i>w</i> 21	3.256		2.455	
<i>w</i> 22	169.8		166.9	
<i>w</i> 23	215.5		138.2	
<i>w</i> 24	-289.06		-189.54	
BW2 Model (Equation 21)		0.792		0.187
<i>b</i> w20	283.7		268.2	
<i>b</i> w21	164.4		71.33	
BW3 Model (Equation 22)		0.827		0.170
<i>b</i> w30	375.9		286.5	
<i>b</i> w31	166.6		76.05	

(Ds) as driving variables (Equation 4 in Aphalo and Jarvis, 1993). The original leaf model was also adapted to describe daytime canopy Gs, using T_{canopy} instead of T_{leaf} . The AJ2 model (Equation 15; Table 4.1) is a variation of the AJ model, which includes absorbed PPF (PPF_{abs}) as an additional term. Preliminary best subsets regression analysis indicated that this additional coefficient reduced the root mean square error (RMSE) of the regression against the observed Gs. The inclusion of the PPF_{abs} term improved the fit more than the addition of the interaction term ($Ds * T_{\text{canopy}}$) suggested by Aphalo and Jarvis (1993).

Leuning (LN). The LN model (Equation 16; Table 4.1) is another modification of the BWB model (Leuning, 1995). It includes the CO_2 compensation point, Γ , to improve the behavior at low Cs, and uses a hyperbolic function of Ds for improved humidity response, rather than a linear relation with Ds as proposed in the BWB and AJ models. The LN model also includes D_0 , an empirical coefficient reflecting sensitivity of the stomata to Ds.

Whitfield (WF and WF2). The WF model (Equation 19; Table 4.1) describes evaporative fluxes in terms of the sensitivity (α) of leaf conductance to solar radiation. It assumes that leaf conductance is proportional to the absorbed radiation, and treats canopy conductance as a function of the radiation intercepted by the canopy. Furthermore, the WF model assumes that canopy conductance varies during the day due to changes in leaf water potential (Whitfield, 1990). The model follows Choudhury and Idso (1985), who related canopy water vapor exchange to intercepted radiation (Q, Equation 17) and vapor pressure deficit, where Q depends on LAI, incident radiation (Q_0), solar elevation (β), and the canopy extinction coefficient (K).

$$Q = Q_0 * [1 - \exp(-K * LAI / \sin\beta)] \quad (17)$$

The intercepted radiation integrates radiation within the canopy over all the leaf layers, thus canopy conductance expressed as a function of Q is shown in Equation 18.

$$G_c = \alpha * Q_0 * [1 - \exp(-K * LAI / \sin\beta)] = \alpha * Q \quad (18)$$

The WF model assumes that α changes simultaneously with radiation and leaf water potential. We obtain the WF model (Equation 19; Table 4.1) by assuming that variations in daytime G_s are described by α , and that α varies quadratically with fPD, the time of day normalized for the photoperiod. This equation is suitable for describing diurnal changes in G_s based on measures of Q . However, this model was originally formulated for field conditions at ambient CO_2 concentrations. We added an additional term, $1/C_s$, in the WF2 model (Equation 20; Table 4.1) to accommodate for changes in CO_2 concentration because an increase in CO_2 concentration reduces G_s (Jarvis, 1976).

Improved BWB Models (BW2 and BW3). The decline in the daytime course of G_s was found to be more rapid than predicted by the BWB model (Monje and Bugbee, 1996). In view of these findings (described in Chapter 3), the BW2 model (Equation 21; Table 4.1) was developed by modifying the BWB model to include diurnal fluctuations in G_s . A nondimensional parameter (varying from 0 to 1) was used to describe the diurnal course of G_s , fGs. This parameter was determined empirically by nonlinear regression from measured values of G_s normalized to the maximum G_s in the parameterization data set (typically G_s measured at $400 \mu\text{mol mol}^{-1}$). The fGs function was dependent on fPD, C_s , and relative humidity. The empirical equation and parameters (a-i) are given in Table 4.3. The BW3 model

Table 4.3. *Parameterization coefficients for fGs functions*

$fG_s = a + b \cdot fPD + c \cdot C_s + d \cdot RH + e \cdot fPD \cdot \exp(f \cdot fPD) + g \cdot \exp(-h \cdot fPD) + i \cdot fPD^{0.5}$		
Parameter	Wheat	Soybean
<i>a</i>	-0.15939	0.18149
<i>b</i>	3.7327	-0.04825
<i>c</i>	-4.903e-4	-6.347e-4
<i>d</i>	0.01183	0.01167
<i>e</i>	-3.5406	3.36733
<i>f</i>	0.15926	-3.86356
<i>g</i>	0.25341	0.14823
<i>h</i>	0.41173	0.02356
<i>i</i>	-0.0500	0.01221

(Equation 22; Table 4.1) was a modified version of the BW2 model, which includes absorbed PPF to improve predictions of G_s in young canopies that have not reached full cover.

Canopy transpiration models

Two separate algorithms were implemented to calculate canopy transpiration using the chosen canopy stomatal conductance model. The first model is the Big Leaf model written as an analog of Ohms' Law (Equation 2), which treats the canopy as a single leaf with the stomatal conductance equal to G_c (Equation 3). Tr is calculated from the product of G_c and the canopy-air vapor pressure gradient. Although the second model is also another form of

the Big Leaf model, it uses the chamber gA and the modeled daytime G_s to determine T_r from the Penman-Monteith equation (Equation 23; Jones, 1992).

$$T_r = (S \cdot R_{net} + \rho \cdot C_p \cdot gA \cdot D_s) / (\lambda \cdot (S + \gamma \cdot (gA / G_s))) \quad (23)$$

where, ρ = the density of dry air,
 C_p = the specific heat of air,
 D_s = the vapor pressure deficit,
 S = the slope of the curve relating saturation vapor pressure to temperature,
 γ = the psychrometric constant, and
 λ = the latent heat of vaporization of water.

Model validation

The calibrated model must perform well in different plant growth chambers for it to be useful because controlled environment research is typically conducted in chambers that differ in volume, environmental controls, and lighting. The eight stomatal conductance and the two transpiration models were compared using the approach of predictive validation described by Power (1993). The procedure first evaluates the predictive properties of each model and then selects the model with the highest predictive validity. Bias and accuracy statistics are used to choose the model that most consistently and precisely predicts system behavior. This comparative method uses Theil's inequality coefficient (U^2) for producing both an index of predictive performance and for indicating the source of predictive errors. It also employs the Janus coefficient (J^2) as a measure of the relative in and out of sample predictive performance (Power, 1993). The out of sample predictive validity was used as an index to evaluate and quantify the portability of the model to other chamber systems. The goal of the validation procedure was used to rank the eight competing models in their ability to provide

the best prediction, to identify the models with the best out of sample predictive performance, and to select the best single model for predicting canopy transpiration in wheat and in soybean.

Another factor considered for comparing alternative models was the model complexity. The Akaike information criterion (AIC, Equation 24) was calculated for each of the models.

$$\text{AIC} = L(Y|M) + 2*P \quad (24)$$

where, AIC = Akaike information criterion,
L(Y|M) = Likelihood of the model M given the data Y,
P = number of parameters in model M.

The model selection criterion is that the best model is the one with the lowest AIC, and therefore the lowest degree of complexity (Hilborn and Mage, 1997). The likelihood that the model M gives the best fit was calculated from the $\log(\text{SSQ})$, where SSQ is the residual sum of squares. This measure of fitness is penalized by adding 2 to the $\log(\text{SSQ})$ for every parameter used in the model. Thus, the best model under this criterion includes the lowest degree of complexity and minimizes the residual sum of squares.

The portability of these validated models to other chamber systems was evaluated by running the model, once parameterized and calibrated, with environmental inputs obtained in a completely different chamber system. Transpiration data from a soybean canopy grown in the Biomass Production Chamber (BPC) from the NASA Kennedy Space Center was used to test the performance of the best predictive soybean model.

Model sensitivity

Sensitivity analysis of the best wheat and soybean canopy transpiration models to several variables was performed. Two methods were used. The first method is a simple graphical method for evaluating model sensitivity to changes in a single environmental input. Equation 25 gives the relative sensitivity, S_i , of function $F = f(p_1, p_2, \dots, p_n)$ to a single variable, p_i . In this sensitivity analysis, F is canopy transpiration and the environmental variables (p_i) are: aerodynamic resistance (r_A), T_{air} , relative humidity, CO_2 concentration, and PPF.

$$S_i = (\partial F / \partial p_i) / (F / p_i) \propto (\Delta F / F) / (\Delta p_i / p_i) \quad (i = 1, 2, \dots, n) \quad (25)$$

The sensitivity of Tr to variables p_i was studied by plotting $(\Delta Tr / Tr \times 100)$ against $(\Delta p_i / p_i \times 100)$ for values of P_i equal to $\pm 1, 5, 10, 20,$ and 40% above a reference set of conditions where $r_A = 7 \text{ s m}^{-1}$, $T_{air} = 20^\circ\text{C}$, $P_{net} = 20 \mu\text{mol m}^{-2} \text{ s}^{-1}$, $[CO_2] = 600 \mu\text{mol mol}^{-1}$, and $PPF = 500 \mu\text{mol m}^{-2} \text{ s}^{-1}$. The second test was designed to distinguish the effects of interactions between the five environmental variables used in evaluating the single parameter effects. This test was performed using the best wheat canopy transpiration model. Two analyses were done using a fractional factorial design involving the five environmental variables, whereby the altered level was ± 10 percent of the nominal value. A half factorial design was used to reduce the number of runs, and for five factors, there are five main effects, 10 two-factor interactions, and each test required 16 runs of the model. Although this design reduces the number of model runs, single parameter effects are aliased with higher order effects, i.e., three- and four-factor effects. The factorial effect totals were calculated in a spreadsheet using the Yates' method (Cochran and Cox, 1957).

Results and discussion

There are significant differences in canopy architecture and physiology between the plant species chosen for this study. Canopy architecture is important in determining how radiation for driving transpiration is distributed within the canopy, as well as for determining the leaf area index that can be packed into a given volume. Wheat has an erectophile canopy architecture with narrow vertical leaves, while soybean has a broad leaves arranged in a planophile architecture. There are also physiological differences in how sugars and starch accumulate in these plant species when they are grown at elevated CO₂ concentrations. These differences affect canopy stomatal conductance, transpiration, and canopy energy balance. They may also have a significant impact on which model is best suited to describe the nonlinear relations associated with energy fluxes of plant communities.

We adapted and evaluated eight canopy stomatal conductance models for predicting canopy transpiration in CEs. The majority of these models were developed for predicting leaf scale stomatal conductances and have been incorporated into many canopy level transpiration models. The eight models can be separated into two broad categories. The first category includes the family of BWB models (AJ, AJ2, LN, BW2, and BW3). These models are improved variations of the widely used BWB model, which relates stomatal conductance to P_{net} , CO₂ concentration, and relative humidity at the leaf surface (Ball *et al.*, 1987). The AJ, AJ2, and LN models have been developed to improve the semi-empirical relation embodied in the BWB by relating stomatal conductance to leaf temperature and water vapor deficit, instead of relating it to humidity at the leaf surface, h_s . The BW2 and BW3 models are

variations of the BWB model that attempt to improve model performance by solely incorporating terms that account for the diurnal changes in stomatal conductance described in Chapter 3. The second category includes the WF and WF2 models. These models relate canopy stomatal conductance to the amount of PPF absorbed by the canopy and include time-dependent parameters for incorporating diurnal variations in stomatal conductance.

Model calibration

Extensive data sets consisting of several days of wheat and soybean canopy gas exchange measurements were made at various combinations of PPF, CO₂ concentration, and relative humidity. These data were used to parameterize these eight models for each species. The canopy stomatal conductance parameterization data sets for the wheat and soybean stomatal conductance models included over 500 data points. These data sets also included corresponding measurements of canopy temperature, net photosynthesis, transpiration rate, air temperature, relative humidity, time of day, CO₂ concentration, PPF, and the fraction of PPF absorbed. The parameterization coefficients obtained by nonlinear regression for each model and for each species are shown in Table 4.2.

The parameterization coefficients for the fGs functions used by the BW2 and BW3 models are shown in Table 4.3. The relation between fGs and the time of the photoperiod (fPD) was found to be significantly more sensitive to changes in CO₂ concentration in soybean compared to wheat (Fig. 4.2). These differences in sensitivity to CO₂ concentration probably reflect differences in sugar translocation between the two species; wheat typically accumulates

soluble sugars while soybean accumulates starch when exposed to elevated CO₂ (Farrar and Williams, 1991).

Model validation

The transpiration models using the Penman-Monteith equation (Equation 21; Fig. 4.3B, D) were found to give slightly more accurate predictions of canopy transpiration than the Ohm's Law analog equation (Equation 2; Fig. 4.3A, C) for both wheat and soybean canopies. Two separate methods were devised to rank the eight models of canopy G_s . They were first ranked according to their predictive capability using the predictive validation procedure is found in Powers (1983). The statistics used to rank the wheat and soybean canopy stomatal conductance models during the predictive validation procedure are shown in Tables 4.4 and 4.5. The tables include a critical value of key statistics in the first column. The values in the tables marked by a (†) indicate the value at the 5% level of significance. Briefly, the models were ranked according to how well each statistic compared with the critical value denoting significance. According to this ranking procedure, the best predictive wheat canopy G_s model was the BW2 model, and the best predictive soybean model was the AJ2 model. Generally, the BWB-type and AJ models ranked higher than the WF models. However, the best predictive wheat model included the time dependent fG_s parameter, whereas the best soybean model did not. This was an unexpected result since soybean was more sensitive to changes in CO₂ (Fig. 4.2). This suggests that differences in C allocation in response to elevated CO₂ may play a considerable role in helping to explain the mechanisms determining stomatal conductance.

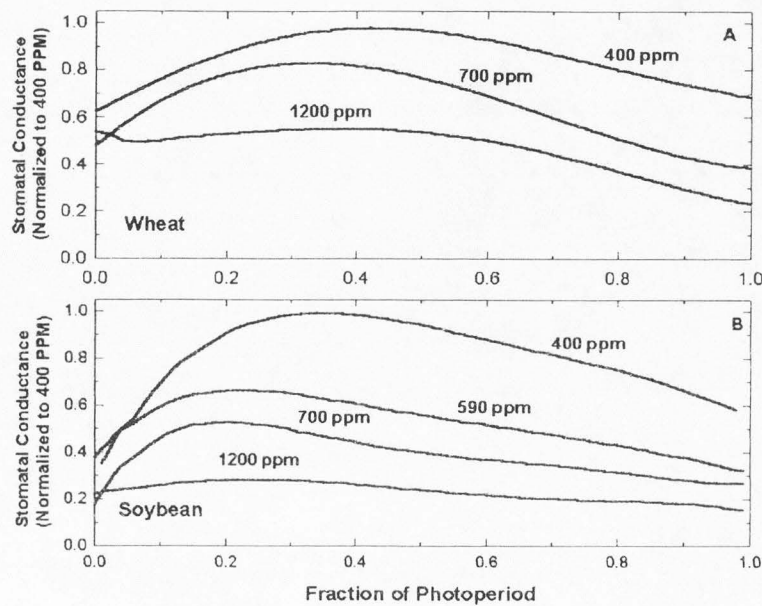


Figure 4.2 The fGS functions for (A) wheat and (B) soybean. These functions describe the response of canopy stomatal conductance to CO₂ enrichment as a function of the photoperiod. Soybean canopy stomatal conductance was more sensitive to elevated CO₂ than wheat.

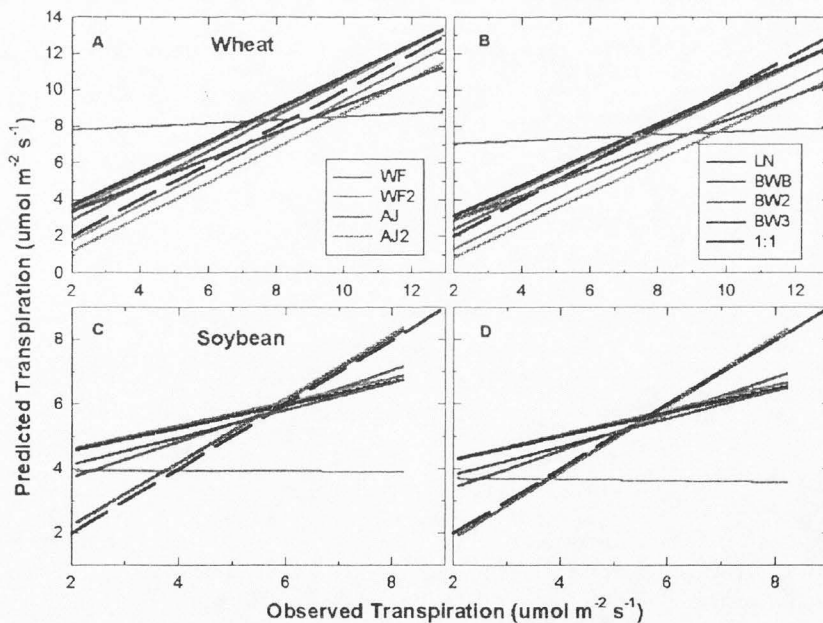


Figure 4.3 A comparison between predicted vs. observed transpiration. This figure compares the accuracy of the eight canopy G_s models and the two transpiration models. Wheat canopy transpiration calculated (A) using the eight canopy G_s models and the Ohms' Law analog model, and (B) using the Penman-Monteith equation; (C) the Ohms' Law analog model, and (D) the Penman-Monteith model for soybean.

The second ranking procedure was according to the degree of model complexity embodied by the AIC (Equation 24). This ranking was devised to avoid selecting extremely complex models because as the number of model parameters increases then the ease of use and predictive capacity of the model generally decreases (Hilborn and Mangel, 1997). The AIC was plotted against the number of parameters in each model (Fig. 4.4) and the models were ranked in terms of their complexity (Tables 4.4 and 4.5). The simplest and highest ranking model according to this criterion was the BWB model since it only required two parameters. This model also ranked third in the predictive ranking for both plant species. These considerations suggest that the BWB model is the best model for predicting canopy stomatal conductance since it is the simplest and because its predictive accuracy is adequate.

The stomatal conductance models are also compared in Fig. 4.5. In wheat, the BWB models appear to overpredict at lower values of stomatal conductance, while the AJ type models underpredict stomatal conductance (Fig. 4.5A). In soybean, the best models are the AJ type models but they fail to give accurate predictions of stomatal at the higher values of stomatal conductance (Fig. 4.5B).

The sensitivity analysis plot of the wheat BW2 model shows that transpiration sensitivity ($\Delta Tr/Tr$) increases as changes in PPF, relative humidity, and air temperature ($\Delta p/p$) increase, but transpiration sensitivity decreases for changes in CO_2 and rA (Fig. 4.6A). In soybean, the sensitivity of transpiration increases with increasing changes in PPF and temperature, it decreases with changes in CO_2 and relative humidity, and it is insensitive to changes in rA (Fig. 4.6B). These analyses suggest that small changes in air temperature and

Table 4.4. Comparison of wheat canopy stomatal conductance models in predicting canopy transpiration using the Penman-Monteith equation. Three statistics (Bias, *W*, and *Q*) and the Janus coefficient were used to determine the predictive model ranking (see text).

† denotes the value required for significance at the $p = 0.05$ level. * denotes statistical significance at the $p = 0.05$ level.

Statistic (Critical Value)†	BWB	AJ	AJ2	LN	WF	WF2	BW2	BW3
Number of Parameters	2	3	4	4	3	4	11	11
model Mean (8.33)	8.26	6.07	6.37	7.10	7.65	7.06	8.01	8.35
model Std. Dev. (2.33)	2.30	21.5	2.35	1.89	1.69	2.60	2.27	2.15
model Variance (5.42)	5.28	5.03	5.51	3.57	2.85	6.74	5.14	4.61
Mean Percent Error	2.04	44.1	36.9	18.2	12.7	21.7	4.75	0.16
RMSE	1.77	6.81	5.52	3.49	7.51	4.07	1.29	1.32
Mean Absolute Error (%)	13.9	45.4	38.42	22.8	32.4	25.4	12.34	12.5
Bias (0.00)	0.072	2.26	1.95	1.23	0.678	1.26	0.317	-0.023
W (1.96)†	0.562*	17.7	15.3	9.64	5.31	9.92	2.48**	-0.17*
Q-statistic (1.17)†	0.761*	2.92	2.37	1.50	3.22	1.74	0.556*	0.568*
Theil's U ² Statistic (0.00)	0.024	0.163	0.120	0.065	0.122	0.072	0.019*	0.018
Ub	0.003	0.751	0.693	0.434	0.061	0.395	0.078	0.000
Uv	0.000	0.001	0.000	0.055	0.054	0.018	0.003	0.025
Uc	0.997	0.248	0.307	0.510	0.885	0.588	0.920	0.975
Janus Coefficient (J ²) (1.00)	1.66	0.54	1.87	2.83	2.74	0.36	1.01	1.44
Predictive rank	3	7	6	4	8	5	1	2
Log (SSQ)	3.26	3.54	3.48	3.36	3.31	3.37	3.27	3.26
AIC	7.26	9.54	11.48	11.36	9.31	11.37	25.27	25.26
Complexity rank	1	3	6	4	2	5	7	8

Table 4.5. Comparison of soybean canopy stomatal conductance models in predicting canopy transpiration using the Penman-Monteith equation. Three statistics (Bias, *W*, and *Q*) and the Janus coefficient were used to determine the predictive model ranking (see text). † denotes the value required for significance at the $p = 0.05$ level. * denotes statistical significance at the $p = 0.05$ level.

Statistic (Critical Value)†	BWB	AJ	AJ2	LN	WF	WF2	BW2	BW3
Number of Parameters	2	3	4	4	3	4	11	11
model Mean (6.02)	5.85	6.20	6.27	5.67	3.61	6.49	5.95	5.82
model Std. Dev. (1.02)	0.87	1.47	1.51	0.78	0.51	1.98	0.65	0.71
model Variance (1.04)	0.76	2.15	2.27	0.61	0.26	3.92	0.43	0.51
Mean Percent Error	6.83	3.53	2.44	10.1	75.6	1.06	4.54	7.13
RMSE	0.76	0.97	1.03	1.04	7.94	2.14	0.82	0.98
Mean Absolute Error (%)	12.8	14.0	14.4	15.8	75.8	18.3	13.3	15.1
Bias (0.00)	0.352	0.002	-0.08	0.532	2.591	-0.29	0.251	0.377
W (1.96)	7.26	0.05*	-1.54	10.9	53.4	-6.0	5.17	7.77
Q-statistic (1.17)	0.75*	0.95*	1.01*	1.01*	7.78	2.09	0.80*	0.95*
Theil's U ² Statistic (0.00)	0.022	0.024	0.025	0.032	0.598	0.046	0.023	0.028
Ub	.163	0.000	0.005	0.273	0.846	0.040	0.077	0.146
Uv	.029	0.207	0.229	0.054	0.032	0.431	0.163	0.096
Uc	.808	0.793	0.765	0.673	0.122	0.530	0.76	0.758
Janus Coefficient (1.0)	1.47	1.30	1.26	1.50	2.42	3.40	1.34	1.49
Predictive rank	3	2	1	6	8	7	4	5
Log (SSQ)	2.78	2.75	2.75	2.82	4.25	2.78	2.76	2.79
AIC	6.78	8.75	10.75	10.83	10.25	10.78	24.77	24.79
Complexity rank	1	2	4	6	3	5	7	8

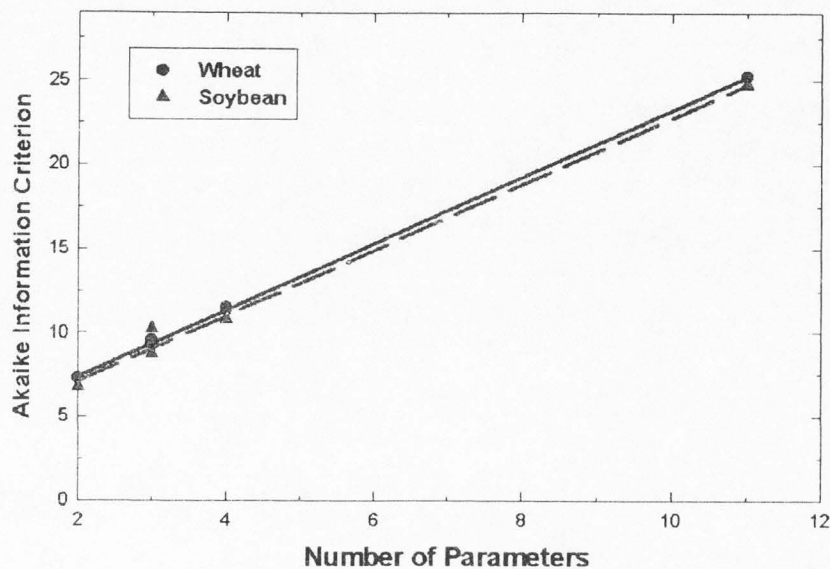


Figure 4.4 The Akaike information criterion (AIC) as a function of model complexity. The greater the number of parameters then the likelihood that a given model gave the best fit was reduced.

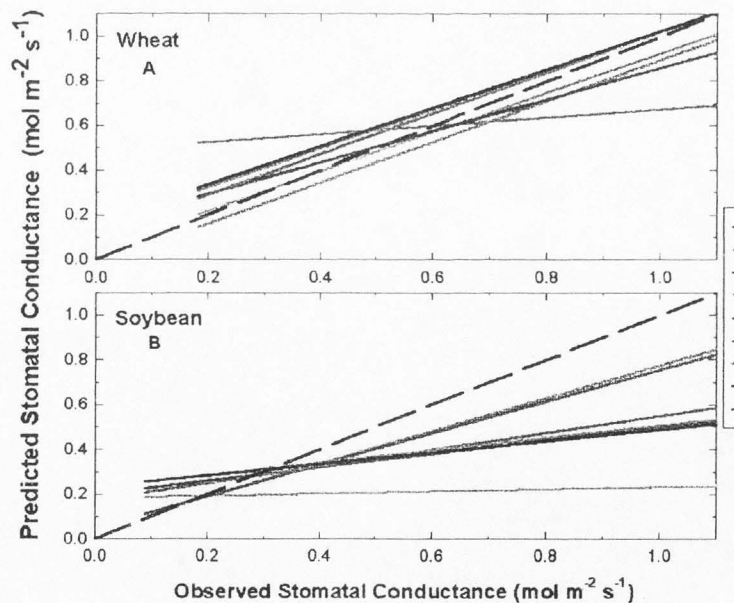


Figure 4.5 A comparison between predicted vs. observed wheat (A) and soybean (B) canopy GS for the eight stomatal conductance algorithms. The best predictive model for wheat was the BW2 model and the best predictive model for soybean was the AJ2 model.

relative humidity result in large changes in transpiration, and that these changes are particularly large in the soybean AJ2 model. The sensitivity analysis plots also show that changes in CO₂ and relative humidity are nonlinearly related to transpiration. This analysis suggests that input variables such as CO₂ concentration, relative humidity, and air temperature must be accurately determined. The results of the half factorial design in wheat confirm that $\pm 10\%$ changes in the five environmental variables result in significant changes in transpiration ($P < 0.05$), and that the significant two-factor effects include PPF*CO₂, PPF*T_{air}, CO₂*T_{air}, PPF*RH, CO₂*RH, T_{air}*RH, T_{air}*rA, and RH*rA ($P < 0.05$). The only two-factor effects that did not significantly alter transpiration were PPF*rA and CO₂*rA.

Model performance

The responses of canopy stomatal conductance and transpiration (Fig. 4.7) to water vapor pressure deficit predicted by the wheat BW2 model are compared with the observed response in the wheat validation data set (predictive ranking #1; Table 4.4). Generally, the model predicts the overall data fairly well but it is more tightly grouped than the observed data. Although the predicted and the observed data sets have practically the same variance, the largest source error is due to differences due to imperfect covariation in the two data sets. This is quantified by the covariance proportion in Theil's inequality coefficient (Uc variable in Table 4.4; BW2 model). This source of error is probably caused by improper description of diurnal fluctuations in stomatal conductance by the fGs function. This inability to properly describe the diurnal changes in stomatal conductance may have been introduced by the limited

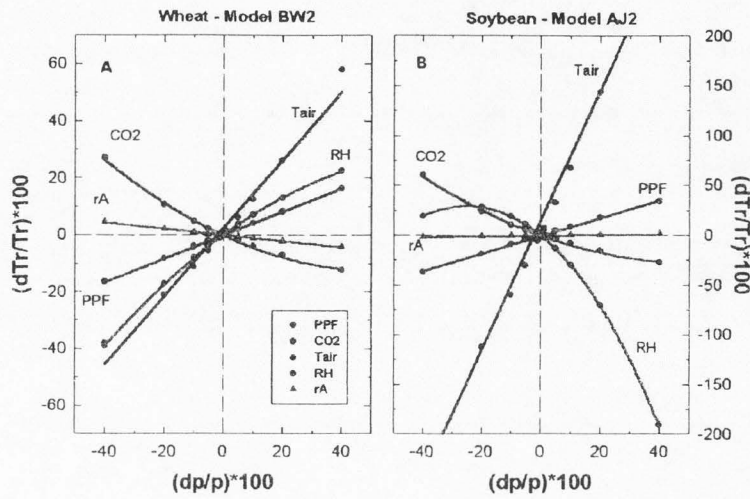


Figure 4.6 Single parameter sensitivity plots for the wheat BW2 model (A) and the soybean AJ2 model (B).

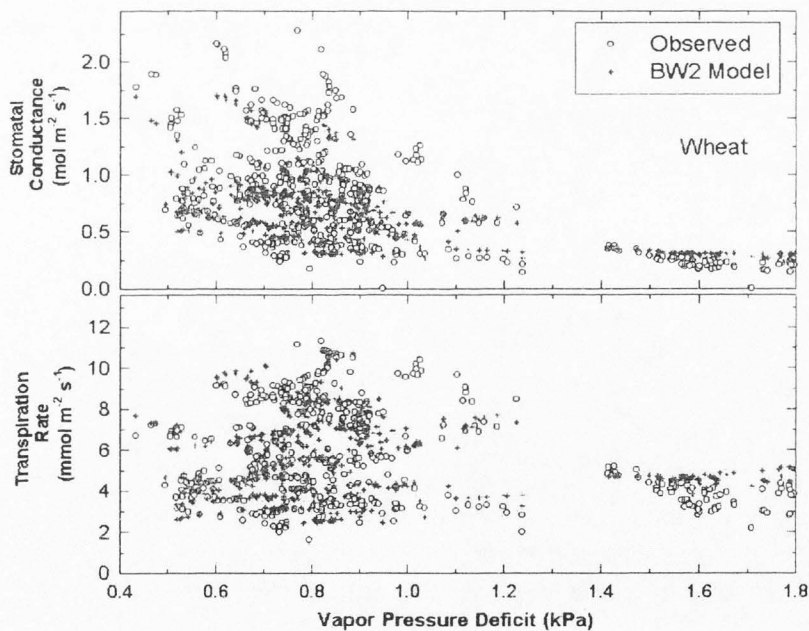


Figure 4.7 A comparison between predicted vs. observed wheat canopy stomatal conductance (A) and transpiration rate (B) as a function of vapor pressure deficit. The wheat BW2 model performed reasonably well, and it did not distort the responses of canopy G_s and transpiration to VPD contained in the wheat validation data set.

data set used to obtain the fGs function or by experimental errors in the measurement of chamber air temperature.

The performance of the AJ soybean model in predicting transpiration in another chamber system was evaluated against a data set collected in the Biomass Production Chamber (BPC) at the NASA Kennedy Space Center (Fig. 4.8). The AJ model (predictive ranking #2; Table 4.5) was used to predict transpiration from a soybean canopy using inputs from the BPC, which is vastly different than the growth chambers we used to parameterize and validate the AJ model. The AJ model was used because only a limited data set was available. The data set included daily measurements of canopy photosynthesis (Fig. 4.8A), dark respiration, and transpiration from a 20 m² soybean crop. The soybean variety 'McCall' used in the BPC was different from the 'Hoyt' variety used to develop the AJ model, and the BPC canopy was grown using the nutrient film technique. The model essentially calculated transpiration rates from P_{net}, C_s, D_s, and T_{canopy} (Equation 14), but since there was no canopy temperature available, it was assumed that it was +1 °C higher than T_{air} in the day and -0.5 °C lower in the dark. The transpiration was greatly overestimated (318 liters; +62.7%) during days 11-30, then it was underestimated (370 liters; -14.3%) between days 30-55, and the model overestimated the overall amount of water transpired by 6.1% (days 11-92). These results are encouraging and they indicate that reasonable predictions are possible in other chamber systems if more pertinent environmental and plant growth data were available.

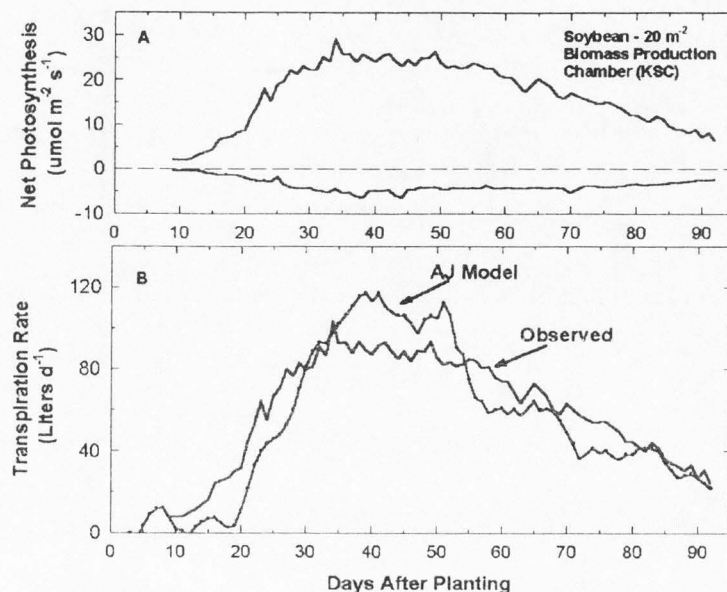


Figure 4.8 Soybean canopy photosynthesis and dark respiration (A) measured in the 20 m² Biomass Production Chamber (BPC) at the Kennedy Space Center. The C flux data plus additional environmental information was used to predict transpiration (B) using the soybean AJ model (model rank #2; Table 4.5). The model overestimated average life cycle transpiration in the BPC by 6.1%.

Conclusions

The transpiration models developed in this study differ from the majority of the existing canopy transpiration models because canopy stomatal conductance is not calculated from leaf scale measurements. The models are based on and were calibrated with canopy-scale measurements. The predictive accuracy of these models was evaluated using a statistical procedure for evaluating model predictive validity. The degree of model complexity was also determined for each model. The transpiration models using the Penman-Monteith equation gave slightly better predictions of transpiration than the Ohm's Law analog model in both wheat and soybean canopies. Although the best predictive canopy G_s models were the BW2

model for wheat and the AJ2 model for soybean, the BWB model was ranked as the best model for predicting canopy stomatal conductance since it is the simplest and because its predictive accuracy is comparable to the best predictive models in both species.

References

- Aphalo PJ, Jarvis PG.** 1993. An analysis of Ball's empirical model of stomatal conductance. *Annals of Botany* **72**, 321-327.
- Ball JT, Woodrow IE, Berry JA.** 1987. A model predicting stomatal conductance and its contribution to the control of photosynthesis under different environmental conditions. In: Biggens J, ed. *Progress in Photosynthesis Research*. The Hague: Martinus Nijhoff Publishers, 221-224.
- Bugbee B, Monje O.** 1992. The limits of crop productivity. *BioScience* **42**, 494-502.
- Choudhury BJ, Idso SB.** 1985. An empirical model for stomatal resistance of field-grown wheat. *Agricultural and Forest Meteorology* **36**, 65-82.
- Cochran WG, Cox GM.** 1957. *Experimental designs*. New York: John Wiley and Sons.
- Collatz GJ, Ball JT, Grivet C, Berry JA.** 1991. Physiological and environmental regulation of stomatal conductance, photosynthesis and transpiration: a model that includes a laminar boundary layer. *Agricultural and Forest Meteorology* **54**, 107-136.
- De Pury DGG, Farquhar GD.** 1995. Simple scaling of photosynthesis from leaves to canopies without the errors of big-leaf models. *Plant, Cell and Environment* **20**, 537-557.
- Evans JR, Farquhar GD.** 1991. Modelling canopy photosynthesis from the biochemistry of the C₃ chloroplast. In: Boote KJ, Loomis RS, eds. *Modelling crop photosynthesis from biochemistry to canopy*. CSSA Special Publication Number 19. Madison: Crop Science Society of America, Inc., 1-16.
- Farrar JF, Williams ML.** 1991. The effects of increased atmospheric dioxide and temperature on carbon partitioning, source-sink relations and respiration. *Plant, Cell and Environment* **14**, 819-830.
- Harley PC, Thomas RB, Reynolds JF, Strain BR.** 1992. Modelling photosynthesis of cotton grown in elevated CO₂. *Plant, Cell and Environ.* **15**, 271-282.

- Hilborn R, Mangel M.** 1997. *The ecological detective: confronting models with data.* Princeton: Princeton University Press, 159-160.
- Jarvis PG.** 1976. The interpretation of the variations in leaf water potential and stomatal conductance found in canopies in the field. *Philosophical Trans. Of the Royal Soc. London.* **273B**, 593-610.
- Jones HG.** 1992. *Plants and microclimate: A quantitative approach to environmental plant physiology* New York: Cambridge University Press.
- Leuning R.** 1995. A critical appraisal of a combined stomatal-photosynthesis model for C₃ plants. *Plant, Cell and Environment* **18**, 339-357.
- Long SP.** 1991. Modification of the response of photosynthetic productivity to rising temperature by atmospheric CO₂ concentrations: has its importance being underestimated? *Plant, Cell and Environ.* **14**, 729-739.
- Monje O, Bugbee B.** 1996. Characterizing photosynthesis and transpiration of plant communities in controlled environments. *Acta Hort. ISHS. 1996* **440**, 123-128.
- Monje O, Bugbee B.** 1998. Adaptation of plant communities to elevated CO₂: radiation capture, canopy quantum yield, and carbon use efficiency. *Plant, Cell, and Environment.* **21**, 315-324.
- Mott KA, Parkhurst DF.** 1991. Stomatal response to humidity in air and in helox. *Plant, Cell and Environment* **14**, 509-515.
- Power M.** 1993. The predictive validation of ecological and environmental models. *Ecological Modelling* **68**, 33-50.
- Raupach MR, Finnigan JJ.** 1988. Single layer models of evaporation from plant canopies are incorrect but useful, whereas, multilayer models are correct but useless: Discuss. *Australian Journal of Plant Physiology* **15**, 705-716.
- Sage RF.** 1990. A model describing the regulation of ribulose-1,5-bisphosphate carboxylase, electron transport, and triose phosphate use in response to light intensity and CO₂ in C₃ plants. *Plant Physiology* **94**, 1728-1734.
- Sellers PJ, Berry JA, Collatz GJ, Field CB, Hall FG.** 1992. Canopy reflectance, photosynthesis and transpiration. III. A reanalysis using improved leaf models and a new canopy integration scheme. *Remote Sensing Environment* **42**, 187-216.

Smart DS, Chatterton NJ, Bugbee BG. 1994. The influence of elevated CO₂ on fructan synthesis in intact wheat canopies. *Plant, Cell and Environment* **17**, 435-442.

Valentini R, Gamon JA, Field CB. 1995. Ecosystem gas exchange in a California grassland: Seasonal patterns and implications for scaling. *Ecology* **76**, 1940-1952.

Whitfield DM. 1990. Canopy conductance, carbon assimilation and water use in wheat. *Agricultural and Forest Meteorology* **53**, 1-18.

CHAPTER 5

SUMMARY AND CONCLUSIONS

Abstract

The purpose of this study was to develop a model for predicting canopy transpiration rates (Tr) of wheat and soybean in controlled environments. The Tr model could serve as a diagnostic tool for the design of plant growth chambers in spacecraft and in other controlled environment applications. The approach used in this study employed simultaneous measurements of canopy transpiration (Tr), photosynthesis (P_{net}), canopy temperature (T_{canopy}) referenced to air temperature (T_{air}), and net radiation (R_{net}) to calibrate eight models for predicting the response of canopy stomatal conductance (G_s) to environmental conditions typically found in controlled environments. These measurements allowed us to solve the energy balance equation exactly, and to determine sensible heat flux (H) by subtraction from the energy balance equation ($H = R_{net} - LE - P_{net}$). Several technical difficulties associated with the determination of the aerodynamic conductance (g_A) in plant growth chambers and the measurement of canopy temperature using infrared transducers were also resolved. The algorithms for calculating G_s were then incorporated into a model based on the Penman-Monteith equation to predict Tr . The algorithms with the best predictive validity were selected, and model sensitivity to input parameters was determined using statistical methods. This effort resulted in the development of several experimental methods for measuring G_s in controlled environments, as well as in the validation of eight predictive models of canopy G_s . These models were ranked by their predictive validity, and by their degree of complexity. The

single model for simulating G_s in wheat and soybean that met these criteria was the BWB model. The best predictive models for each crop were then used to simulate the response of canopy G_s to vapor pressure deficit (VPD) and CO_2 concentration, and the simulations were compared against observed data.

*Measurement of canopy temperature
and aerodynamic conductance*

The goals of the research outlined in Chapter 2 were to compute canopy G_s from direct measurements of canopy surface conductance (G_c), to explore the relation between radiative (ΔT_{IR}) and aerodynamic (ΔT_A) canopy-air temperature differences, and to quantify the degree of coupling between canopy Tr and G_s in controlled environments. G_c was determined from direct measurements of Tr and the canopy-air vapor pressure gradient. Plots of canopy H versus (ΔT_{IR}) were used to calculate the chamber aerodynamic conductance, g_A , which was used to calculate G_s from G_c . This approach was used because it was not possible to use the log-wind profile approximation to determine chamber aerodynamic conductance, as is typically done in the field (Hatfield, 1985). The degree of coupling between Tr and G_s was determined from the ratio between G_s and g_A , and quantified by the decoupling coefficient, Ω (Jarvis and McNaughton, 1986).

A consistent offset between the radiative T_{canopy} (measured with infrared transducers) and the aerodynamic T_{canopy} (determined from sensible heat flux measurements) was found. Comparisons between within-the-canopy air temperature profile and the profile in radiative T_{canopy} , obtained by placing the infrared transducer at several depths within the canopy,

suggest that the aerodynamic ΔT_A is being determined by the energy balance of all the leaf layers of the canopy, and that the difference between the radiative and the aerodynamic canopy temperatures exists because infrared transducers measure mostly leaf temperatures from the uppermost layers of the canopy. This finding is corroborated by measurements of radiative canopy temperatures in the dark, suggesting that the infrared transducers view mostly the upper, warmer leaf layers. Thus, although infrared transducer output is weighted towards the center of their field of view where they would 'see' deeper into the canopy, they are probably not seeing enough depth to accurately represent the true T_{canopy} profile. Another finding was that the offset between radiative and aerodynamic T_{canopy} also depends on incident photosynthetic photon flux (PPF), which results because the canopy temperature profile also varies with the incident PPF.

The failure of the uncorrected infrared transducer measurements to give the appropriate aerodynamic T_{canopy} may result in positive canopy-air temperatures when the actual sensible heat flux is negative. However, the radiative T_{canopy} can still be used to determine the correct g_A needed for determining G_s , and to calculate the appropriate offset correction to determine the aerodynamic T_{canopy} that solves the energy balance equation. The chamber g_A for wheat ($5.5 \text{ mol m}^{-2} \text{ s}^{-1}$ or 0.14 m s^{-1}) and for soybean ($2.5 \text{ mol m}^{-2} \text{ s}^{-1}$ or 0.06 m s^{-1}) canopies is slightly higher than the range of typical values of aerodynamic conductances of field crops (ranging from $3.2\text{-}10 \text{ mol m}^{-2} \text{ s}^{-1}$ or $0.08\text{-}0.25 \text{ m s}^{-1}$; O'Toole and Real, 1986). These values suggest that the conditions in the chamber correspond to highly turbulent, windy conditions in the field.

Canopy stomatal conductance

The canopy G_s for wheat at $400 \mu\text{mol mol}^{-1} \text{CO}_2$ ($2.08 \text{ mol m}^{-2} \text{s}^{-1}$) in this study is similar to field canopy G_s values ($1.82 \text{ mol m}^{-2} \text{s}^{-1}$; Hatfield, 1985) at sea level, under optimal available soil water. Soybean canopy G_s was $1.08 \text{ mol m}^{-2} \text{s}^{-1}$, nearly one-half the values found in wheat, probably due to less leaf area and the lower growth PPF of the soybean canopy. Soybean canopy G_s was also slightly higher than typical conductances measured in field crops (O'Toole and Real, 1986). The decoupling coefficient measured in our chambers was similar to field values. These results suggest that the approach developed in this study for estimating canopy G_s from surface G_c measurements in controlled environments yields values of similar magnitude to conductances reported in field studies.

A major finding in this study was that G_s of hydroponically-grown plants in the dark was high, unlike the low G_s typically observed at night in field conditions. In the dark, wheat G_s ranged from $0.2\text{-}0.5 \text{ mol m}^{-2} \text{s}^{-1}$ and soybean G_s ranged from $0.2\text{-}0.3 \text{ mol m}^{-2} \text{s}^{-1}$. Although these values of G_s in the dark are small compared to daytime G_s , they resulted in large Tr rates since the gradient for water loss was greater at night. This occurred because chamber humidity could not be controlled sufficiently to prevent it from falling during the dark period. Thus, a significant amount of water was transpired since the canopy spent a large portion of the day in darkness. This became apparent when canopy Tr was measured in wheat for an entire life cycle (Fig. 5.1A). The ratio of dark:light transpiration rose from 0.6 early in the life cycle to nearly 0.8 as the canopy matured (Fig. 5.1B). The evaporative cooling at night

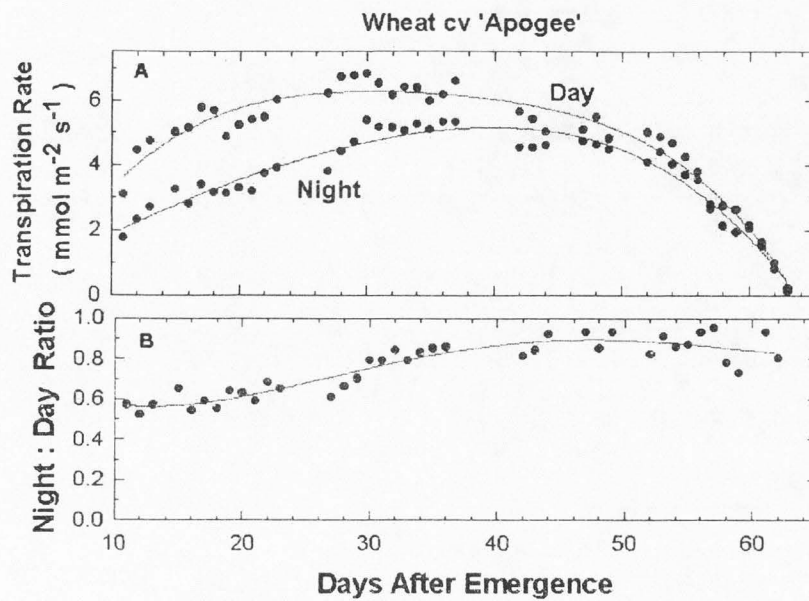


Figure 5.1 (A) Average daytime and nighttime canopy transpiration rates measured for the life cycle of a wheat (cv. Apogee) crop. (B) The ratio of nighttime to daytime transpiration rate increases as the life cycle progresses.

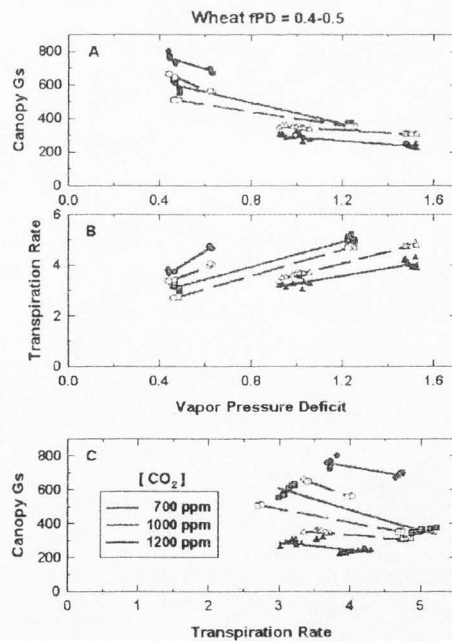


Figure 5.2 Canopy G_s (A), Tr (B), and G_s vs. Tr (C) as a function of vapor pressure deficit (VPD) measured at 700 (red), 1000 (green), and 1200 (blue) $\mu\text{mol mol}^{-1}$ CO_2 . The measurements were made in two successive days at the same time of day. The predicted (dashed lines) response to vapor pressure deficit follows the observed (solid line) values. Canopy G_s was found to decrease as Tr increased (C).

caused plant temperature to be several degrees lower than air temperature measured above the canopy, and sensible heat flux warmed the canopy at night.

The coupling coefficient (Chapter 2) indicates the amount of feedback between stomatal conductance and the saturation deficit within the chamber. It is a measure of how well canopy G_s obtained in our system may apply to other systems, such as field conditions or other chambers. We found that feedback indeed occurs in our chambers, that the amount of feedback is reduced in elevated CO_2 , and that the coupling coefficient became larger as g_A increased. The coupling coefficient in soybean was lower than in wheat, probably because the lower wind speeds above the soybean canopy resulted in a smaller chamber g_A . The coupling for the soybean canopy approaches values observed in field studies, where small changes in G_s have little effect on canopy transpiration, and transpiration is dominated by net radiation (Meinzer and Grant, 1989).

Diurnal fluctuations in canopy stomatal conductance

Canopy G_s of well-watered canopies decreased diurnally at constant PPF and CO_2 by 20-30% from the beginning to the end of the photoperiod (Chapter 3). Although these diurnal fluctuations in stomatal conductance have been observed in field experiments (Körner, 1995), and in trees (Meinzer *et al.*, 1993), they have not been possible to quantify in the field. In field conditions, large diurnal fluctuations in PPF, VPD, and T_{air} confound the diurnal patterns of stomatal conductance. However, these patterns are readily observed in CEs when environmental parameters are held constant. This repeatable diurnal decrease in G_s was of

great importance in this study because it influenced how data were collected during the development of the Tr model, as it was not possible to obtain environmental response curves in a single day. This diurnal pattern resulted in the collection of 'whole-day' data points to obtain CO₂ or PPF response curves. Thus, data collection of response curves was limited to periods of the life cycle with relatively constant growth rates, in order to avoid confounding effects caused by changes in ontogeny.

The magnitude of the diurnal decrease in the G_s of wheat and soybean depended on the ambient CO₂ concentration to which the canopy was exposed. Higher ambient CO₂ concentrations increased the magnitude of the diurnal reductions, and caused them to begin earlier in the photoperiod. The diurnal patterns in G_s were similar in wheat and soybean. The magnitude of the diurnal reductions in G_s became more pronounced as CO₂ was increased. In wheat, the effect of CO₂ saturates after 900 μmol mol⁻¹, but the pattern in soybean appeared to saturate after CO₂ concentration was raised above 600 μmol mol⁻¹.

The responses of these diurnal fluctuations to CO₂ concentration were used to study competing explanations of the mechanisms controlling canopy G_s. In elevated CO₂, smaller diurnal reductions in G_s are expected if stomatal aperture is primarily being determined by leaf and stem water status because Tr is reduced, which results in a more favorable leaf water potential. Leaf water potential reflects the diurnal status of water reserves within the plant responsible for supplying the transpiration stream. In field conditions, plant water reserves are replenished from soil water during the night, the transpiration stream depletes these reserves in the day, and the stomata are not affected until a critical leaf water potential is reached. This

hypothesis argues that reduced stomatal conductance in elevated CO_2 would cause a slower depletion of the water reserves within the leaves and stems of the canopy (Lynn and Carlson, 1990), and the critical water potential at which stomatal closure was triggered would occur after longer times into the photoperiod as chamber CO_2 increased.

On the other hand, we would expect no attenuation in the diurnal course of G_s at low chamber CO_2 concentrations (i.e., $400 \mu\text{mol mol}^{-1}$) if stomatal aperture is controlled by the sugar accumulation hypothesis proposed by Lu *et al.* (1997). This competing hypothesis argues that G_s would remain constant until sufficient sucrose accumulated on guard-cell walls to elicit stomatal closure. Since net photosynthesis also increases as CO_2 concentration is increased, we would expect that stomatal closure occurs earlier in the photoperiod at $600 \mu\text{mol mol}^{-1}$ than at $400 \mu\text{mol mol}^{-1}$ because sucrose accumulation in the guard-cell walls would occur at a faster rate. Then, at even higher CO_2 concentrations (i.e., $>900 \mu\text{mol mol}^{-1}$), apoplastic sucrose would always be sufficiently high as photosynthesis is maximal such that stomatal aperture would be permanently reduced compared to lower levels of CO_2 enrichment.

The data measured in this study support the sugar accumulation hypothesis as the primary cause of the observed diurnal reduction of G_s . However, diurnal measurements of leaf water potential were not made in this study and although the sugar accumulation hypothesis appears to explain the observed data, further study is warranted. The results from this study suggest that diurnal patterns in leaf and stem carbohydrate concentrations, leaf water potentials, and canopy and foliar stomatal conductances should be measured

simultaneously at several CO₂ concentrations. Such data should help further clarification of the mechanisms controlling the diurnal patterns in G_s we observed in soybean and wheat.

The diurnal fluctuations in G_s also affect the relation between G_s and Tr. If G_s collected during the course of a day in constant environmental conditions is plotted against Tr, then G_s appears to *increase* in response to an increase in Tr. However, this is an artifact caused by diurnal rhythms and Tr decreases because G_s declines as the day progresses. The diurnal rhythm distorts the response of G_s to Tr, which normally declines in response to increasing Tr, except under very dry atmospheres Tr decreases because G_s declines (Monteith, 1995). The traditional decrease in G_s as Tr increases was observed only when G_s measured at different VPDs was compared *at the same fraction* of the photoperiod (Fig. 5.2). These results underscore the importance of characterizing the diurnal patterns of canopy stomatal conductance in transpiration studies conducted in controlled environments.

Model development and validation

The Tr model was developed by calibrating eight separate stomatal conductance models with canopy G_s measurements, and using the predicted G_s to calculate Tr, and the energy balance components (Chapter 4). The models were calibrated using an independent data set from the data set used in the validation procedure. Model calibration was accomplished by parameterizing responses of wheat and soybean canopies to short-term (hours to one day) environmental changes. The calibrated stomatal conductance models were incorporated into a canopy transpiration model based on the Penman-Monteith equation. Sensitivity analyses was conducted to test the relative importance of both environmental and

stomatal factors in determining transpiration rates. Model inputs were ranked with respect to their effect on transpiration and the precision required in specifying model inputs was determined. This analysis suggests that input variables such as CO₂ concentration, relative humidity, and air temperature must be accurately determined to better than $\pm 10\%$ since this results in significant changes in Tr.

The validation procedure of Power (1983) was used to select the best predictive models, and model complexity was ranked using the Akaike information criterion (Hilborn and Mangel, 1997). The models were validated against independent transpiration data sets obtained in the same chamber and several statistics were used to rank the models according to their ability to simulate canopy transpiration. In wheat, the modified Ball-Woddrow-Berry (BWB) models appear to overpredict at lower values of stomatal conductance, while the Aphalo-Jarvis (AJ) models underpredict stomatal conductance. In soybean, the best models are the AJ-type models but they fail to give accurate predictions of stomatal at the higher values of stomatal conductance. The best predictive wheat model (BW2) included a time-dependent fG_s parameter, whereas the best soybean (AJ2) model did not. The model with the lowest complexity and which ranked third in predictive validity was the BWB model. This was the only canopy G_s model that predicted canopy G_s equally well in wheat and soybean.

The calibrated soybean AJ model was used to predict data from inputs collected in another chamber. This was a critical test since the usefulness of the model will depend on the validity of its predictions in different chamber systems. The cumulative amount of transpired water of a 20 m² chamber was predicted using life cycle canopy photosynthesis measurements

and nominal values for humidity, PPF, and air temperature. Although the model predicted the total amount of transpired water to within 6% of the observed amount, there were large discrepancies (up to 60% from the observed transpiration rates) during the early period of crop growth. However, it was not possible to determine if these differences were due to errors in the model inputs or due to measurement errors in the observed transpiration rates themselves. Nevertheless, we found that the soybean model performed well and that it will be useful for simulating transpiration in other environmental scenarios in the 20 m² chamber.

Canopy responses to environment

The calibrated models were used to explore the response of canopy G_s and Tr to two dominant environmental factors: vapor pressure deficit and atmospheric CO_2 concentration. As in most experiments, the response of stomata to environmental changes was simulated by varying either VPD or CO_2 concentration independently while maintaining the other variables constant. The models employed the canopy photosynthesis routine (Chapter 4) for the stomatal conductance models because net photosynthesis measurements were not available to conduct these simulation experiments.

We first examined canopy responses in wheat (Fig. 5.3a, b) subjected to changes in VPD at two PPF levels (600 and 1400 $\mu\text{mol m}^{-2} \text{s}^{-1}$). The VPD was changed by altering relative humidity from 50-85%, while maintaining T_{air} (23 °C), CO_2 concentration (400 $\mu\text{mol mol}^{-1}$), and fraction of the photoperiod ($fPD = 0.2$) constant. The wheat BW2 model predicts that canopy G_s and Tr increase at the higher PPF, but it also predicts a linear decrease in G_s as VPD increased in contrast to the exponential relation that is typically observed (Jones,

1998). Modeled T_r increased as VPD increased (Fig. 5.3b), and the relation between G_s and T_r from the VPD experiment depicts the expected decline in G_s as T_r increases (Fig. 5.3c).

A similar simulation was conducted in soybean with the AJ2 model. The predicted response was compared to actual experimental results to evaluate how well the model predicts the humidity response of G_s at four CO_2 concentrations (400, 600, 800, and 1200 $\mu\text{mol mol}^{-1}$). The results were similar to the wheat simulation, the observed response in G_s shows an exponential decrease with VPD (Fig. 5.4a), but the model predicts a linear decrease in response to increased VPD (Fig. 5.4b). This linear response of canopy G_s to increasing VPD is probably caused by the inability of the photosynthesis routine to capture the reduction in P_{net} as VPD increases due to decreasing stomatal conductance. The observed diurnal courses in canopy G_s , P_{net} , T_r , T_{canopy} , and VPD (expressed as a function of the photoperiod, fPD) for the soybean experiment are shown in Fig. 5.5a-e. Soybean canopy G_s initially increased during the first part of the photoperiod and then it declined for the remainder of the day. G_s responded strongly to increasing CO_2 concentrations, especially between 400 and 600 $\mu\text{mol mol}^{-1}$ (Fig. 5.5a). Canopy P_{net} reached its maximum at the beginning of the photoperiod, and declined slightly as the day progressed, probably due to the decrease in G_s (Fig. 5.5b). Generally, canopy T_r decreased, T_{canopy} increased, and chamber VPD decreased at the higher CO_2 concentrations (Fig. 5.5c-e). These trends continued as the photoperiod progressed, for example, the canopy became hotter and chamber VPD increased as evaporative cooling decreased diurnally. Canopy T_r remained identical between 400 and 600

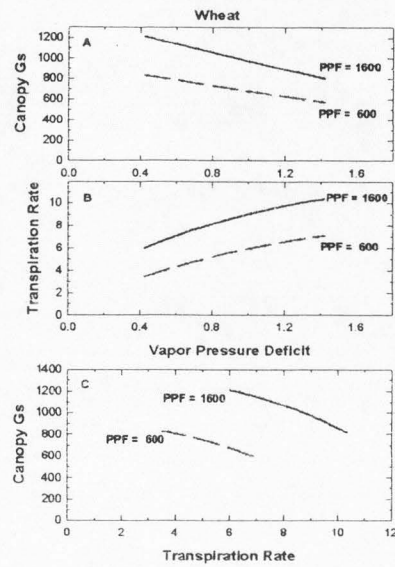


Figure 5.3 Simulated canopy G_s (A), Tr (B), and G_s vs. Tr (C) as a function of vapor pressure deficit at two PPF levels (600 and 1400 $\mu\text{mol m}^{-2} \text{s}^{-1}$). The VPD was changed by altering relative humidity from 50-85%, while maintaining T_{air} (23°C), CO_2 concentration ($400 \mu\text{mol mol}^{-1}$), and fraction of the photoperiod ($f_{\text{PD}} = 0.2$) constant. The wheat BW2 model predicts that canopy G_s and Tr increase at the higher PPF, but it also predicts a linear decrease in G_s as VPD increased in contrast to the exponential relation that is typically observed. Modeled Tr increased as VPD increased, and the relation between G_s and Tr from the VPD experiment depicts the expected decline in G_s as Tr increases (C).

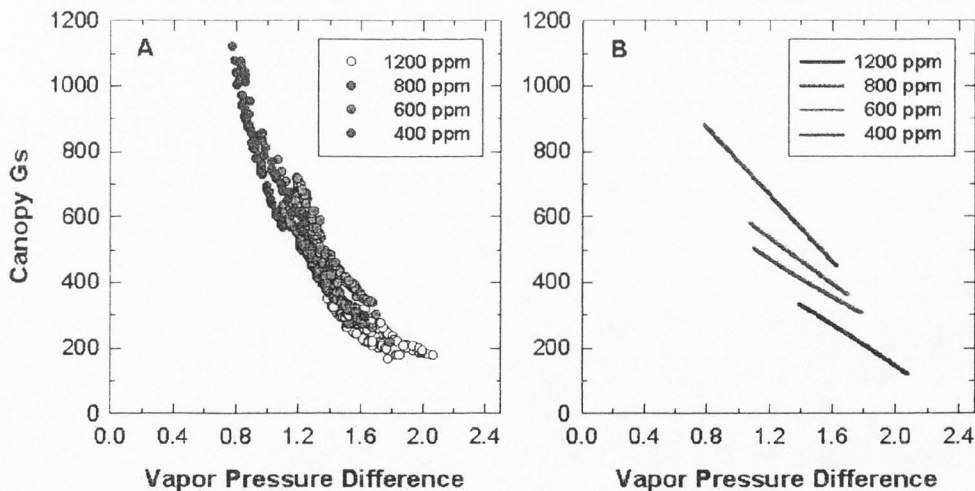


Figure 5.4 Observed (A) and simulated (B) canopy G_s in soybean at four CO_2 concentrations (400, 600, 800, and 1200 $\mu\text{mol mol}^{-1}$). The results were similar to the wheat simulation, the observed response in G_s shows an exponential decrease with VPD, but the model predicts a linear decrease in response to increased VPD.

$\mu\text{mol mol}^{-1}$, cooling decreased diurnally. Canopy Tr remained identical between 400 and 600 $\mu\text{mol mol}^{-1}$, even though canopy G_s was almost doubled, because chamber VPD increased by about 1 kPa and the gradient for transpiration was reduced.

The modeled diurnal courses in canopy G_s , P_{net} , Tr , T_{canopy} , and VPD for the soybean experiment are shown in Fig. 5.6a-e. The inputs used in the simulation were PPF, the fraction of PPF absorbed, CO_2 concentration, relative humidity, T_{air} , aerodynamic conductance, and the time of day. Curves for diurnal course of G_s have similar shapes to those in Fig 5.5a, although the model predicts a flatter response and lower values of G_s than was observed, especially at 400 $\mu\text{mol mol}^{-1}$. The modeled values of P_{net} as a function of CO_2 concentration are similar to the observed data; however, the model again does not predict the observed diurnal decline in P_{net} (Fig 5.5b). This suggests that the canopy photosynthesis model algorithm does not adequately couple net photosynthesis and stomatal conductance. The model reproduces key features in the data such as: 1) the relative differences in canopy Tr as CO_2 concentration increases (Fig 5.5c), 2) the similarity in the shapes of the curves for the diurnal course in canopy Tr , and 3) the relative differences in T_{canopy} and chamber VPD as the day progresses. Although the modeled diurnal course of G_s is similar to the observed trend, there is a large discrepancy in the absolute values of G_s . Although the AJ2 soybean model consistently underpredicted G_s , even when the actual P_{net} was used as an input during the validation procedure (Chapter 4), the model predicts values of canopy Tr comparable to the observed data.

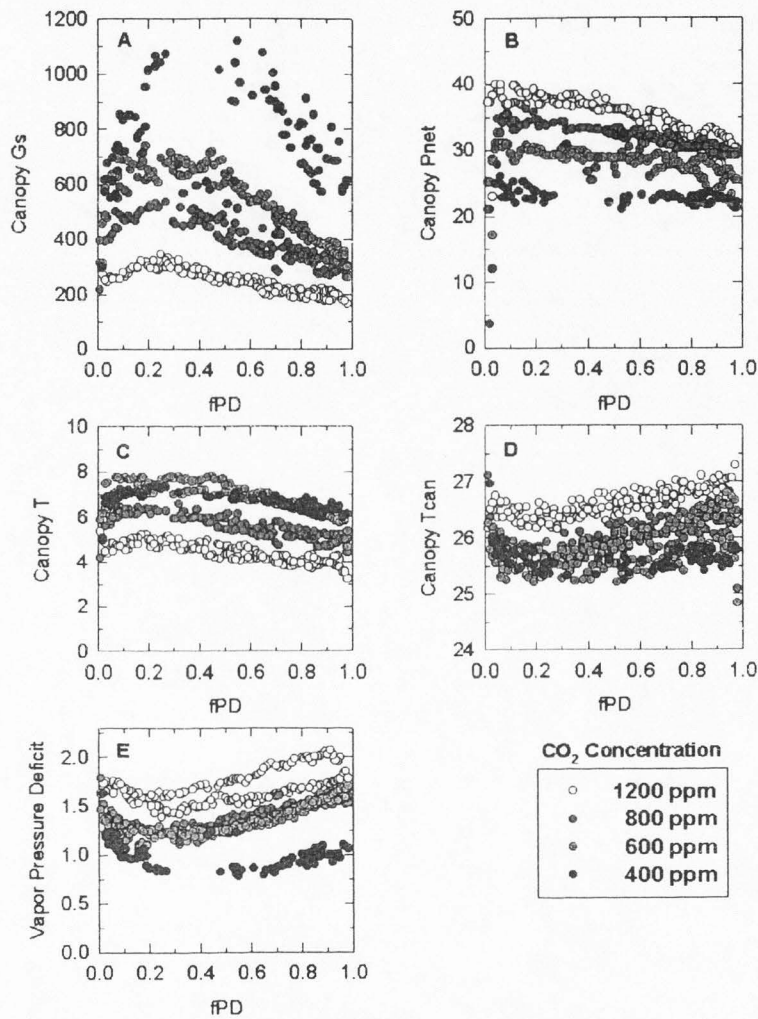


Figure 5.5 The observed diurnal courses in canopy G_s (A), P_{net} (B), T_r (C), T_{canopy} (D), and chamber VPD (E) as a function of the photoperiod (fPD) for the soybean experiment described in Fig. 5.4. Soybean G_s initially increased during the first part of the photoperiod and then it declined for the remainder of the day. G_s responded strongly to increasing CO_2 concentrations, especially between 400 and 600 $\mu mol mol^{-1}$. Canopy P_{net} reached its maximum at the beginning of the photoperiod, and declined slightly as the day progressed. Canopy T_r decreased, T_{canopy} increased, and chamber VPD decreased at the higher CO_2 concentrations.

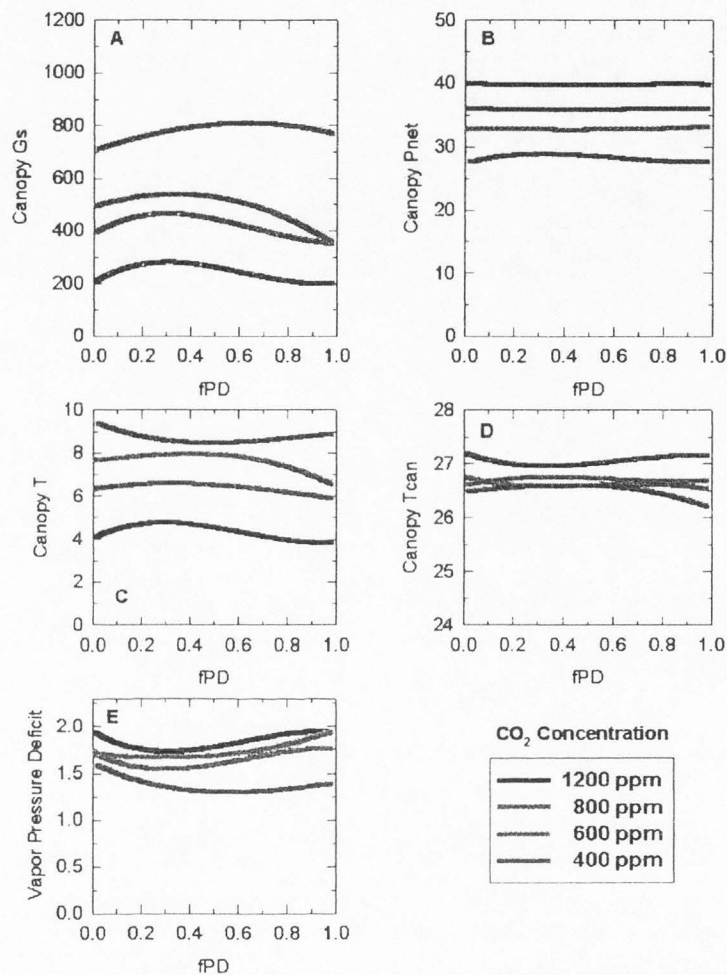


Figure 5.6 The simulated diurnal courses in canopy G_s (A), P_{net} (B), T_r (C), T_{canopy} (D), and chamber VPD (E) as a function of the photoperiod (fPD) for the soybean experiment described in Fig. 5.4. The inputs used in the simulation were PPF, the fraction of PPF absorbed, CO_2 concentration, relative humidity, T_{air} , aerodynamic conductance, and the time of day. The modeled curves for diurnal course of G_s have similar shapes to the observed data, although a flatter response and lower values of G_s than observed are predicted. The modeled values of P_{net} as a function of CO_2 concentration are similar to the observed data, but the model does not predict the observed diurnal decline in P_{net} .

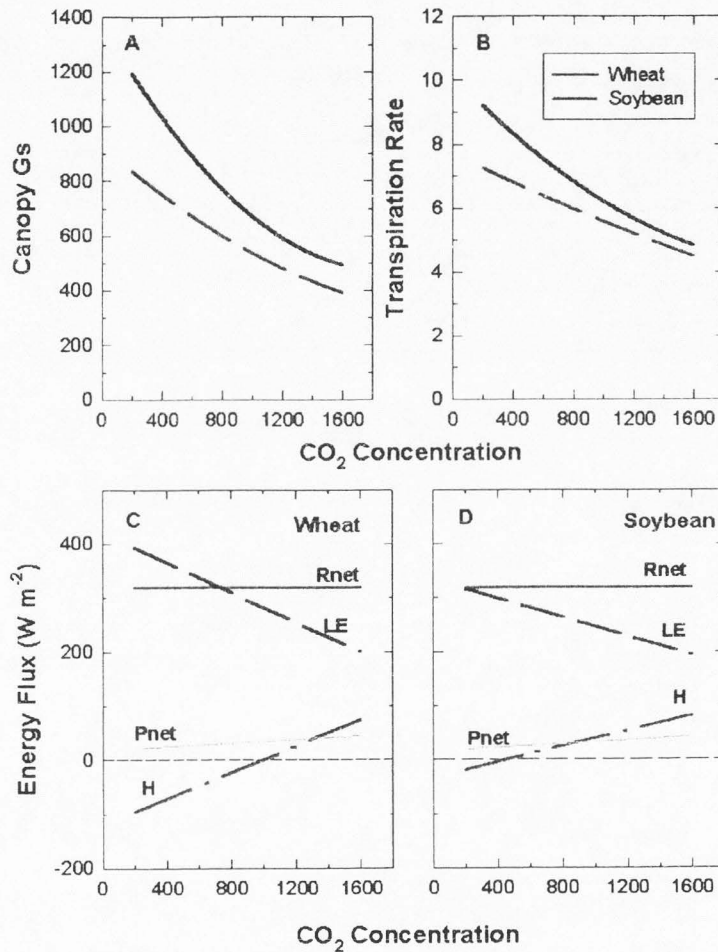


Figure 5.7 The responses of daytime wheat and soybean G_s (A) and Tr (B) to CO_2 concentration at a PPF of $1400 \mu\text{mol m}^{-2} \text{s}^{-1}$ were simulated with the same inputs as in the wheat experiment. (Fig. 5.3). The model predicts higher G_s and Tr in wheat compared to soybean, and nonlinear relation between G_s and T with increasing CO_2 concentration. The CO_2 response of the energy balance components for wheat (C) and soybean (D).

The response of daytime wheat and soybean G_s to CO_2 concentration at a PPF of $1400 \mu\text{mol m}^{-2} \text{s}^{-1}$ was simulated with the same inputs as in the wheat experiment of Fig. 5.3. Although soybean would never be grown at this high, constant PPF, we can use the model to simulate what we might observe under these conditions. Another concern is that the model cannot predict the effects of long-term acclimation to CO_2 enrichment and therefore does not take into account changes in number or frequency of stomata, nor considers adaptive changes in leaf area (Morison, 1998). The model predicts that wheat has a higher G_s and Tr than soybean and that both species exhibit nonlinear decreases in G_s and Tr when exposed to increasing CO_2 concentration (Fig. 5.7a, b). The CO_2 response of the energy balance components for each species is shown in Figs. 7c and 7d. The model predicts that latent heat flux (LE) decreases in both species resulting in an increase in H as CO_2 concentration rises. Thus, the wheat canopy is warmer than air temperature after $800 \mu\text{mol mol}^{-1}$, while soybean canopy temperature is below air temperature only at below $400 \mu\text{mol mol}^{-1}$. This simulation shows how radiant energy from the lamps may be partitioned within a growth chamber for each plant species, and how this partitioning is affected by changes in ambient CO_2 concentration. This type of information is what is needed for the design of plant growth chambers in controlled environment applications.

Conclusions

The models developed in this study differ from the majority of the existing canopy Tr models because canopy G_s is not calculated from leaf scale measurements. Instead, it is derived from measurements of surface conductance and the chamber aerodynamic

conductance. Several technical difficulties associated with the determination of the aerodynamic conductance in plant growth chambers and the measurement of T_{canopy} using infrared transducers were resolved for this purpose. Simultaneous measurements of canopy T_r , P_{net} , T_{canopy} referenced to T_{air} , net radiation, and sensible heat flux were used to develop and to calibrate eight separate models of canopy G_s with data collected in controlled environments. The algorithms for calculating G_s were then incorporated into a transpiration model based on the Penman-Monteith equation and used to predict T_r . The best predictive models for wheat and soybean were selected from this suite of models using a statistical procedure for evaluating model predictive validity. The best predictive canopy G_s models were the BW2 model for wheat and the AJ2 model for soybean. However, the simplest model was the BWB model, which required only two empirical parameters to model canopy G_s for wheat and soybean equally well.

Simulation experiments were used to explore the response of canopy G_s to VPD and CO_2 concentration. The inputs used in these simulations were PPF, the fraction of PPF absorbed, CO_2 concentration, relative humidity, T_{air} , aerodynamic conductance, and the time of day. Canopy photosynthesis, used in the stomatal conductance models, was modeled because net photosynthesis measurements were not available to conduct these simulation experiments. The wheat and soybean models predicted a linear decrease in G_s as VPD increased in contrast to the exponential relation that is typically observed. However, this was not observed during the model validation phase (Chapter 4), which used measured values of canopy photosynthesis. This suggests that the canopy photosynthesis model algorithm does

not adequately couple net photosynthesis and stomatal conductance. Nevertheless, the model predicts an increase in T_r as VPD increases, and the expected decline in G_s as T_r increases. The model also reproduces key features in diurnal courses of canopy T_r as a function of CO_2 concentration increases, as well as relative differences in T_{canopy} and chamber VPD as the day progresses. Although the modeled diurnal course of G_s is similar to the observed trend, the calibrated models consistently underpredict the absolute values of G_s , yet they predict values of canopy T_r comparable to the observed data. These results suggest that the models developed in this study will be useful diagnostic tools for the design of controlled environment chambers because they predict canopy stomatal behavior that is consistent with data measured in controlled environments.

References

- Hatfield JL.** 1985. Wheat canopy resistance determined by energy balance techniques. *Agronomy Journal* **77**, 279-283.
- Hilborn R, Mangel M.** 1997. *The ecological detective: confronting models with data*. Princeton: Princeton University Press, 159-160.
- Jarvis PG, McNaughton KG.** 1986. Stomatal control of transpiration: Scaling up from leaf to region. *Advances in Ecological Research* **15**, 1-49.
- Jones, HG.** 1998. Stomatal control of photosynthesis and transpiration. *Journal of Experimental Botany* **49**, 387-398.
- Körner Ch.** 1995. Leaf diffusive conductances in the major vegetation types of the globe. In: Schulze ED, Caldwell M.M., eds. *Ecophysiology of photosynthesis*: The Hague: Springer-Verlag, 463-490.
- Lu P, Outlaw WH Jr, Smith BG, Freed GA.** 1997. A new mechanism for the regulation of stomatal aperture size in intact leaves. *Plant Physiology* **114**, 109-118.

- Lynn BH, Carlson TN.** 1990. A stomatal resistance model illustrating plant vs. external control of transpiration. *Agricultural and Forest Meteorology* **52**, 5-43.
- Meinzer FC, Goldstein G, Holbrook NM, Jackson P, Cavelier J.** 1993. Stomatal and environmental control of transpiration in a lowland tropical forest tree. *Plant, Cell, and Environment* **16**, 429-436.
- Meinzer FC, Grant DA.** 1989. Stomatal control of transpiration from a developing sugarcane canopy. *Plant, Cell, and Environment* **12**, 635-642.
- Morison, JIL.** 1998. Stomatal response to increased CO₂ concentration. *Journal of Experimental Botany* **49**, 443-452.
- Monteith JL.** 1995. A reinterpretation of stomatal responses to humidity. *Plant, Cell and Environment* **18**, 357-364.
- O'Toole JC, Real JG.** 1986. Estimation of aerodynamic and crop resistances from canopy temperature. *Agronomy J.* **78**, 305-310.
- Power M.** 1993. The predictive validation of ecological and environmental models. *Ecological Modelling* **68**, 33-50.

CURRICULUM VITAE

OSCAR MONJE

Education

A.A.	New Mexico Military Institute	1980
B.S.	Utah State University, Chemistry	1984
M.S.	Utah State University, Plant Science Dept. (major area of study: Crop Physiology)	1993
Ph.D.	Utah State University, Plants, Soils, & Biomet. Dept (major area of study: Crop Physiology)	1998

Experience

Teaching Assistant, Plants, Soils & Biomet. Dept., USU,	1989-92
Research Assistant, Plants, Soils & Biomet. Dept., USU,	1992-93
Research Associate, Plants, Soils & Biomet. Dept., USU,	1993-97
Research Associate, Space Dynamics Lab, USU,	1997-98
Postdoctoral Fellow, Plants, Soils & Biomet. Dept., USU,	1998-present

Professional Memberships

American Society for Gravitational and Space Biology

Research Experience

Project Scientist on NASA SBIR 97-109.05 entitled "Moisture and O₂ Content Sensor Suite for Nutrient Delivery Systems". Funded by NASA through a subcontract from Orbital Technologies Corporation (ORBITEC) to the Space Dynamics Lab. 1998.

Research Associate on NASA cooperative agreement "Crop Production Optimization using CO₂ Gas-Exchange". 1995-1997.

Research Associate on grower funded project to study fungicide toxicity to crop plants. 1994-1995.

Research Associate on a NASA cooperative agreement to model carbon, water, and energy fluxes in crop plant canopies. 1994-1996.

Principal Investigator in USU Gas Away Special Program. Designed, built, and flew a biological flight experiment aboard STS-64. 1985-994.

Research Technician in EPA funded project to study the effects of UV radiation on photosynthesis. USU Range Science Department. 1984-1985.

Publications in Refereed Journals

Monje, O., G.E. Bingham, F.B. Salisbury, W.F. Campbell, J.G. Carman, B.K. Eames, V. Sytchev, M.A. Levinskikh, and I. Podolsky. 1998. Canopy Photosynthesis and Transpiration in Microgravity: Gas Exchange Measurements Aboard Mir. *Adv. In Space Res.* (In review).

Monje, O. and B. Bugbee. 1998. Adaptation to High CO₂ Concentration in an Optimal Environment: Radiation Capture, Canopy Quantum Yield and Carbon Use Efficiency. *Plant, Cell and Environment* 21:315-324.

Bugbee, B., M. Droter, **O. Monje**, and B. Tanner. 1997. Evaluation and Modification of Commercial Infra-red transducers for Leaf Temperature Measurement. *Adv. In Space Res.* (In press).

Monje, O. and B. Bugbee. 1996. Characterizing Photosynthesis and Transpiration of Plant Communities in Controlled Environments. *Acta Hort. ISHS* 440:123-128.

Bugbee, B., **O. Monje**, and B. Tanner. 1996. Quantifying Energy and Mass Transfer in Crop Canopies. *Adv. in Space Res.* 18:149-156.

Bugbee, B., B. Spanarkel, S. Johnson, **O. Monje**, and G. Koerner. 1994. CO₂ Crop Growth Enhancement and Toxicity in Wheat and Rice. *Adv. in Space Res.* 14:257-267.

Bugbee, B. and **O. Monje**. 1992. The Limits of Crop Productivity: Theory and Validation. *BioScience* 42:494-502.

Monje, O. and B. Bugbee. 1992. Inherent Limitations of Nondestructive Chlorophyll Meters: A Comparison of Two Types of Meters. *HortScience* 27:69-71.

Conference Proceedings

Monje, O., C.M.U. Neale, and R. Ahmed. 1997. Correction of Bi-directional Effects in Video Imagery. Proceedings of the 16th Biennial Workshop on Videography and Color Photography in Resource Assessment. Weslaco, TX.

McCormack, A., B. Bugbee, **O. Monje**, and R. Sirko. 1994. A Method for Modeling Transpiration in CELSS. Am. Inst. of Aeronautics and Astronautics 94-4573.

Published Abstracts

Monje, O., G.E. Bingham, F.B. Salisbury, W.F. Campbell, J.G. Carman, B.K. Eames, V. Sytchev, M.A. Levinskikh, and I. Podolsky. 1998. Canopy Photosynthesis and Transpiration in Microgravity: Gas Exchange Measurements Aboard Mir. 1998 Biennial COSPAR meeting.

Monje, O., B. Bugbee, and G. E. Bingham. 1998. Modeling Canopy Transpiration: Lessons from Controlled Environments. 28th Crop Simulation Workshop. Beltsville, MD.

Bugbee, B., M. Droter, and **O. Monje**. 1996. Infra-red Thermometry: Accurate Measurement of Leaf to Air Temperature Gradients in CELSS. 1996 Biennial COSPAR meeting.

Droter, M., **O. Monje**, and B. Bugbee. 1996. Calibration of Commercial Infrared Transducers for Biological Applications. 6th Infrared Radiometric Sensor Calibration Symposium, Logan, UT.

Bugbee, B., M. van Iersel, and **O. Monje**. 1995. Continuous Gas-Exchange Measurements in a Ten chamber System. Agronomy Abstracts. 1995 Annual Meeting.

Monje, O., and B. Bugbee. 1995. Adapting Field Transpiration Models to Controlled Environments. Agronomy Abstracts. 1995 Annual Meeting.

Bugbee, B., **O. Monje**, and B. Tanner. 1994. Optimizing Crop Productivity: New Sensors for Measurement of CO₂, Temperature, and Air Velocity. Adv. Space Res.

Monje, O., A. McCormack, and B. Bugbee. 1994. Measurement of Effective Canopy Temperature: The missing Link to Modeling Transpiration in Controlled Environments. Am. Soc. Gravitational and Space Biol. Bulletin 94.

Bugbee, B. and **O. Monje**. 1993. Elevated CO₂ Increases Respiration but Improves Carbon Use Efficiency. Agronomy Abstracts. 1993 Annual Meeting.

Monje, O., B. Tanner, L. Hipps, and B. Bugbee. 1993. Evaluation of Low-cost Infrared Transducers for Measurement of Canopy Temperature. Agronomy Abstracts. 1993 Annual Meeting.

Bugbee, B., **O. Monje**, S. Johnson, and Gus Koerner. 1993. Studies on Resource Optimization of Wheat. NASA Principal Investigators meeting, Washington, DC.

Bugbee, B. and **O. Monje**. 1992. The Energy Cascade Approach to Crop Modeling. Agronomy Abstracts. Agronomy Abstracts 92:122.

Monje, O., and B. Bugbee. 1992. Elevated CO₂ Improves Carbon Use Efficiency in Wheat. Agronomy Abstracts 92:128.

Monje, O., and B. Bugbee. 1992. Monitoring and Control of Plant Growth in a CELSS. Am. Soc. Grav. and Space Biology Bulletin 6:84.

Monje, O., and B. Bugbee. 1990. Uses of Canopy Gas Exchange in CELSS Research. Am. Soc. of Grav. and Space Biol. Bulletin 4:48.

Monje, O., and B. Bugbee. 1989. Design and Calibration of a Meter for In-flight Measurements of Chlorophyll. Am. Soc. of Gravitational and Space Biology Bulletin 3:57.

Monje, O. 1988. Design of Photometric Probes for the Study of Plant Physiology in Microgravity. CELSS Research Conference, Texas A & M, College Station, Texas.

Monje, O. 1988. Design of a Student-built Life Support System for GAS Biological Experiments. Get Away Special Symposium, Cocoa Beach, Florida.